



Title	スペクトル線の衝突拡がりと原子間相互作用の研究
Author(s)	播磨, 弘
Citation	大阪大学, 1983, 博士論文
Version Type	VoR
URL	https://hdl.handle.net/11094/1457
rights	
Note	

The University of Osaka Institutional Knowledge Archive : OUKA

<https://ir.library.osaka-u.ac.jp/>

The University of Osaka

**STUDIES OF COLLISIONAL BROADENING OF SPECTRAL LINES
AND
INTERACTION BETWEEN ATOMS**

1983

Hiroshi Harima

STUDIES OF COLLISIONAL BROADENING
OF SPECTRAL LINES AND INTERACTION
BETWEEN ATOMS

(スペクトル線の衝突拡がりと原子間相互作用の研究)

播磨 弘

Abstract

It is well known that atomic spectral lines show broadenings, shifts and asymmetries when light-emitting (or absorbing) atoms collide with other atoms. This phenomenon, called the collision broadening, is determined by the interaction potentials between the colliding atoms, and by the collision dynamics. Therefore we can make use of this phenomenon as a powerful diagnostic tool to study these interatomic interactions. With the development of line-broadening theories, such attempts have become very popular for some diatomic systems such as alkali-rare-gas pairs. In recent years, these pairs have been widely investigated because of the potentiality as a future gas-laser source. For alkaline-earth-rare-gas pairs, on the other hand, only a few data have been published so far. This is due partly to experimental difficulties. Spectra of alkaline-earth elements which are collisionally broadened by rare gases have received much attention from astrophysical interest, i.e. in the analysis of stellar spectra. In addition, it is interesting to compare these spectra with those of alkali-rare-gas pairs, because both pairs have similar electronic configurations to each other.

The present work reports on spectral-profile measurements of alkaline-earth (Ca, Sr and Ba) resonance lines. These lines are collisionally broadened by various rare gases at pressures below one atmosphere. The measured spectral regions are classified into two groups by the distance from the line center, i.e. the line-core- (near the line center) and the wing- (far apart from the line

center) regions. In the present work, profiles of the line-core regions have been analysed by a classical theory called the impact limit of the phase-shift theory. Profiles in the wing regions have been analysed by a classical theory called the quasi-static limit, a classical theory called the auto-correlational (AC) method, and a quantum theory called the Unified-Franck-Condon (UFC) method. From the line-core-region spectra we can obtain information mainly on the long-range interatomic potentials, while from the wing-region spectra we can deduce the short-range interactions.

In Chapter 1, we classify various broadening mechanisms by the species of perturbers and give a brief review on line-broadening experiments on alkaline-earth-rare-gas pairs.

In Chapter 2, we introduce line-broadening theories used in the present work. They are composed of

- (1) the classical phase-shift theory which predicts two limiting cases, i.e. the impact and the quasi-static limits,
- (2) the general treatment based on the classical phase-shift theory (AC method),
- (3) and the quantum UFC theory.

In Chapter 3, we introduce representative methods to calculate interatomic potentials. They are used in the discussions when we compare the experimentally deduced interatomic potentials with theoretical predictions.

In Chapter 4, we describe the experiments by a shock tube. The atomic pairs studied are as follows.

- (1) Ca-Ar and Ba-Ar pairs for absorption measurements.
- (2) Ca^+ -Ar pair for an emission measurement.

The shock tube can easily produce high temperatures upto 1×10^4 K.

We have measured the profiles at 4000~4600 K for (1) and at 7600~7700 K for (2). We have found from these measurements that if the interatomic distance (denoted hereafter as R) between the colliding atoms is large, the dominant interatomic interaction is the van der Waals type which varies as R^{-6} .

In Chapter 5, we describe the experiments by a heat-pipe cell. We have investigated the following pairs by absorption measurements:

- (1) Sr-rare gas (Ar and Xe),
- (2) Ba-rare gas (He, Ne, Ar, Kr and Xe).

The profiles have been measured at temperatures near 1000 K. We have found from these measurements for Sr (or Ba)-heavy-rare-gas (Ar, Kr and Xe) pairs, the van der Waals interaction is dominant at large R , however repulsive interactions occur at intermediate R ($\sim 6\text{\AA}$). For Ba-light-rare-gas (He and Ne) pairs repulsive interaction is dominant for wide ranges of R .

In Chapter 6, we describe the experiments by a discharge cell. We have measured some atomic lines of argon collisionally broadened by the same species of atoms. In the Ar-Ar collision, we can expect the broadening mechanism is quite different from previous ones. Therefore the comparison of profiles between these cases is interesting. We have found that for the transitions which terminate upon the resonance state the resonance interaction is dominant at large R , and it varies as R^{-3} . However when the transition terminates upon a metastable state, the van der Waals interaction is dominant just like the previous measurements of foreign-gas broadening.

In Chapter 7, we give the concluding remarks.

Contents

	page
Abstract	(1)
Chapter 1. Introduction	1
1.1 Historical background	1
1.2 Contribution of the presentwork	6
Chapter 2. Theory of collision broadening	9
2.1 Introduction	9
2.2 Classical treatment by the phase-shift theory	10
2.2.1 Impact limit	14
2.2.2 Quasi-static limit	20
2.2.3 General case	23
2.3 Quantum treatment by the UFC theory	25
Chapter 3. Interatomic potential	32
3.1 Introduction	32
3.2 Long-range interaction	35
3.2.1 Resonance interaction	36
3.2.2 Van der Waals interaction	38
3.3 Short-range interaction	41
3.3.1 General remarks	41
3.3.2 Gombás' pseudopotential	43
3.3.3 Fermi potential	45
3.4 Model potential of Baylis	47

	page
Chapter 4. Shock-tube experiments	52
4.1 Principle of shock tube	52
4.2 Absorption measurement for Ca-Ar and Ba-Ar pairs	55
4.2.1 Introduction	55
4.2.2 Experimental apparatus	56
(a) Shock tube	56
(b) Optical arrangement	57
4.2.3 Results	58
4.2.4 Discussions	61
(a) Lorenzian width	61
(b) Optical cross section and van der Waals coefficient	64
4.3 Emission measurement for Ca ⁺ -Ar pair	66
4.3.1 Introduction	66
4.3.2 Experimental setup	67
4.3.3 Method of analysis	69
4.3.4 Results and Discussions	71
Chapter 5. Heat-pipe-cell experiments	75
5.1 Introduction	75
5.2 Experiment	77
5.2.1 Absorption cell	77
5.2.2 Optical arrangement and data reduction	80
5.3 Results and discussions	83
5.3.1 Sr-rare gas	83
(a) Observed profile	83
(b) UFC analysis	86
(c) Interatomic potentials	90

	page
5.3.2 Ba-rare gas	94
(a) Observed spectra	94
(b) UFC and AC analyses	98
(c) Interatomic potentials	101
Chapter 6. Discharge-cell experiments	108
6.1 Introduction	108
6.2 Experiment	110
6.3 Results and discussions	116
Chapter 7. Conclusions	122
Acknowledgement	126
References	127
List of publications	132

Chapter 1. Introduction

1-1. Historical background

The broadening of atomic spectral lines is an important problem which commonly appears in optical spectra from gaseous materials. With the development of theories, it has become very popular to use this phenomenon as a powerful diagnostic tool for laboratory and astrophysical plasmas.

The broadening mechanism may be divided into three groups:

- (1) Natural broadening due to the finite lifetime of the excited state.
- (2) Doppler broadening due to the thermal motion of the emitting (or absorbing) atoms.
- (3) Collision broadening due to collisions between the emitting (or absorbing) atoms with surrounding particles.

In most cases we interpret a broadened spectrum as a convolution of these factors plus instrumental function.

Theoretically, the treatments of natural and Doppler broadenings are now well established (see e.g. Mitchell and Zemansky 1971), while for collision broadenings continuous efforts have been made starting from the pioneering work of Michelson (1895).

Collision broadenings (3) may further be divided by the species of the collision perturbers:

- (3a) Stark broadening due to collisions with charged particles, such as ion and electron.
- (3b) Neutral-gas broadening due to collisions with neutral atoms.

Stark broadening is most extensively studied by Griem (1964, 1974) mainly for ionized hydrogen and helium plasma and compared with experiments. These species are familiar in the spectroscopy of laboratory plasmas. In astrophysical plasmas, in addition to the above, neutral gas broadening becomes the problem. For example in "cool" stars such as the Sun, which has an effective temperature of about 6000K, the perturbing particles are predominantly neutral hydrogen atoms. If we limit the topic to neutral gas broadening, with which the present work is concerned, collision pairs most extensively studied are perhaps rare-gas-rare-gas, alkali-rare-gas and alkali-alkali systems. One of the strong motivations for these work is the potentiality of gas lasers, such as excimer lasers (Phelps 1972, York and Gallagher 1974).

Next most commonly studied system is alkaline-earth-rare-gas pair. Alkaline earth is the element familiar in stellar spectra. Take Ca-He pair as an example. As previously mentioned, the collision with hydrogen atoms plays an important role in the Ca line observed in solar spectra. However, because of high temperatures required to dissociate hydrogen molecules, it has not yet been proved possible to perform reliable laboratory measurements of collision broadening by hydrogen atoms. Then the possibility has been discussed to replace the hydrogen atoms by light rare gases like helium. Ayres (1977) discussed how to scale broadenings by rare gases to yield that by hydrogen atoms. From such analyses the abundance of Ca in the sun has been discussed (O'Neill and Smith 1980). In the followings, we will see some more details of experiments on alkaline-earth resonance lines collisionally

broadened by rare gases, since they are the main topic of this work.

For this purpose we will firstly classify the measured spectral regions into two groups depending on the distance from the line center:

- (a) Line-core regions which is near the line center (typically the distance from the line center $\Delta\lambda$ is $|\Delta\lambda| \lesssim 1\text{\AA}$).
- (b) Wing regions which is far apart from the line center.

As we will see in the next chapter, these regions are analysed in somewhat different manners and are closely related to relatively long- and short- range interatomic potentials, respectively.

Line-core measurements for various pairs of neutral alkaline-earth and rare-gas elements have been performed mainly by English and Russian groups (see e.g. Hindmarsh and Farr 1972, Penkin and Shabanova 1968). Since most of the experiments were carried out by conventional furnaces, the temperatures were relatively low, typically below 1000K. In order to observe the spectra at higher temperatures, e.g. near 6000K like the solar atmosphere, other techniques become necessary. One of the preferable techniques is the shock tube, since this does not yield "extra" electrons like electrical-discharge experiments. In the latter case the electrons may severely influence the spectra by Stark broadening. Because of the high temperatures, the shock tube is also suitable for treating ionized species. Experiments on alkaline-earth elements with this technique is quite few (e.g. Hammond 1975, Baur and Cooper 1977), which is one of the motivations for the present shock-tube study at high temperatures.

In contrast to the line-core regions, wing data on alkaline-

earth resonance lines have been reported on limited pairs such as Ca-Ar (Corney and McGinley 1981). This is partly because there is an experimental difficulty. In the wing regions the line intensity generally drastically falls off (down to a few orders of magnitude). Therefore to facilitate the experiment we have to increase the atomic densities to raise the sensitivity. However the vapor pressure of alkaline-earth elements are relatively low, compared to e.g. alkalis (Honig and Kramer 1969), therefore difficult at temperatures of conventional furnaces. In the present work, wing spectra of Sr and Ba broadened by various rare gases are reported, using furnace technique at temperatures near 1000K. This is probably the first extensive studies on these elements up to date, in the meaning that it provides line intensities in "absolute" values for a wide spectral range.

Neutral-gas broadenings (3b) may further be divided by the species of the collision pertubers:

(3b1) Foreign-gas broadening due to collisions with different species of atoms.

(3b2) Resonance broadening due to collisions with the same species as the emitting (or absorbing) atoms.

As described in Chapter 3 the interaction mechanism shows a clear distinction, especially at long-range interatomic-distance, between these two cases. This difference will appear in the line-core profile, e.g. the position of the line center shifts linearly on the perturber's density in foreign-gas broadening, whereas it does not shift in resonance broadening. In this sense, the comparison between these cases is interesting. In the present

work, the resonance broadening of argon is studied. We treat transitions between some excited states, which are the candidates for the energy pooling states in excimer lasers.

As shown in the next chapter, interaction potentials between the colliding atoms play essential roles in the formation of broadened spectra. Conversely, if we had a well-established theory on broadening and a theoretical potential, we can predict the profile and judge if the potential is correct or not by comparing the profile with observations. This technique has the advantage that it yields information on excited state potentials, which are generally inaccessible by other conventional techniques such as beam scattering experiments (e.g. Buck and Pauly 1968).

From the viewpoint of theoretical calculations of potentials, the most commonly studied system is alkali-rare gas. Since alkalis have simple atomic structures, namely single-valence electron, such calculations are relatively easy (e.g. Baylis 1969a,b, Pascale and Vandeplanque 1974). For alkaline-earth-rare-gas systems, on the other hand, sophisticated calculations are quite rare, especially for the short-range interatomic distance. In the present work, experimentally deduced potentials are presented for Ca, Sr, Ba-rare-gas systems and compared with existing theoretical calculations. When there is no appropriate theoretical potentials, we have made some calculations to compare with experiments.

1-2. Contribution of the present work

Chapter 2 briefly reviews some line-broadening theories which are commonly used for the analysis of neutral-gas broadening. As a classical treatment, the phase-shift theory is introduced. The theory predicts two limiting cases, i.e. the impact and the quasi-static limit. The former one corresponds to, so to speak, the limit of high temperature and low perturber density, and the latter to the opposite limit. Most of the present observations are analysed by these methods, but at some positions in the wing spectra where "singularities" are observed (they are called satellite or shoulder) these treatments are invalid. Then, a quantum treatment called the UFC (Unified-Franck-Condon) theory (Szudy and Baylis 1975) is introduced to apply to these cases.

Chapter 3 introduces representative methods to calculate interatomic potentials. They depend on the interatomic distance in question. We first discuss the long-range interaction by a standard perturbation method, which is the most common approach. If the atoms are different, the leading term is the well-known van der Waals force, to which some detailed explanations are given. In the short range, where the overlap of electron clouds can not be neglected, both perturbation method with charge exchange and variational method appear reasonable. Since these are in general quite complicated calculations, much effort has been made to simplify them by modeling the potentials into various styles (Düren 1980). The pioneering and probably the simplest treatment is that of Baylis (1969a,b), which is here briefly

reviewed. Though he originally applied this to alkali-rare gas collision, it may also be applicable to the present problem of $\text{Ca}^+ \text{-Ar}$, since Ca^+ has similar electronic structure to alkali (single valence electron).

The present works were performed with three experimental apparatus, i.e. a shock tube, a heat-pipe cell and a discharge cell. Experimental conditions vary drastically depending on the apparatus, e.g. the shock-tube produces temperatures between roughly 4000 and 8000K, while the others between room temperature and 1000K.

Chapter 4 describes the shock-tube experiments. The transitions in question are as follows:

- (1) $\text{Ca} 4227\text{\AA}$ resonance line ($4s^2 \text{ }^1\text{S}_0 - 4s4p \text{ }^1\text{P}_1$) broadened by Ar.
- (2) $\text{Ba} 5535\text{\AA}$ resonance line ($6s^2 \text{ }^1\text{S}_0 - 6s6p \text{ }^1\text{P}_1$) broadened by Ar.
- (3) $\text{Ca}^+ 3968$ and 3933\AA resonance line doublet ($4s^2 \text{ }^2\text{S}_{1/2} - 4p^2 \text{ }^2\text{P}_{1/2, 3/2}$) broadened by Ar.

The measured spectral region is the line core for all cases. The first two were measured at temperatures between 4000 and 5000K, while the last one between 7000 and 8000K. Since such data at high temperatures are quite scarce, they give interesting comparison with existing low temperature results. For example, van der Waals coefficients for Ca, Ba-Ar pairs have been deduced to compare with data at temperatures below 1000K.

Chapter 5 describes the heat-pipe cell experiment. This is a technique commonly used to confine a metallic vapor with rare gases. The transitions in question are as follows:

(1) Sr 4607\AA resonance line ($5s^2 1S_0 - 5s 5p 1P_1$) broadened by Ar and Xe.

(2) Ba 5535\AA resonance line broadened by He, Ne, Ar, Kr and Xe.

The measured spectral region lies in the wing area, where the distance from the line center is $1 \leq |\Delta\lambda| \leq 50\text{\AA}$. Structures like satellite have been observed clearly for collisions with heavy rare gases. They are analysed in detail by the classical phase-shift theory and the quantum UFC treatment. It has been found the experimental interaction potentials have wells at some short interatomic distance. The result is compared with theoretical calculations and discussed.

Chapter 6 describes the discharge-cell experiment for the following transitions:

(1) Ar 8115\AA line ($1s_5 - 2p_9$, in Paschen notation).

(2) Ar 8104\AA line ($1s_4 - 2p_7$).

(3) Ar 8408\AA line ($1s_2 - 2p_3$).

These lines are broadened by the collision with argon itself in the ground state. Here using a tunable diode laser as the light source of absorption measurement, very narrow line-core regions ($|\Delta\lambda| \lesssim 0.02\text{\AA}$) have been measured. The 8104 and 8408\AA lines have been found to have small or no collision shift, which indicates the existence of resonance interaction.

Chapter 7 summarizes the experimental findings and discussions in the present work and shows the remaining problems.

Chapter 2. Theory of collision broadening

2.1 Introduction

To know the development of general line-broadening theories, the following review articles would be most appropriate: Unsöld (1955), Traving (1960), Breene (1961, 1981), Baranger (1962), Griem (1964, 1974), Cooper (1967), Sobelman (1972), Peach (1980) and Sobelman et al (1981).

If we limit the topic to neutral-gas broadenings, the following articles are also appropriate. They include experimental results up to the respective date:

Weisskopf (1933), Margenau and Watson (1936), Chen and Takeo (1957) and Hindmarsh et al (1972).

In this chapter for the classical phase-shift theory, we follow mainly the treatment of the last two articles and that of Sobelman et al (1981).

The quantum treatment by the UFC theory is developed by Szudy and Baylis (1975). To remove the inapplicability of the classical theory to the wing satellite, they described the perturber's motion by an approximate formula based on the WKB approximation.

2.2 Classical treatment by the phase-shift theory

The theory of spectral line broadening caused by the interaction of a light-emitting (or absorbing) atom with surrounding particles is closely related to the general theory of atomic collisions. For example in many calculations of spectral profiles we must consider scattering amplitude, cross section and so on. These values are often important observables in atomic collisions.

We first make the following assumptions to simplify the problem, as are often employed in the general theory of atomic collisions. In the following we shall call the light-emitting (or absorbing) atom as an active atom and the perturbing particle as a perturber.

- (a) The relative motion of an active atom and a perturber is quasi-classical. This assumption enables us to use the concept of a trajectory of the perturber.
- (b) This trajectory is straight.
- (c) The interaction with the nearest perturber plays the principal role in the broadening (the assumption of binary interaction), so that multiparticle interactions can be neglected.
- (d) The perturbation is adiabatic, i.e. the collision does not induce transitions between different states of the active atom.

The assumptions (a) and (b) may be valid in most thermal collisions at low temperatures, where perturbers penetrating deeply into the active atom are relatively few, and on the average the perturbation

is not strong. The assumption (c) is valid when the density of perturber is low, typically below one atmosphere. Then the effect of many perturbers on an active atom can be separated in time. The assumption (d) is valid when the active atom has no closely lying states near the upper or lower state of the transition.

In this approach the active atom is described by an atomic oscillator, and intensity distribution $I(\omega)$ in question is given by the power spectrum of the oscillation $f(t)$. Thus

$$I(\omega) = \lim_{T \rightarrow \infty} \frac{1}{2\pi T} \left| \int_{-T/2}^{T/2} f(t) \exp(-i\omega t) dt \right|^2. \quad (2.1)$$

If $f(t)$ is treated as a stationary random quantity, (2.1) can be rewritten in a more convenient form by the Wiener-Khintchine theorem, as

$$I(\omega) = \frac{1}{\pi} \text{Re} \int_0^{\infty} \Phi(s) \exp(-i\omega s) ds, \quad (2.2)$$

where $\Phi(s)$ is the autocorrelation function of $f(t)$

$$\Phi(s) = \lim_{T \rightarrow \infty} \frac{1}{T} \int_{-T/2}^{T/2} f(t) f(t + s)^* dt. \quad (2.3)$$

Time averaging can be replaced by averaging over the statistical assembly of quantities defining the function $f(t)$ if the ergodic hypothesis is used. We shall denote such averaging by $\langle \rangle$, then (2.3) can be rewritten as

$$\Phi(s) = \langle f(0)^* f(s) \rangle, \quad (2.4)$$

where we can drop t .

Next we shall consider $f(t)$. Usually the atomic oscillator is described by an elastically-bound oscillating electron. In this case the displacement of the electron, hence the time-varying dipole moment of the oscillator, corresponds to $f(t)$. It may be written as

$$f(t) = A(t) \exp \left[i \int_{-\infty}^t \omega(t') dt' \right] , \quad (2.5)$$

where $A(t)$ is the amplitude, $\omega(t')$ is the instantaneous frequency of the oscillator at time $t = t'$ and we assumed that at $t = -\infty$ there is no interaction. Eq.(2.5) already includes the previous binary approximation (c), because multi-perturber effect is replaced by successive collisions of the nearest perturbers and the phase factor is expressed by the time integral from $-\infty$ to t . If we put the unperturbed frequency of the oscillator as ω_0 , the frequency will remain at ω_0 after completion of each collision and $A(t)$ will remain constant, because there is no transfer of energy from the perturber to the oscillator due to the adiabatic assumption (d). Here we further assume that the oscillator may change the phase by $\gamma(t)$ given by

$$\gamma(t) = \frac{1}{\hbar} \int_{-\infty}^t \Delta V(t') dt' , \quad (2.6)$$

as the result of successive collisions, where $\Delta V(t')$ is the interaction at time t' . Then $f(t)$ is rewritten as

$$f(t) = \exp \left[i \omega_0 t + i \gamma(t) \right] , \quad (2.7)$$

where ω_0 is the unperturbed frequency and we have put $A(t) = 1$.

If (2.7) is put into (2.1), we get

$$\begin{aligned} I(\omega) &= \lim_{T \rightarrow \infty} \frac{1}{2\pi T} \left| \int_{-T/2}^{T/2} \exp \left[-(\omega - \omega_0)t + i\beta(t) \right] dt \right|^2 \\ &= \lim_{T \rightarrow \infty} \frac{1}{2\pi T} \left| \int_{-T/2}^{T/2} \exp \left[-\Delta\omega t + i\beta(t) \right] dt \right|^2, \end{aligned} \quad (2.8)$$

where we put $\Delta\omega = \omega - \omega_0$. This is written again by the Wiener-Khintchine theorem as

$$I(\Delta\omega) = \frac{1}{\pi} \operatorname{Re} \int_0^\infty \Phi(s) \exp(-i\Delta\omega s) ds, \quad (2.9)$$

where $\Phi(s)$ is given by (2.3) with $f(t) = \exp[i\beta(t)]$ as

$$\begin{aligned} \Phi(s) &= \lim_{T \rightarrow \infty} \frac{1}{T} \int_{-T/2}^{T/2} \exp \left[i\beta(t+s) - i\beta(t) \right] dt \\ &= \langle \exp[i\beta(s)] \rangle. \end{aligned} \quad (2.10)$$

In the following, two limiting cases, impact and quasi-static limits, are discussed starting from this general result.

2.2.1 Impact limit

This limit is based on the assumption that the decisive factor in the broadening of a line is the disruption of the coherence of the oscillations of an atomic oscillator during collisions. In other words if the duration of collision is small as compared with the mean time between collisions, then one can neglect radiation during collisions and consider the collisions to be instantaneous. Therefore the collisions are manifested only in phase shifts δ .

Using this assumption of instantaneous collision, it is possible to calculate the correlation function $\Phi(s)$ as follows. We shall firstly make a differential equation for $\Phi(s)$. The difference $\Delta\Phi(\Delta s) = \Phi(s + \Delta s) - \Phi(s)$ can be written, from (2.10), as

$$\begin{aligned}\Delta\Phi &= \langle \exp[i\delta(s + \Delta s)] \rangle - \langle \exp[i\delta(s)] \rangle \\ &= \langle \exp[i\delta(s)] \cdot \exp[i\Delta\delta] \rangle - \langle \exp[i\delta(s)] \rangle,\end{aligned}\quad (2.11)$$

where $\Delta\delta$ is the additional phase shift in time Δs

$$\Delta\delta = \frac{\partial\delta}{\partial s} \Delta s. \quad (2.12)$$

Since collisions are instantaneous, the phase shift $\Delta\delta$ does not depend on $\delta(s)$. Therefore, eq.(2.11) is written as

$$\begin{aligned}\Delta\Phi &= \langle \exp[i\delta(s)] \rangle \left\{ \langle \exp[i\Delta\delta] \rangle^{-1} \right\} \\ &= \Phi(s) \cdot \langle \exp[i\Delta\delta]^{-1} \rangle.\end{aligned}\quad (2.13)$$

The average $\langle \rangle$ over ensemble can be calculated by taking over all possible conditions which causes a phase change in the time interval ΔS . If we put

n : the perturber density

\bar{v} : the mean relative velocity of colliding atoms

ρ : impact parameter (namely the distance at the closest approach),

the number of collisions occurring in ΔS is $2\pi\rho d\rho \bar{v} n \Delta S$ with impact parameters between ρ and $\rho + d\rho$ (see Fig.2.1, where the straight trajectory assumption (b) is employed).

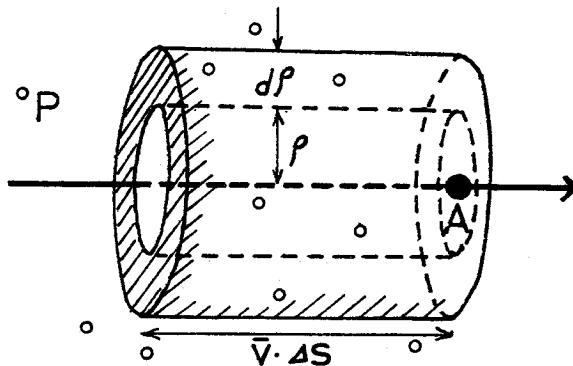


Fig.2.1 The number of collisions between the time interval Δs .

Perturbers (○) within the shaded volume collide with the active atom (●), with impact parameters between ρ and $\rho + d\rho$.

Thus, if $\Delta\gamma$ is a function of ρ only, we can write

$$\begin{aligned} \langle \exp [i \Delta\gamma] \rangle^{-1} &= \Delta S n \bar{v} \int_0^\infty \left\{ \exp [i \gamma(\rho)] \right\}^{-1} 2\pi \rho d\rho \\ &\equiv -\Delta S n \bar{v} (\alpha_r - i \alpha_i), \end{aligned} \quad (2.14)$$

where we have defined optical cross sections as

$$\alpha_r \equiv \int_0^\infty [1 - \cos \gamma(\rho)] 2\pi \rho d\rho, \quad (2.15)$$

$$\alpha_i \equiv \int_0^\infty \sin \gamma(\rho) 2\pi \rho d\rho. \quad (2.16)$$

Thus eq.(2.13) is rewritten as

$$\Delta \Phi = -\Phi \cdot \Delta S n \bar{v} (\alpha_r - i \alpha_i), \quad (2.17)$$

or in a differential form

$$\frac{d\Phi}{ds} = -\Phi \cdot n \bar{v} (\alpha_r - i \alpha_i). \quad (2.18)$$

This has the solution

$$\Phi(s) = \exp [-n \bar{v} (\alpha_r - i \alpha_i) s]. \quad (2.19)$$

By substituting (2.19) into (2.9), we get

$$I(\Delta\omega) = \frac{n \bar{v} \alpha_r / \pi}{(\Delta\omega - n \bar{v} \alpha_i)^2 + (n \bar{v} \alpha_r)^2}. \quad (2.20)$$

This is a Lorentzian distribution, whose HWHM (half width at half maximum) γ and shift β are given by

$$\gamma = n \bar{v} \alpha_r, \quad (2.21)$$

$$\beta = n \bar{v} \alpha_i. \quad (2.22)$$

It is easy to see from (2.15) and (2.16) that if $\gamma(\rho)$ increases rapidly as ρ decreases, the rapidly oscillating term $\sin \gamma(\rho) 2\pi\rho$ yields no contribution to the integral. Thus the contribution to α_i comes from large values of ρ , while that to α_r comes from small values of ρ . Therefore for the width τ , "strong" (namely ρ is small, hence $\gamma(\rho)$ is large) collisions contribute greatly. This is originally the physical idea of Weisskopf (1933), who considered the broadening arises essentially from collisions which cause phase changes of $\gamma \geq 1$ radian.

All that remains to press this calculation to a numerical conclusion is to evaluate $\gamma(\rho)$ and then perform the integration in (2.15) and (2.16). Since R , the interatomic distance, is given by the straight assumption (b) as

$$R = \sqrt{\rho^2 + (\bar{v}t)^2} , \quad (2.23)$$

where t is the time taken from the time of closest approach (see Fig.2.2), $\gamma(\rho)$ is rewritten from (2.6) as

$$\gamma(\rho) = \frac{2}{\bar{v}\hbar} \int_0^{\infty} \frac{\Delta V(R) R}{\sqrt{R^2 - \rho^2}} dR . \quad (2.24)$$

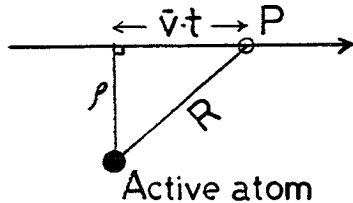


Fig.2.2 Straight trajectory.

A perturber (\bullet) follows a straight trajectory with impact parameter ρ , and with velocity \bar{v} .

Take for example

$$\Delta V(R) = \frac{\Delta C}{R^p} , \quad (2.25)$$

which is the commonly-known p -th inverse power potential with a coefficient ΔC , then we find by putting into (2.24)

$$\gamma(\rho) = \sqrt{\pi} \frac{\Gamma(\frac{p-1}{2})}{\Gamma(\frac{p}{2})} \frac{\Delta C}{\hbar \bar{v} \rho^{p-1}} \quad (2.26)$$

From (2.26), (2.15), (2.16), (2.21) and (2.22) we get

$$\text{for } p = 3 \quad \gamma = \pi^2 \left(\frac{\Delta C_3}{\hbar} \right) n , \quad (2.27)$$

$$p = 4 \quad \gamma \approx 5.7 \left(\frac{\Delta C_4}{\hbar} \right)^{2/3} \bar{v}^{1/3} n , \quad \beta = \gamma \tan \frac{\pi}{3} , \quad (2.28)$$

$$p = 6 \quad \gamma \approx 4.08 \left(\frac{\Delta C_6}{\hbar} \right)^{2/5} \bar{v}^{3/5} n , \quad \beta = \gamma \tan \frac{\pi}{5} . \quad (2.29)$$

From (2.26) we get the Weisskopf radius ρ_w , which is defined as threshold of strong collision by the condition $\gamma(\rho_w) = 1$, i.e.

$$\rho_w = \left[\sqrt{\pi} \cdot \frac{\Gamma(\frac{p-1}{2})}{\Gamma(\frac{p}{2})} \frac{\Delta C}{\hbar \bar{v}} \right]^{\frac{1}{1-p}} . \quad (2.30)$$

Finally we discuss the spectral region $\Delta \omega$ to which this impact limit applies. From (2.19) significant contributions to $\Phi(s)$ occur when $n \bar{v} \alpha_r s \lesssim 1$ (otherwise $\exp(-n \bar{v} \alpha_r s)$ is too small). Therefore the times of interest s in determining the profile

are less than about $(n\bar{v}\alpha_r)^{-1}$, while s must be much larger than the time for which there is a non-vanishing perturbation, i.e. the duration τ_c of a typical collision (since respective collision is assumed statistically independent). Therefore

$$\tau_c \ll s \lesssim (n\bar{v}\alpha_r)^{-1}. \quad (2.31)$$

This agrees to the picture of Lorentz (1906), who considered the mean time between collisions is given by $T = (n\bar{v}\alpha)^{-1}$ and is much larger than collision duration τ_c . From the properties of the Fourier transform, times of interest is given by $s \sim \Delta\omega^{-1}$ for the frequency separation $\Delta\omega$, therefore with (2.31)

$$\Delta\omega \ll \tau_c^{-1}. \quad (2.32)$$

If we estimate by $\tau_c \sim \rho_w / \bar{v}$, $\Delta\omega \ll 10^{12} \text{ sec}^{-1}$ with typical values of $\rho_w (\sim 10^{-7} \text{ cm})$ and $\bar{v} (\sim 10^5 \text{ cm/sec})$, or in wavelength for visible light $\Delta\lambda \ll 1\text{\AA}$.

2.2.2 Quasi-static limit

In the previous limit we assumed collisions occur instantaneously, so neglected the contribution that arises in collision duration to the line intensity. In the quasi-static limit on the other hand, we assume perturbers move very slowly, so we must include all contributions.

We start from the general result for $I(\Delta\omega)$ and $\Phi(s)$, i.e. (2.9) and (2.10). When $\gamma(s)$ is a slowly-varying function of s , main contributions to $I(\Delta\omega)$ comes from small values of s if $\Delta\omega$ is large. In this case we expand $\gamma(t+s)$ in Taylor series about t , and take only the first two terms i.e.

$$\gamma(t+s) = \gamma(t) + \frac{d\gamma}{dt} s = \gamma(t) + \Delta\omega \cdot s, \quad (2.33)$$

then we get

$$\Phi(s) = \langle \exp(i\Delta\omega \cdot s) \rangle. \quad (2.34)$$

If $P(\Delta\omega)$ is the probability of occurrence $\Delta\omega$, we may write

$$\Phi(s) = \int_{-\infty}^{\infty} \exp(i\Delta\omega s) P(\Delta\omega) d\Delta\omega.$$

Leaving the contributions from small s , we get

$$I(\Delta\omega) = P(\Delta\omega). \quad (2.35)$$

Therefore, to calculate $I(\Delta\omega) d\omega$ we must find the probability $P(R) dR$ of the nearest perturber to be between R and $R + dR$, where R satisfies from (2.6)

$$\Delta\omega = \frac{\Delta V(R)}{\hbar} \quad . \quad (2.36)$$

$P(R)$ is calculated as follows. If an active atom is surrounded by perturbers of density n , the probability of finding a perturber in a volume element $dV (= 4\pi R^2 dR)$ is given by $n \cdot dV$. $P(R)dR$ is given as the product of $n \cdot dV$, and the probability of perturbers not being at any volume element V_i ($i = 1 \dots N$, with $N = V/dV$) within R ,

$$\begin{aligned} P(R)dR &= \prod_i^N (1 - n dV_i) n dV \\ &= (1 - n dV)^N n dV \\ &= \exp(-nV) n dV \quad (N \rightarrow \infty) \\ &= \exp\left(-\frac{4\pi}{3} R^3 n\right) \cdot 4\pi R^2 n dR . \end{aligned} \quad (2.37)$$

Therefore (2.35) is

$$I(\Delta\omega)d\omega = \exp\left(-\frac{4\pi}{3} R^3 n\right) 4\pi R^2 n dR . \quad (2.38)$$

Since we practically treat the case of $n \sim 10^{19} \text{ cm}^{-3}$ and $R \sim 10^{-8} \text{ cm}$, the exponential factor can be omitted

$$I(\Delta\omega) = 4\pi R^2 n \frac{dR}{d\omega} = n\hbar \cdot 4\pi R^2 \left[\frac{d\Delta V(R)}{dR} \right]^{-1} , \quad (2.39)$$

where we used (2.36) and identity

$$\frac{dR}{d\omega} = \left[\frac{d\Delta V(R)}{dR} \right]^{-1} \frac{d\Delta V(R)}{d\omega} .$$

Eq. (2.39) can be calculated if we have an explicit form for $\Delta V(R)$. For p-th inverse-power potential $\Delta V(R)$, eq. (2.25), we get

$$I(\Delta\omega) = \frac{4\pi}{p} n\left(\frac{\Delta C}{h}\right)^{\frac{3}{p}} \Delta\omega^{-\frac{p+3}{p}}. \quad (2.40)$$

To conclude, the basic idea of the quasi-static limit is that perturbers move very slowly and the line intensity is proportional to the probability of finding the perturbers at the distance corresponding to $\Delta\omega$. Contrary to the impact limit, the quasi-static formula predicts profiles at large $\Delta\omega$, namely the wing region.

2.2.3 General case

There have been many attempts (e.g. Margenau and Watson 1936, Lindholm 1945 and Holstein 1950) to span a bridge over the impact and quasi-static limits to describe the spectral region of intermediate $\Delta\omega$. Here is introduced the treatment of Anderson (1952). His idea is based on the preceding assumptions listed as (a)~(d) except for (c), the binary assumption. He proposed the interactions responsible for $\Phi(s)$ are scalar and additive, so $\gamma(t)$ of (2.6) is given by

$$\gamma(t) = \frac{1}{\hbar} \int_{-\infty}^t \Delta V(R) dt' = \frac{1}{\hbar} \int_{-\infty}^t \sum_{i=1}^N \Delta V(R_i) dt' , \quad (2.41)$$

where N perturbers at R_i ($i = 1, 2 \dots N$) perturb an active atom simultaneously at $t = t'$. For weak perturbations, this scalar additivity is not a strong requirement. Thus from (2.10)

$$\Phi(s) = \langle \exp \left[i \sum_{i=1}^N \gamma_i(s) \right] \rangle_{\text{phase space of } N \text{ perturbers}} \quad (2.42)$$

where we have put

$$\gamma_i(s) = \frac{1}{\hbar} \int_{-\infty}^s \Delta V(R_i) dt' . \quad (2.43)$$

Anderson (1952) further assumes perturbers' paths are mutually independent, then the average over N perturbers can be computed by considering just one perturber at a time uncoupled from the rest, therefore

$$\Phi(s) = \langle \exp[i\gamma(s)] \rangle_{\text{phase space of one perturber}}^N \quad (2.44)$$

In this case to make the spatial average we must take the average over x which denotes the perturber's initial position by $R^2 = (x + \bar{v}t)^2 + \rho^2$. If there are N perturbers in the space volume with density n ,

$$\begin{aligned} \Phi(s) &= \left\{ \frac{n}{N} \int_0^\infty 2\pi\rho d\rho \int_{-\infty}^\infty dx \exp[i\gamma(s)] \right\}^N \\ &= \left\{ 1 - \frac{n}{N} \int_0^\infty 2\pi\rho d\rho \int_{-\infty}^\infty dx (1 - \exp[i\gamma(s)]) \right\}^N \\ &= \exp \left[-n \int_0^\infty 2\pi\rho d\rho \int_{-\infty}^\infty dx (1 - \exp[i\gamma(s)]) \right], \quad (2.45) \end{aligned}$$

where we used the relation $(1 - x)^N \approx \exp(-Nx)$ which is valid for small x .

Kielkopf (1981) writes (2.45) using the spatial unit $u = \bar{v}s$ (cm), rather than time s , as $\Phi(u/\bar{v}) = \exp(\alpha + i\beta)$ with

$$\alpha(u) = n \int_0^\infty 2\pi\rho d\rho \int_{-\infty}^\infty dx \{1 - \cos[\gamma(x, \rho, u)]\} \quad (2.46)$$

$$\beta(u) = n \int_0^\infty 2\pi\rho d\rho \int_{-\infty}^\infty dx \sin[\gamma(x, \rho, u)] \quad (2.47)$$

and

$$\gamma(x, \rho, u) = \frac{1}{\bar{v}} \int_0^u \Delta V \left([(x + y)^2 + \rho^2]^{1/2} \right) dy \quad (2.48)$$

with $y = \bar{v}t$, then the line intensity $I(\Delta\omega)$ is written from (2.9) as

$$I(\Delta\omega) = \frac{1}{\pi \bar{v}} \int_0^\infty \exp[-\alpha(u)] \cos \left[\Delta\omega \frac{u}{\bar{v}} - \beta(u) \right] du. \quad (2.49)$$

2.3 Quantum treatment by the UFC theory

In some cases "satellites" appear in the wing region of the intensity distribution. Usually they are found as a shoulder or a maximum followed in some cases by small oscillations. In the classical-static limit eq. (2.39), they appear at frequency which satisfies $d\omega/dR = 0$ leading to a singularity in $I(\omega)$. For a quantitative treatment of such observations eq. (2.39) is therefore insufficient. This fault comes from the static model of perturbers, therefore to remove the difficulty we must include the atomic motion into the theory. The theoretical work on this subject is recently well advanced by Szudy and Baylis (1975), who called the method UFC (Unified-Franck-Condon) theory due to the analogy with the Franck-Condon approximation for molecular transitions. The basic idea comes from the treatment of Jablonsky (1945) who introduced WKB wave functions to describe perturber's motion, and that of Baranger (1958) who derived a quantum expression of the autocorrelation function. The theory is briefly outlined in the following.

The system considered consists of a single active atom immersed in a gas of N perturbers in a macroscopic volume V . The starting point is the expression of Baranger for the single-perturber correlation function (Baranger 1958)

$$\varphi(s) = \sum_{if} p_i |\langle f | i \rangle|^2 e^{\pm \omega_{fi} s}, \quad (2.50)$$

where $|i\rangle$ and $|f\rangle$ are the initial and final perturber states, p_i is the probability of finding the perturber in $|i\rangle$, and $\hbar\omega_{fi}$ is the

difference of perturber state energies between $|f\rangle$ and $|i\rangle$ for emission (+) or absorption (-). To derive (2.50) we used Born-Oppenheimer approximation to separate electronic and nuclear motions. N-perturbers correlation function $\Phi(s)$ is derived like the classical result (2.45), namely

$$\Phi(s) = \exp[-ng(s)] , \quad (2.51)$$

where n is the perturber density and

$$g(s) = V \left(1 - \varphi(s) \right) = V \sum_{if} p_i |\langle f | i \rangle|^2 (1 - e^{\mp i \omega_{fi} s}) . \quad (2.52)$$

The assumption used here is, like the classical case, that perturbers are independent.

Szudy and Baylis (1975) calculate $g(s)$ as follows. The states $|i\rangle$ and $|f\rangle$ are described as $\psi_{i(f)\ell}(R)Y_\ell^m/R$ because the interactions V_i and V_f are functions of interatomic distance R only. Here Y_ℓ^m is the usual spherical harmonics. Since Y_ℓ^m is orthonormal, the overlap integral $\langle f | i \rangle$ is non-zero only when $|i\rangle$ and $|f\rangle$ have the same quantum numbers ℓ and m , and if so

$$\begin{aligned} \langle f | i \rangle &= \int_0^R \psi_{f\ell}^*(r) \psi_{i\ell}(r) dr . \\ &\equiv A_\ell(\mp \omega_{fi}) . \end{aligned} \quad (2.53)$$

$\psi_{i(f)\ell}(R)$ satisfies the equation

$$\left[-\frac{d^2}{dR^2} + k_j^2(R) \right] \psi_{j\ell}(R) = 0 , \quad (2.54)$$

where $j=i$ and f , and $k_j(R)$ is given with the reduced mass μ as

$$k_j^2(R) = \frac{2\mu}{\hbar^2} [E_j - V_j(R)] - \frac{\ell(\ell+1)}{R^2} . \quad (2.55)$$

With some minor approximations for $V \sum_{i,f} p_i$ in eq. (2.52), $g(s)$ is reduced to

$$g(s) = \left\langle \frac{4\hbar R^2}{E_i} \sum_{\ell=0}^{\infty} (2\ell+1) \int_{-\infty}^{\infty} d\omega_{fi} k_f^{-1} (1 - e^{\mp i\omega_{fi}s}) |A_{\ell}(\mp\omega_{fi})|^2 \right\rangle , \quad (2.56)$$

where $\langle \dots \rangle$ is the average over k_i or equivalently over initial energies E_i . Eq. (2.56) is the basic formula of the UFC theory to calculate $I(\Delta\omega)$ with (2.51) and (2.9). The calculated result is

$$I(\Delta\omega) = \frac{n}{\pi} \cdot \frac{\zeta^2 J(\zeta)}{(\Delta\omega - \beta)^2 + \gamma^2} , \quad (2.57)$$

where

$$\zeta = \Delta\omega - n \kappa \quad (2.58)$$

with

$$\kappa = \mp \left\langle \frac{4\hbar R^2}{E_i} \sum_{\ell=0}^{\infty} (2\ell+1) \int_{-\infty}^{\infty} d\omega_{fi} k_f^{-1} |A_{\ell}(\mp\omega_{fi})|^2 \omega_{fi} \right\rangle , \quad (2.59)$$

and

$$J(\zeta) = \left\langle \frac{\pi\hbar R^2}{E_i k_f} \sum_{\ell=0}^{\infty} (2\ell+1) |A_{\ell}(\zeta)|^2 \right\rangle , \quad (2.60)$$

where A_{ℓ} is now to be evaluated for the energy difference

$$E_f - E_i = \hbar \omega_{fi} = \hbar \zeta, \quad (2.61)$$

and γ and β correspond to the impact width and shift, given by

$$\gamma - i\beta = ng'(\infty). \quad (2.62)$$

Next step is to calculate A_ℓ by using WKB wavefunctions for $\psi_{i(f)j}$ as Jablonsky (1945) did. From (2.54) and (2.55) we get the WKB solution

$$\psi_{j\ell}(R) = \left[\frac{2k_j}{Rk_j(R)} \right]^{1/2} \cos \gamma_j(R), \quad (2.63)$$

where the phase is

$$\gamma_j(R) = \int_{R_t}^R k_j(R') dR' + \frac{\pi}{4} \quad (2.64)$$

for $j = i$ and f (R_t is the classical turning point). From (2.63) and (2.53) we get

$$A_\ell(\zeta) = \frac{[k_i k_f]^{1/2}}{R} \int_{R_t}^R \frac{\cos \gamma_-(R')}{[k_i(R') k_j(R')]^{1/2}} dR', \quad (2.65)$$

where $\gamma_- = \gamma_i - \gamma_f$ and the rapidly oscillating term from $\gamma_+ = \gamma_i + \gamma_f$ has been neglected in derivation. The cosine term predicts the oscillatory behavior of the band strength.

As the final step, we apply the following stationary phase approximation to A_ℓ and reduce $I(\omega)$ to a calculable form for the wing region. We find in (2.65) at large ζ the integrand usually contributes significantly in the neighborhood of the points $R = R_c$ where with (2.64)

$$\beta'_-(R_c) = k_i(R_c) - k_f(R_c) = 0 \quad . \quad (2.66)$$

With (2.55) and (2.61) we find

$$\hbar \xi = \frac{1}{\gamma} (E_f - E_i) = \frac{1}{\gamma} \left[V_f(R_c) - V_i(R_c) \right] = \Delta V(R_c) \quad . \quad (2.67)$$

Eq. (2.67) has in general complex solutions R_c . If they are real, they represent "transition points": positions at which, according to the classical formulation of the Franck-Condon principle, the transitions occur. In this meaning, R_c is called the Condon point. Although Szudy and Baylis (1975) have given a detailed discussion on complex Condon points, we shall not repeat it here. There are some ways to approximate $\beta'_-(R)$ near $R = R_c$, one is to expand in Taylor series

$$\beta'_-(R) = \beta'_-(R_c) + \frac{1}{2} \beta''(R_c)(R-R_c)^2 + \frac{1}{6} \beta''(R_c)(R-R_c)^3 + \dots \quad (2.68)$$

If $\beta'_-(R)$ is written as a cubic function of R , it is shown that A_1 is evaluated as an Airy function. Szudy and Baylis introduce a more refined cubic expansion than (2.68) called "uniform approximation" to treat a pair of Condon points.

Here we introduce the final result of Szudy and Baylis (1975) to describe the wing region intensity.

$$I(\Delta \omega) = \frac{4\pi n \xi^2}{\xi^2 + \gamma^2} \sum_c \frac{(R_e R_c)^2 \exp[-V_i(R_e R_c)/kT]}{|\Delta V'(R_c)/\hbar|} |36\pi Z_c|^{1/2} L(Z_c) \quad , \quad (2.69)$$

where the summation is over all Condon points R_c with complex ones. $R_e R_c$ means the real part and Z_c and $L(Z_c)$ are given as follows. Z_c is a dimensionless parameter, defined for real R_c as

$$z_c = \frac{1}{2} \left(\frac{\mu}{kT} \right)^{1/3} \left[\frac{\Delta V'(R_c)}{\hbar} \right] \left[\frac{\Delta V''(R_c)}{\hbar} \right]^{-4/3}, \quad (2.70)$$

and for complex R_c as

$$z_c = -\frac{1}{2} \left(\frac{\mu}{kT} \right)^{1/3} \left| (I_m R_c)^2 \frac{\Delta V'(R_c)}{\hbar} \right|^{2/3}. \quad (2.71)$$

$L(z_c)$ is called the line-shape function and defined as

$$L(z_c) = \int_0^{\infty} s^{-2} \left| A_i(-z_c s) \right|^2 \exp(-s^3) ds, \quad (2.72)$$

where A_i is the Airy function. For $\beta^2 \gg \tau^2, \beta^2$, (2.69) is approximated to

$$I(\Delta\omega) = 4\pi n \sum_c \frac{(R_e R_c)^2 \exp[-V_i(R_e R_c)/kT]}{\left| \Delta V'(R_c)/\hbar \right|} \left| 36\pi z_c \right|^{1/2} L(z_c). \quad (2.73)$$

This is the formula used in the present work. The procedure to calculate $I(\Delta\omega)$ for a $\Delta\omega$ is as follows:

(1) Calculate r_c by (2.67) and (2.58), in our case they are reduced to

$$\hbar \Delta \beta \approx \hbar \Delta \omega = \Delta V(R_c).$$

(2) Calculate z_c by (2.70) and (2.71).

(3) Calculate $L(z_c)$ by (2.72).

(4) Substitute these values and make summation as (2.73).

Eq.(2.73) predicts the classical quasi-static limit (2.39) as a special case. For real R_c with $z_c \gg 1$, we can put

$|36\pi z_c|^{1/2} L(z_c) \approx 1$, and (2.73) is reduced to

$$I(\Delta\omega) = \sum_c n \hbar \cdot 4 \pi R_c^2 \left[\frac{d\Delta V(R)}{dR} \right]_{R=R_c}^{-1}, \quad (2.74)$$

if we can neglect the Boltzmann factor.

Chapter 3. Interatomic potentials

3.1 Introduction

We have seen in the preceding chapter that collisionally broadened profiles are essentially determined by the interaction potentials between atoms. Conversely, starting from an experimental result of broadened profile we can deduce an empirical potential by a broadening theory. In the present work, such empirical potentials have been deduced by the preceding broadening theories, and compared with theoretical predictions. In this chapter, some representative methods to calculate the theoretical potentials are introduced.

According to the interatomic distance R in question, the methods may be divided into three groups.

- (1) In the long range, typically at $R \gtrsim 10\text{\AA}$, the charge overlap between atoms is well neglected and the dominant interaction comes from the electrostatic force. In this region, the standard perturbation theory is the most common and useful approach.
- (2) In the intermediate range, typically at $r_A + r_B \lesssim R \lesssim 10\text{\AA}$ (r_A or r_B is a measure of respective atomic radius), the charge overlap can not be neglected. In this region both the perturbation theory with exchange interaction, and the variational method appear reasonable.
- (3) In the short range, at $R \lesssim r_A + r_B$, the repulsive interaction due to charge overlap is important. The

diatomic system is treated in this case as a molecule, to which variational methods, e.g. SCF (Self-Consistent-Field) method, are usually applied.

Here we shall mainly discuss regions of (1) and (2), since as we will see later interatomic potentials roughly at $R \gtrsim 5\text{\AA}$ are treated in the present work.

Although bound states of some diatomic molecules have been studied in detail (see e.g. Hertzberg 1950), these discussions are mainly based on simple hypothetical electronic interactions such as the Lennard-Jones form

$$V(R) = C_{12}R^{-12} - C_6R^{-6} . \quad (3.1)$$

More realistic calculations including excited states have been developed recently, since Baylis (1969a,b) made the pioneering work on alkali-rare-gas pairs. Baylis presented a model potential to describe the whole range of R . After his work, considerable efforts have been made to refine the short-range potentials to explain many observations mainly for alkali-rare-gas pairs. These pairs have received much experimental interest as described in Chapter 1, and in addition, the theoretical treatment of the atoms can be simplified as follows:

- (i) Alkalies are treated at large R by the hydrogenic models, which are composed of a valence electron and a frozen core made of a nucleus plus closed shells.
- (ii) Rare gases have relatively large energy separation, so that we may neglect the electronic excitation for them.

Since alkaline-earth atoms have similar electronic structures to alkalis (two valence electrons plus closed shells), we can expect the methods which were originally applied to alkali-rare-gas pairs are applicable to the present problems, alkaline-earth (neutral or ion)-rare-gas pairs, with slight modifications.

In the following, we shall firstly review the perturbation method to treat long-range interactions for two cases, i.e. when the colliding atoms are identical (resonance interaction) or different (van der Waals interaction). Next we introduce two approximate methods to calculate repulsive interaction due to charge overlap, which are widely used to replace the laborious molecular treatment, e.g. ab initio SCF calculations. Such replacement may be valid when we treat only small charge overlap. Finally introduced is the method of Baylis (1969a,b).

3.2 Long-range interaction

When interatomic distance R is large and the charge overlap between atoms is well neglected, we can expand the interaction $V(R)$ in a Taylor series of R^{-1} . The result is, for neutral atoms (Margenau 1931)

$$\begin{aligned}
 V(R) = & \frac{e^2}{R^3} \sum_{ij} \left[x_i x_j + y_i y_j - 2z_i z_j \right] \\
 & + \frac{3}{2} \frac{e^2}{R^4} \sum_{ij} \left[r_i^2 z_j - z_i r_j^2 + (2x_i x_j + 2y_i y_j - 3z_i z_j)(z_i - z_j) \right] \\
 & + \frac{3}{4} \frac{e^2}{R^5} \sum_{ij} \left[r_i^2 r_j^2 - 5z_i^2 r_j^2 - 5r_i^2 z_j^2 - 15z_i^2 z_j^2 + 2(4z_i z_j - x_i x_j - y_i y_j)^2 \right] \\
 & + \dots , \tag{3.2}
 \end{aligned}$$

where e is the electronic charge and $\mathbf{r}_i = (x_i, y_i, z_i)$ and $\mathbf{r}_j = (x_j, y_j, z_j)$ denote the position of i -th electron of one atom and that of j -th electron of the other (the Z axis is taken along the R direction). The terms proportional to R^{-3} and R^{-4} denote the dipole-dipole and dipole-quadrupole energies, and the R^{-5} term denotes two parts, i.e. the interaction between two quadrupoles and that of dipole-octupole. The next step is to calculate the interaction energy $\Delta E(R)$ by the standard perturbation method by putting $V(R)$ as the perturbation on the diatomic system. In the following two subsections, we introduce the result of London (1930) who firstly made such a calculation.

3.2.1 Resonance interaction

This is characteristic of the case when the interacting atoms, one of which is excited, are identical. Since they are identical, they can exchange the excitation energy with one another. London's calculation (London 1930) shows that the first order perturbation term is not zero. The leading term is found to be

$$\Delta E = \frac{\delta e^2 \hbar f}{4\pi m \omega_0} \frac{1}{R^3}, \quad (3.3)$$

where m is the electron mass, ω_0 is the angular frequency of the transition, f is the oscillator strength and the numerical factor δ takes the value -2 (1) if the magnetic quantum number m_J of the excited state is 0 (± 1). According to the sum rule, the average of ΔE over all states of different m_J 's is zero.

In order to calculate the line broadening accurately it is necessary to take into consideration the degeneracy of levels and the dependence of the interaction on the angular variables. Foley (1946) calculated the mean square value over all m_J to get

$$\Delta E = \frac{\sqrt{3} e^2 \hbar f}{8\pi m \omega_0} \left(\frac{2J+1}{2J'+1} \right)^{1/2} \frac{1}{R^3}, \quad (3.4)$$

where J and J' denote the statistical weight of the upper and lower states of the transition respectively. Then we can readily calculate the impact broadening γ by (2.27) with the coefficient ΔC_3 defined by $\Delta E = \Delta C_3 R^{-3}$. Recent calculations of γ are reviewed by Hindmarsh and Farr (1972). They give 2γ as

$$2 \gamma = k_{JJ'} \left(\frac{2J+1}{2J'+1} \right)^{1/2} \frac{4\pi e^2 f}{m \omega_0} n, \quad (3.5)$$

where the numerical factor $k_{JJ'}$ depends on J and J' and the approximations made to take an average over all m .

It is easy to see how the resonance effect affects the radiation process. When an excited atom passes by an unexcited atom of the same kind, there must be a finite probability that the energy of the excitation will be transferred from the first to the second atom, without the intervention of radiation. This results in a reduction of the lifetime of the excited atom, and yields the corresponding broadening of the line.

3.2.2 Van der Waals interaction

When the colliding atoms are unlike (foreign-gas broadening), London's calculation (London 1930) shows that the first order perturbation energy is zero, but that there is a second-order term with the leading term for two atoms in the state k and ℓ .

$$\Delta E = -\frac{1}{R^6} \frac{3 e^4 \hbar^4}{2m^2} \sum_{\substack{k'=k \\ \ell'=\ell}} \frac{f_{kk'} f_{\ell\ell'}}{(E_{k'} - E_k)(E_{\ell'} - E_\ell)(E_{k'} + E_{\ell'} - E_k - E_\ell)}, \quad (3.6)$$

where one atom is in state $|k\rangle$, the other in state $|\ell\rangle$, $f_{kk'}$ and $f_{\ell\ell'}$ are the oscillator strengths of transitions $k \rightarrow k'$ for the first and $\ell \rightarrow \ell'$ for the second atom, and E_k and E_ℓ are the energies of the states of the two atoms. It must be noted that the calculation was done by neglecting the electron-exchange effect, by assuming that atoms are nondegenerate. Eq. (3.6) is usually negative and numerically much larger for the excited state than for the ground state, except for the highly-excited states.

This expression may be greatly simplified if the perturber has a much greater energy separation than the other (i.e. if it has a lower polarizability); this is the present case when perturber is rare gas. If $E_\ell (\ell')$ corresponds to rare gas, $|E_k - E_k| \ll |E_\ell - E_\ell|$, thus (3.6) may be approximated to

$$\begin{aligned} E &= -\frac{1}{R^6} \frac{3 e^4 \hbar^4}{2m^2} \sum_{\ell'} \frac{f_{\ell\ell'}}{(E_{\ell'} - E_\ell)^2} \cdot \sum_{k'} \frac{f_{kk'}}{E_{k'} - E_k} \\ &= -\frac{1}{R^6} \frac{3 e^2 \hbar^2}{2m} \alpha_B \sum_{k'} \frac{f_{kk'}}{E_{k'} - E_k}, \end{aligned} \quad (3.7)$$

where we have defined the static dipole polarizability of the perturber α_B as

$$\alpha_B = \frac{e^2 \hbar^2}{m} \sum_{\ell'} \frac{f_{\ell\ell'}^2}{(E_{\ell'} - E_{\ell})^2}. \quad (3.8)$$

If the active atom is hydrogenic, namely if it has single optical electron, (3.6) may be further approximated by (Dalgarno and Kingston 1960)

$$\Delta E = -R^{-6} e^2 \alpha_B \langle k | r^2 | k \rangle, \quad (3.9)$$

where r^2 is the square of the radius of the electron. If we use the Bates-Damgaard-type wavefunctions (Bates and Damgaard 1949) for $|k\rangle$, we find C_6 in $\Delta E = -C_6 R^6$ to be

$$C_6 = \frac{1}{2} e^2 \alpha_B a_0^2 n^{*2} \left\{ 5n^{*2} + 1 - 3\ell(\ell+1) \right\}, \quad (3.10)$$

where a_0 ($\equiv \hbar^2 / me^2$) is the Bohr radius, ℓ is the orbital-angular-momentum quantum number and n^* is the effective principal quantum number given by

$$n^* = \sqrt{\frac{R}{E}}, \quad (3.11)$$

where R and E are the Rydberg constant and the ionization energy. Mahan (1969) extended (3.9) to include angular dependence of the wavefunction for $|k\rangle$. The result is

$$C_6 = \frac{1}{2} e^2 \alpha_B \langle k | r^2 (1 + 3\cos^2\theta) | k \rangle \quad (3.12)$$

$$= \frac{1}{2} e^2 \alpha_B a_0^2 n^2 \left\{ 5n^2 + 1 - 3\ell(\ell+1) \right\} \frac{5\ell(\ell+1) - 3(m_\ell^2 + 1)}{(2\ell+3)(2\ell-1)} , \quad (3.13)$$

where θ is the angle between the vectors corresponding to r and R , and m_ℓ is the magnetic quantum number.

Eq. (3.6) is generally hard to calculate, since it requires a knowledge of every energy level and oscillator strength. Eqs. (3.10) and (3.13) are obtained by replacing the summation in (3.6) by some net values. To remove this difficulty, several treatments by the variational method have been proposed to evaluate C_6 for the collision of atoms in the ground S state. The three commonly used approximate formulae may be written in the form (Kramer et al 1970)

$$C_6 = \frac{3}{2} \alpha_A \alpha_B \frac{\bar{\omega}_A \bar{\omega}_B}{\bar{\omega}_A + \bar{\omega}_B} , \quad (3.14)$$

where α_A is the static dipole polarizability of the active atom, $\bar{\omega}_A$ is some average energy for transitions from the initial state of the active atom, and α_B and $\bar{\omega}_B$ are defined likewise for the perturber (in the following we drop the subscripts A and B).

- (1) In London (1930) approximation, two common choices for $\bar{\omega}$ are the ionization potential and resonance transition energy.
- (2) In Slater and Kirkwood (1931) approximation,

$$\bar{\omega} = (N/\alpha)^{1/2} , \quad (3.15)$$

where N is the number of the outermost electrons.

- (3) In Kirkwood (1932) - Müller (1936) approximation,

$$\bar{\omega} = \frac{2}{3} \langle r^2 \rangle / \alpha . \quad (3.16)$$

3.3 Short-range interaction

3.3.1 General remarks

In this section we treat the case when there is a charge overlap of colliding atom. In our region (roughly $5 \lesssim R \lesssim 10 \text{ \AA}$) the electrostatic interaction is still important, therefore to calculate the interaction we must consider both factors.

For the electrostatic interaction, the discussion in the preceding section is still available here, but it needs some slight modifications. As an example, the van der Waals interaction may be modified as follows. Koide (1976) introduced a damped dispersion interaction to include the charge-overlap effect such as

$$\Delta E = -\chi(R) C_6 R^{-6}, \quad (3.17)$$

where C_6 is the usual van der Waals coefficient and $\chi(R)$ is the damping factor satisfying

$$(R:\text{small}) \ 0 \leftarrow \chi(R) \rightarrow 1 (R:\text{large}). \quad (3.18)$$

By $\chi(R)$ we can compensate for the defect that the R^{-1} series expansion (3.2) is invalid at small R where the charge overlap can not be neglected.

The other factor, i.e. the repulsive interaction due to charge overlap is usually calculated by a variational method such as the SCF method. In such ab initio calculations, we usually construct antisymmetrized products of electron orbitals. The ground-state eigenfunction is then approximated usually by the normalized

product or linear combination of products which minimize the energy. Straightforward application of such calculations becomes prohibitively difficult when we treat complex atoms with several electrons.

However, in our case of small charge overlap, we can greatly simplify the problem by assuming the perturbers (rare gas) and core electrons of the active atom remain unperturbed. This assumption is valid for intermediate range of R , where the perturbations are much smaller than the excitation energies of rare gas and core electrons of active atom. For example, alkali-rare-gas pair is treated as a three body problem, namely a valence electron of alkali, its unperturbed (or frozen) core and a rare gas. Thus the repulsive interaction between these three bodies may be written as

$$v = v_{eA} + v_{eB} + v_{AB} , \quad (3.19)$$

where v_{eA} (v_{eB}) denotes the interaction between the valence electron and the alkali core (rare gas) and v_{AB} the interaction between alkali core and rare gas. When a rare gas approaches an alkali, it will firstly have a repulsive interaction with the valence electron (v_{eB}) and then with the alkali core (v_{AB}). Thus in the intermediate range of R , v_{eB} is important in the first place.

There are two common approximate calculations for v_{eB} called the Gombás' pseudopotential and Fermi potential. Since they only treat electron-rare gas collision, they are well adapted to the study of collision between highly-excited atom and rare gas, where the core of the excited atom plays only a negligible role.

3.3.2 Gombás' pseudopotential

The pseudopotential of Gombás (1967) is based on the Thomas-Fermi statistical model of the atom. Instead of treating electrons as indistinguishable fermions, it is convenient to think of them as Boltzmann, i.e. distinguishable, particles with an added pseudointeraction that causes to mimic fermions. The total state of an N -electron system may then be written as a simple product of N one-electron states $\alpha(1) \beta(2) \dots \gamma(N)$. Now the Pauli exclusion principle is satisfied simply by the condition that the states labeled by $\alpha, \beta, \dots, \gamma$ may be mutually orthogonal. Assume that the electrons labeled $1 \sim (N-1)$ occupy the $N-1$ lowest levels of the system. Because of the orthogonality condition, the N -th electron must occupy a state of some minimum, say $E_F - E_0$ above the ground state. Furthermore this state will be spatially correlated with the lowest $N-1$ states.

A pseudopotential that leads to a similar behavior is derived by treating the electron distribution at each point as part of a free-electron gas. The minimum energy E_F is then $\frac{1}{2} P_F^2 / m + V$, where P_F is the Fermi momentum, m is the electron mass, and V is the actual potential energy of the system. Since the electron density ρ is related to P_F in that the phase-space volume of an electron state is $(2\pi\hbar)^3$ per spin orientation, we obtain

$$\rho = 2 \cdot \left(\frac{4}{3} \pi P_F^3 \right) / (2\pi\hbar)^3. \quad (3.20)$$

Thus we get for the minimum energy of the N -th electron

$$E_F = \left[(3\pi^2 \hbar^3 \rho)^{2/3} / 2m \right] + V. \quad (3.21)$$

In other words, in the free-electron model, the N -th electron has a minimum energy at $1r$ of

$$G(1r) = \left[3\pi^2 \hbar^3 \rho(1r) \right]^{2/3} / 2m. \quad (3.22)$$

The repulsive interaction between an electron and rare gas is obtained by putting $\rho(1r)$ as the density distribution of the rare gas.

3.3.3 Fermi potential

We briefly review the approach of Smirnov (1967) and Roueff (1970). We assume that the valence electron of alkali is slightly bound to the core (this is the case when the valence electron is highly excited). Let $E_A = -\frac{1}{2} \beta^2$ be the electron binding energy, \mathbf{R} and \mathbf{R}' the position vector of the electron and rare gas relative to the alkali core and θ' the angle between vectors \mathbf{R} and $\mathbf{R} - \mathbf{R}' (\equiv \mathbf{R}')$ (see Fig. 3.1).

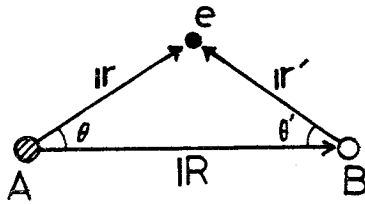


Fig.3.1 The three-body model of an alkali core (A), a rare gas (B) and an electron (e).

We assume $R, r \gg r'$, thus

$$r \approx R - r' \cos \theta' . \quad (3.23)$$

If we write the wavefunctions of the electron in the absence and presence of the rare gas as φ and ψ respectively, they satisfy the Schrödinger equations

$$H_A \varphi = E_A \varphi \text{ and } (H_A + v) \psi = E \psi,$$

from which we get the interaction $V(R)$ by subtraction and integration in the whole space

$$V(R) = E - E_A = \int \varphi^* v \psi d\tau / \int \varphi^* \psi d\tau, \quad (3.24)$$

where v is the interaction operator. By using the exponential nature of the asymptotic form for $\varphi(r) \simeq \beta r^\alpha \exp[-\beta r]$, we get with (3.23)

$$\varphi(r) \simeq \varphi(R) \exp[\beta r' \cos \theta] [1 - (r r' / R) \cos \theta + O(R^{-2})], \quad (3.25)$$

and similarly

$$\psi(r) \simeq \varphi(R) \psi(r') [1 - (r r' / R) \cos \theta + O(R^{-2})]. \quad (3.26)$$

So (3.24) can be expressed as follows:

$$V(R) \simeq \varphi^2(R) \int \exp[\beta r' \cos \theta] v \psi(r') [1 - (2r r' / R) \cos \theta] dr' \quad (3.27)$$

Next we expand $\exp[\beta r' \cos \theta]$ and $\psi(r')$ in Legendre polynomials and integrate over angles, the result is

$$V(R) = -\frac{2\pi\hbar^2}{m\beta} \varphi^2(R) \sum_{l=0}^{\infty} (2l+1) \sin \delta_e. \quad (3.28)$$

The phase shift δ_e can be calculated by the modified effective range theory of O'Malley et al (1961), then the final result is with a correction for the last term (Lewis 1980)

$$V(R) = \frac{2\pi\hbar^2}{m} L \varphi^2(R), \quad (3.29)$$

where L is the scattering length given by

$$L = \left(\frac{1}{L_0} - \frac{\pi \alpha_B \beta}{3L_0^2} - \frac{4\alpha_B \beta^2}{3L_0} l_n \frac{\beta \sqrt{\alpha_B}}{4} \right)^{-1} - \frac{\pi \alpha_B \beta}{5}. \quad (3.30)$$

Here α_B is the rare-gas polarizability, and L_0 is the scattering length for zero kinetic energy of the electron. Eq. (3.29) is called the Fermi potential, since Fermi (1934) first derived this type of potential with $L = L_0$.

3.4 Model potential of Baylis

As previously described (see Fig. 3.1), this model consists of a frozen core, it's valence electron, and a rare gas. In this case, we do not press the restriction $R, r \gg r'$. Therefore the interaction includes many contributions, namely the electrostatic interaction between them and repulsion such as (3.19). Baylis (1969a, b) writes the total Hamiltonian as

$$H = H_A + H_B + T + V , \quad (3.31)$$

where H_A (H_B) is the Hamiltonian of the isolated alkali (rare gas), T is the kinetic energy of the relative motion, and V is the interaction between them. As described in 3.3.1 in ab initio calculations of H , we usually construct antisymmetrized products of one-electron orbitals to satisfy the Pauli exclusion principle. Considerable simplification is effected by using nonorthogonal wavefunctions together with pseudopotentials of the Gombás' type. They replace the antisymmetrization procedure of the total wavefunctions of the system. This is the first major approximation. Thus we put

$$V(\mathbf{r}, \mathbf{R}) = F(\mathbf{r}, \mathbf{R}) + G(\mathbf{r}, \mathbf{R}) + W(\mathbf{R}) , \quad (3.32)$$

where G and W are the Gombás' pseudopotentials due to electron-

rare-gas and alkali-core-rare-gas interactions respectively, and F is the electrostatic interaction. Since we treat adiabatic potentials, we can omit from (3.31) T due to nuclear motion, and we can put $H_B = 0$ since the excitation of rare gas is well neglected here as mentioned previously. Thus Baylis writes (3.31) as

$$H = H_A(\mathbf{R}) + V(\mathbf{R}, \mathbf{R}), \quad (3.33)$$

Then he diagonalize (3.33) in some suitable basis set. Here he makes the second major approximation, i.e. for this basis set he uses a finite number of isolated alkali's atomic state. This is found to be equivalent to applying the variational method to the problem, where the trial wavefunction is chosen as

$$\psi = \sum_i c_i \varphi_i. \quad (3.34)$$

Here φ_i is the eigenfunction of the electron which satisfies the equation

$$H_A \varphi_i = E_i \varphi_i, \quad (3.35)$$

where E_i is the energy of the atomic state given by experimental results (Moore 1971). The minimization condition of $\langle \psi | H | \psi \rangle / \langle \psi | \psi \rangle$ is reduced to solving the secular equation

$$\det \left| V_{ik} + [E_i - V(R)] \delta_{ik} \right| = 0, \quad (3.36)$$

where

$$V_{ik} \equiv \langle \varphi_i | V(\mathbf{R}, \mathbf{R}) | \varphi_k \rangle. \quad (3.37)$$

The third major approximation is to represent the rare gas atom only as a polarizable dipole with polarizability α_B (given by Dalgarno and Kingston 1961) and radius r_0 ($\ll R$). Baylis writes F as

$$F(|r|, |R|) = -\frac{1}{2} \alpha_B |E|^2 (|r|, |R|)$$

$$= \begin{cases} -\frac{1}{2} \alpha_B e^2 \left[\frac{|R|}{R^3} - \frac{|r'|}{r'^3} \right]^2 & \text{for } r' \geq r_0 \end{cases} \quad (3.38)$$

$$= \begin{cases} -\frac{1}{2} \alpha_B e^2 \left[\frac{1}{R^4} + \frac{1}{r_0^4} \right] & \text{for } r' < r_0 \end{cases} \quad (3.39)$$

where $|E|$ is the electric field due to valence electron and to the alkali core (assumed to have a charge $+e$). The attractive potential $F(|r|, |R|)$ dominates at large R and takes the van der Waals form (3.12) asymptotically:

$$F(|r|, |R|) \underset{R \rightarrow \infty}{\sim} -\frac{1}{2} \alpha_B e^2 r^2 (1 + 3 \cos^2 \theta) R^{-6}, \quad (3.40)$$

where θ is the angle between $|r|$ and $|R|$.

G is given by (3.22), i.e.

$$G(|r|, |R|) = \frac{\hbar^2}{2m} \left[3\pi^2 \rho_B(r') \right]^{2/3}, \quad (3.41)$$

where ρ_B' is the charge density of rare gas. Note that the total energy arising from the pseudointeraction of an electron distribution with itself is

$$\int d^3 |r| \int_0^P F(r) d\rho \frac{\hbar^2}{2m} (3\pi^2 \rho)^{2/3} = \frac{3\hbar^2}{10m} (3\pi^2)^{2/3} \int d^3 |r| \rho^{5/3} (|r|). \quad (3.42)$$

If we write the total charge density as $\rho(\mathbf{r}) = \rho_A(\mathbf{r}) + \rho_B(\mathbf{r}')$, $W(R)$ is just the pseudointeraction energy of ρ less than that of ρ_A and ρ_B , thus

$$W(R) = \frac{3\hbar^2}{10m} (3\pi^2)^{2/3} \int d^3\mathbf{r} \left\{ [\rho_A(\mathbf{r}) + \rho_B(\mathbf{r}')]^{5/3} - \rho_A^{5/3}(\mathbf{r}) - \rho_B^{5/3}(\mathbf{r}') \right\}$$

$$\simeq \frac{\hbar^2}{2m} (3\pi^2)^{2/3} \int d^3\mathbf{r} \rho_A(\mathbf{r}) \rho_B^{2/3}(\mathbf{r}') \quad \text{for } \rho_A \ll \rho_B. \quad (3.43)$$

$\rho_{A,B}$ is calculated by the simplified SCF method of Gombás (1967) and expressed as

$$\rho(x) = (1/4\pi) \sum_s \mathcal{G}(s) x^{\alpha(s)} \exp[-2\beta(s)x], \quad (3.44)$$

where the sum extends over all the shells of the rare gas and alkali-core ion (in practice Baylis calculates the outermost shells), and α , β and \mathcal{G} are variationally determined by Gombás (1967).

$V(|\mathbf{r}|, |\mathbf{R}|)$ is shown to be a function only of the magnitudes r and R , and of $\cos\theta$, therefore we can expand V in Legendre polynomials as

$$V(|\mathbf{r}|, |\mathbf{R}|) = \sum_{L=0}^{\infty} V^L(r, R) P_L(\cos\theta), \quad (3.45)$$

where

$$V^L(r, R) = F^L(r, R) + G^L(r, R) + W(R) \delta_{L0}. \quad (3.46)$$

By this expansion we can separate the integration V_{ik} (3.37) into the angular and radial part. Baylis further makes some minor approximations to reduce F , G , and W into calculable forms, which is not repeated here.

This procedure includes one adjustable parameter r_0 . This is determined so that calculated ground-state potentials have the same well depth and position as those experimentally derived (Buck and Pauly 1968). It is the reason why this is called the semiempirical pseudopotential method. Pascale and Vandeplanque (1974) recalculated this by extending the set of basis functions ϕ_i .

Chapter 4. Shock-tube experiment

The present shock-tube experiment consists of absorption measurements for Ca-Ar and Ba-Ar pairs, and an emission measurement for Ca^+ -Ar pair. There is a slight difference in the apparatus between these two cases. First we briefly review the principle of shock-tube, then give the detail of the present experimental setup in the following sections.

4.1 Principle of shock tube

Diaphragm-type (or conventional) shock tubes have been widely used for these 30 years in the study of the shock-wave structure, supersonic beams, high-temperature gases, and weakly ionized plasmas, because they can easily produce high temperatures up to $1 \times 10^4 \text{ K}$, with a relatively large volume in LTE (local thermodynamic equilibrium). A typical application is the study on molecular reactions, such as the vibrational and rotational excitations (see e.g. Kuratani and Tsuchiya 1968). There is another type called electromagnetic shock tube which produces very high temperatures by the use of the electrical discharge, however in the following we limit the topic to the diaphragm type used in this study.

A shock tube consists of a high-pressure region (typically up to 10 atmospheres) called the driver section and a low-pressure region (typically up to 50 Torr) called the test section separated by a thin diaphragm (see Fig. 4.1 (a)). If the diaphragm bursts, a compression wave which rapidly steepens to form a shock wave moves into

the test section, and simultaneously an expansion wave moves into the driver section. Fig. 4.1 (b) is the conventional method called the x-t diagram to show the flow, where the full heavy line denotes the surface of shock wave called shock front, the dashed line the contact surface to separate the two gases, and the chain line the expansion wave. The region is divided into five sections, i.e. ① test section, ② incident- or primary-shock region, ③ low temperature region due to the propagation of expansion wave, ④ driver section at the initial pressure, and ⑤ reflected-shock region. To see the temperature and pressure at certain time t_0 , we cut (b) at $t = t_0$ to get (c) and (d).

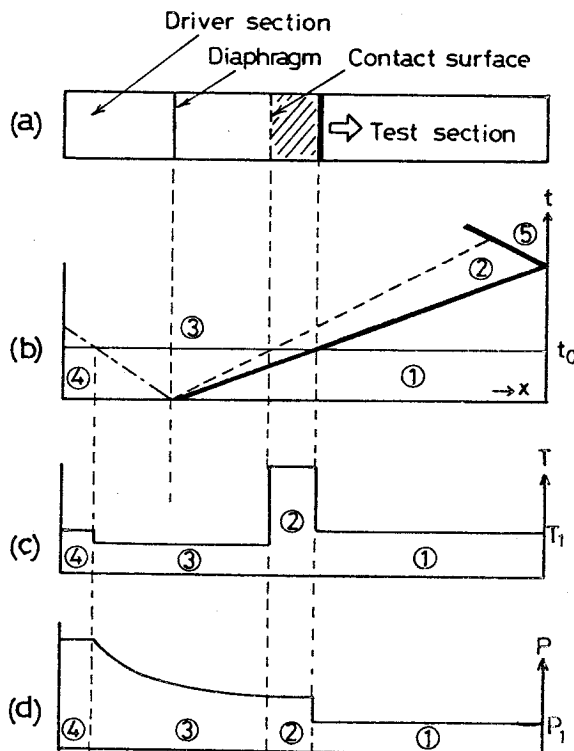


Fig.4.1
Principle of shock tube.
(a):Schematic drawing of a diaphragm-type shock-tube.
(b):x-t diagram showing the progress of shock (heavy solid line) and expansion (chain line) waves following the diaphragm burst (dashed line shows the contact surface).
(c) and (d):temperature and pressure distribution at a time $t = t_0$, respectively.

The region (2) behind the shock front is heated to high temperature by adiabatic compression. An advantage of shock-tube is that the temperature T_2 , the pressure P_2 and the particle density n_2 in this region are easily calculated as follows (see e.g. Kuratani and Tsuchiya 1968)

$$P_2 = \left\{ 1 + \frac{2\gamma_1}{\gamma_1 + 1} (M^2 - 1) \right\} P_1 , \quad (4.1)$$

$$n_2 = \left\{ \frac{(\gamma_1 + 1) M^2}{2 + (\gamma_1 + 1) M^2} \right\} n_1 , \quad (4.2)$$

$$T_2 = \frac{[2 + (\gamma_1 - 1) M^2][2\gamma_1 M^2 - (\gamma_1 - 1)]}{(\gamma_1 + 1)^2 M^2} T_1 , \quad (4.3)$$

where P_1 , n_1 and T_1 denote the initial values of the test section, γ_1 is the heat capacity ratio of the test gas, and M is the Mach number defined as the ratio of the shock velocity U to the sound speed a_1 of the test section.

$$M = U / a_1 \quad (4.4)$$

with

$$a_1 = \sqrt{\gamma_1 P_1 / n_1} . \quad (4.5)$$

For example to know T_2 we substitute measured values of T_1 , U , P_1 , n_1 and known constant γ_1 into (4.3), (4.4) and (4.5). We can similarly calculate the corresponding values for the reflected-shock region (5). Eqs. (4.1) through (4.3) are called the Rankine-Hugoniot relation.

4.2 Absorption measurement for Ca-Ar and Ba-Ar pairs

4.2.1 Introduction

Though there are some previous measurements on alkaline-earth (neutral)-rare-gas systems, they are mostly limited to low temperature regions below 1000K (e.g. Penkin and Shabanova 1968, Chen and Lonseth 1971, Smith 1972 and Bowman and Lewis 1978), and high temperature measurements are quite scarce. To the author's knowledge, there is no report on the broadening of neutral Ca (or Ba) resonance lines at high temperatures caused by rare gases (except for Ca - He, Driver and Snider 1976). Here we study the broadening of these lines by Ar using a shock tube at \sim 4000K, and compare with data at low temperatures.

Ca (or Ba) vapors are heated in Ar buffer gas in the primary shock region (② in Fig. 4.1). Since this region passes an observation window in about 200μ sec., the scanning of the profile must be finished within this time. For this purpose we use a photo-diode array called image sensor. The detail of the experiment is given in the next section, followed by results and discussions.

4.2.2 Experimental apparatus

(a) Shock tube

Fig. 4.2 shows the shock tube along with the evacuating system. The shock tube consists of a copper tube of inner diameter 4.7cm and length 3.4m, and a brass damp tank. The copper tube is separated by a thin aluminium diaphragm into two sections: the driver section which contains hydrogen gas at about 10 atmospherers, and the test section which contains Ar at about 10 Torr with Ca (or Ba). The method to evaporate a metal sample is discussed in detail by Kosasa et al (1976). We generate a shock wave by bursting the diaphragm with needle's attack and measure the shock velocity by two platinum heat probes in the test section. The glass tube serves as the observation window.

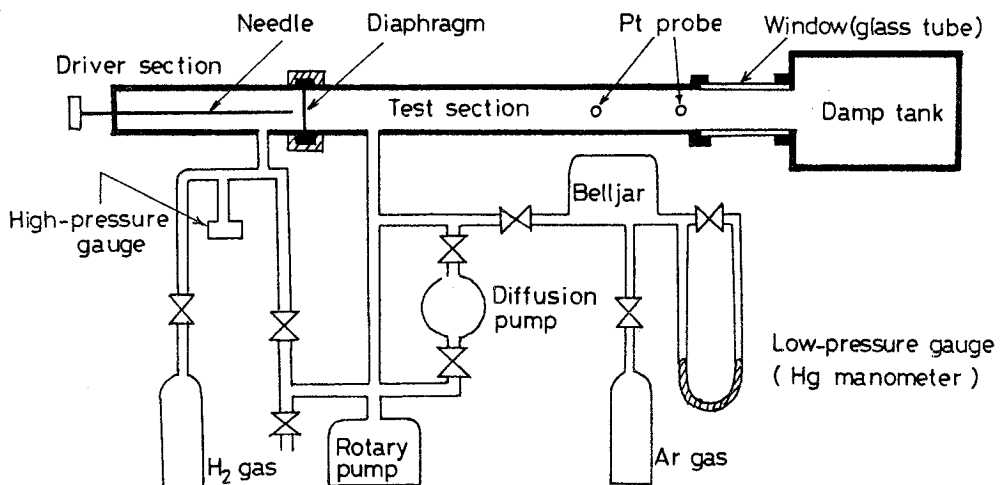


Fig.4.2 Shock tube and the gas-handling system.

(b) Optical arrangement

Fig. 4.3 shows the optical arrangement of the experiment. G is the cross section of the glass-tube window. A continuum-light source FL (Xe-flash lamp) is triggered synchronously with the passage of the shock-heated region through G. The transmitted light is focused on the entrance slit of S_1 about $200 \mu\text{m}$ in width. S_1 is an Ebert-type spectrometer with a focal length 50cm. Using a 1200 grooves/mm grating in the first order, it has a reciprocal linear dispersion of 16.6 \AA/mm in the measured spectral range. The exit slit is removed and the image at this position is re-focused on the image sensor IS by a lense L_3 with a magnifying power of unity. For IS we used MEL512KV (Matsushita Electronics Corp.), which has a photo-diode array of 512 elements (the unit element has the area of $28 \times 464 \mu\text{m}^2$). Details of the signal processing is described by Harima et al (1980).

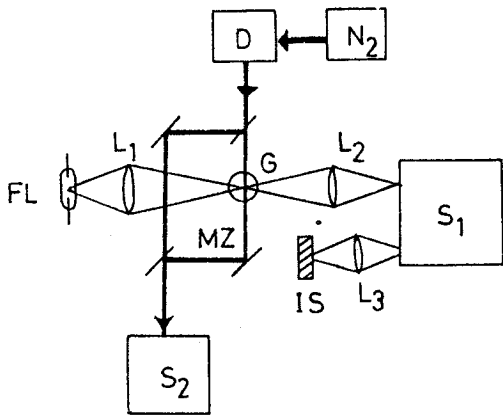


Fig.4.3
Schematic diagram of the optical measurement.
G:glass tube.
FL:Xe-flash lamp.
L:lense.
 S_1 :50 cm spectrometer.
IS:image sensor.
D:dye laser.
MZ:Mach-Zehnder interferometer.
 S_2 :3.4 m spectrograph.

To know the ground-state density of sample vapors we make the hook measurement (Marlow 1967). An N_2 laser-excited dye laser D is triggered simultaneously with the flash lamp FL. The light passes a Mach-Zehnder interferometer MZ whose one arm goes through G. The interference-fringe pattern was observed by an Ebert-Fastie-type spectrograph S_2 of focal length 3.4m. Using a 1200 grooves/mm grating in the first order, it has a dispersion of 2.5 \AA/mm .

4.2.3 Results

Fig.4.4 shows the typical transmission spectra of

- (a) the Ca resonance line at 4227 \AA ($4s^2 \text{ }^1S_0 - 4s4p \text{ }^1P_1$), and
- (b) the Ba resonance line at 5535 \AA ($6s^2 \text{ }^1S_0 - 6s6p \text{ }^1P_1$), where the transition at 5519 \AA between triplet states ($6s6p \text{ }^3P_1 - 6s6d \text{ }^3D_2$) also appears.

The experimental conditions are as follows:

for (a) $T = 4.6 \times 10^3 \text{ K}$, $[\text{Ar}] = 1.5 \times 10^{18} \text{ cm}^{-3}$ and $[\text{Ca}] = 2.5 \times 10^{15} \text{ cm}^{-3}$,
for (b) $T = 4.0 \times 10^3 \text{ K}$, $[\text{Ar}] = 1.4 \times 10^{18} \text{ cm}^{-3}$ and $[\text{Ba}] = 5.4 \times 10^{14} \text{ cm}^{-3}$,

where T denotes the temperature of the shock-heated region, and $[\text{M}]$ ($\text{M} = \text{Ar, Ca or Ba}$) denotes the density of the respective elements.

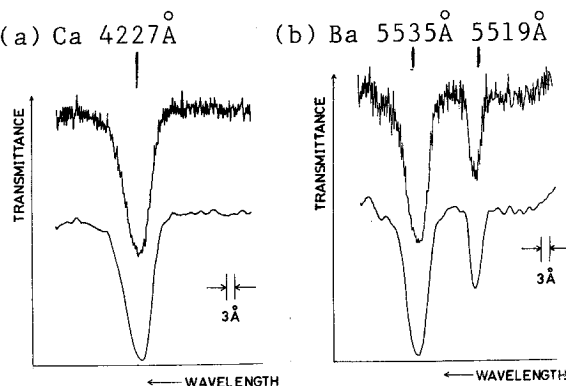


Fig.4.4

Typical transmission spectra of Ca and Ba broadened by Ar. The lower spectra were obtained by smoothing the upper raw spectra.

We can see from Fig. 4.4 that

(1) both resonance lines are nearly symmetric, but have slight tails to the red side.

We have also found by changing $[Ca]$ or $[Ba]$ that

(2) the total absorption W defined by

$$W = \int_0^{\infty} (I_0 - I) / I_0 d\lambda, \quad (4.6)$$

where I_0 and I are the background- and the transmitted-light intensities respectively, has a density dependence approximately

$$W \propto [Ca]^{1/2} \quad (\text{or } [Ba]^{1/2}). \quad (4.7)$$

Before discussing these observations, we consider the effect of the apparatus function (AF) on the profile. If a spectrometer has slit widths x_1 and x_2 for the entrance and the exit slit, and a reciprocal linear dispersion ϕ , its AF may be estimated by a trapezoid whose upper and lower sides are given respectively by $|x_1 - x_2|\phi$ and $(x_1 + x_2)\phi$ (see Fig. 4.5).

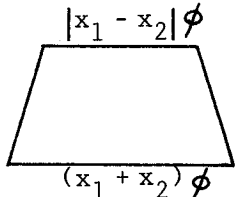


Fig. 4.5 Apparatus function.

x_1 : entrance-slit width.

x_2 : exit-slit width.

ϕ : reciprocal linear dispersion.

In this experiment we can put $x_1 = 200 \mu\text{m}$, $x_2 = 28 \mu\text{m}$ (i.e. the width of the unit of the photo-diode array), and $\phi = 16.6 \text{A/mm}^2$, therefore the present AF is given by a trapezoid whose mean width is $\sim 3 \text{\AA}$. Since the observed spectra have the same order of width, it is well estimated that the spectra are severely distorted by AF.

Thus to discuss the profile characteristics, such as (1), in a straightforward manner we must first remove AF from the observed profile by deconvolution. However it is very difficult in this case, because in the first place we can not determine AF accurately and secondly such a deconvoluted profile is estimated to have many spurious oscillations since the raw data has low S/N ratio due to the thermal noise from the image sensor (see Fig. 4.4). Therefore in the following we discuss the total absorption W . This quantity is not sensitive to such a noise and in addition, as shown below, is not affected by the distortion of the profile due to AF.

If we take AF into account, the integrand of W in (4.6) is given as a convolution of $[I(\lambda) - I_0(\lambda)] / I(\lambda)$ and $K(\lambda')$ (the apparatus function), thus W is written as

$$W = \int_0^{\infty} \left\{ \int_{-\infty}^{\infty} K(\lambda - \lambda_1) [I(\lambda_1) - I_0(\lambda_1)] / I(\lambda_1) d\lambda_1 \right\} d\lambda.$$

DePrima and Penner (1955) have shown that this reduces exactly to (4.6) when $K(\lambda')$ and $[I(\lambda) - I_0(\lambda)] / I(\lambda)$ differ from zero for only a limited range of λ' and λ , and when the range of λ_1 is large enough to include all contributions to W .

4.2.4 Discussions

(a) Lorentzian width

The observed relation (4.7) may be explained as follows. We firstly assume the absorption coefficient $k(\Delta\omega)$ is given by the Lorentzian form (2.20) of the impact limit, i.e.

$$k(\Delta\omega) = \left\{ \frac{2\pi^2 e^2 [M] f}{mc} \right\} \frac{\gamma_L / \pi}{(\Delta\omega - \beta)^2 + \gamma_L^2}, \quad (4.8)$$

where e and m are respectively the electron mass and charge, c is the light speed, f is the oscillator strength, $[M]$ ($M = \text{Ca or Ba}$) is the metal-vapor density, and β and γ_L are the shift and width respectively. The multiplying factor in $\{ \}$ has been introduced so that $k(\Delta\omega)$ satisfies the well-known relation (Mitchell and Zemansky 1971) for the total integrated absorption coefficient

$$\int_0^\infty k(\Delta\omega) d\omega = \frac{2\pi^2 e^2 [M] f}{mc}. \quad (4.9)$$

The transmitted-light intensity $I(\Delta\omega)$ is related to the background intensity I_0 (assumed here to have no $\Delta\omega$ dependence) as

$$I(\Delta\omega) = I_0 \exp [-k(\Delta\omega) \ell], \quad (4.10)$$

where ℓ is the absorption length (in this experiment $\ell = 4.7 \text{ cm}$, i.e. the diameter of the shock-tube). Thus the total absorption W is

$$W = \int_{-\infty}^{\infty} (I - I_0) / I_0 d\Delta\omega$$

$$= \int_{-\infty}^{\infty} \left\{ 1 - \exp \left[-k(\Delta\omega) \ell \right] \right\} d\Delta\omega . \quad (4.11)$$

By substituting (4.8) and neglecting β and γ_L , we get

$$W = 2\sqrt{\pi} \cdot \left(\frac{2\pi e^2 [M] f \ell \gamma_L}{mc} \right)^{1/2} \propto [M]^{1/2} \quad (4.12)$$

if γ_L has not strong dependence on $[M]$. Thus (4.7) can be derived by assuming $\Delta\omega \gg \beta, \gamma_L$, i.e. that $k(\Delta\omega)$ is determined by the wing region of the Lorentzian form (4.8). If we define W in wavelength unit, we multiply (4.12) by $\lambda_0^2 / (2\pi c)$, where λ_0 is the resonance-line wavelength, so we get

$$W = \int_{-\infty}^{\infty} (I - I_0) / I_0 d\lambda \quad (4.13)$$

$$= \lambda_0^2 (2r_e [M] f \ell \gamma_L / c)^{1/2} , \quad (4.14)$$

where $r_e (= e^2 / mc^2)$ is the classical electron radius.

The value $[M] f \ell$ can be obtained by the hook measurement as (Marlow 1967)

$$[M] f \ell = \frac{\pi K \Delta^2}{r_e \lambda_0^3} , \quad (4.15)$$

where K and Δ are respectively the interference-fringe order and the hook separation. From (4.14) and (4.15) we get

$$2\gamma_L = \frac{c W^2}{\pi K \lambda_0 \Delta^2} \text{ (rad.sec.}^{-1}\text{)} . \quad (4.16)$$

This method to deduce γ_L from simultaneous measurements of W and Δ is called the Penkin's total-absorption method (Marlow 1967).

In addition to the width γ_F (the foreign-gas broadening), there are in general other mechanisms which contribute to the Lorentzian width γ_L , such as natural broadening (γ_N), resonance (γ_R) and Stark broadening (γ_s), so that

$$\gamma_L = \gamma_N + \gamma_F + \gamma_R + \gamma_s . \quad (4.17)$$

γ_s may be well neglected in the present experiment, since there are not many charged particles (ion and electron). γ_N is easily calculated by recent measurements of f value (e.g. Miles and Wiese 1969). γ_R may be calculated by the preceding formula (3.5). Thus we can deduce γ_F by subtracting these values from γ_L . Table 4.1 shows typical results.

Table 4.1 Typical results.

	T	Ar	[M]	W	γ	γ_R	γ_N	γ_F
unit	10^3 K	10^{18} cm $^{-3}$	10^{14} cm $^{-3}$	10^{-8} cm	10^9 radian \cdot sec $^{-1}$			
Ca(4227Å)	4.6	1.2	36	8.8	8.7	2.5	0.2	6.0
Ba(5535Å)	4.1	1.6	1.4	2.7	7.7	0.1	0.1	7.5

(b) Optical cross section and van der Waals coefficient

If we assume γ_F is determined by the van der Waals interaction $\Delta V(R) = -\Delta C_6/R^6$ between calcium (or barium) and argon, γ_F and the optical cross section α_r may be related to ΔC_6 from (2.21) and (2.29) as

$$\gamma_F = 4.08 \left(\frac{\Delta C_6}{h} \right)^{2/5} \bar{v}^{3/5} [\text{Ar}] , \quad (4.18)$$

$$\alpha_r = \frac{\gamma_F}{[\text{Ar}] \bar{v}} = 4.08 \left(\frac{\Delta C_6}{h} \right)^{2/5} \bar{v}^{-2/5} . \quad (4.19)$$

Since the present shock tube has a high reproducibility of T and $[\text{Ar}]$, we repeated the measurements in the following conditions about 10 times to obtain the mean value of γ_F , and from the result we calculated ΔC_6 and α_r :

for Ca $T = 4.6(\pm 0.2) \times 10^3 \text{ K}$, $[\text{Ar}] = 1.4(\pm 0.07) \times 10^{18} \text{ cm}^{-3}$,

for Ba $T = 4.1(\pm 0.2) \times 10^3 \text{ K}$, $[\text{Ar}] = 1.6(\pm 0.08) \times 10^{18} \text{ cm}^{-3}$.

Table 4.2 shows the obtained values of ΔC_6 coefficients along with the low-temperature data of Penkin and Shabanova (1968). They also calculated the values in () by using the relation (3.10). We find the present result agrees well with previous experiments but is much smaller than the calculations in (). This is probably due to the erroneous use of (3.10), since it is strictly applicable only to the hydrogen-like atoms. Table 4.3 shows the deduced optical cross section. We can not compare the present result directly with the previous data, since the temperature is quite different.

However if we calculate α_r at the present high temperatures using the above ΔC_6 values of Penkin et al, the result (*) shows a good agreement with ours. Thus to conclude, the observed foreign-gas broadening is well understood by the van der Waals force between calcium (or barium) and argon, and the coefficient agrees well with previous measurements at low temperatures.

Table 4.2 ΔC_6 force constant ($10^{-58} \text{ erg} \cdot \text{cm}^6$).

	Penkin et al (1968)	This work
Ca (4227 \AA)	1.28 (1.83)	1.1
Ba (5535 \AA)	1.42 (2.16)	1.4

Table 4.3 Optical cross section α_r (10^{-16} cm^2).

	Penkin et al (1968)	This work	*
Ca (4227 \AA)	179 (at 850K)	118 ± 19 (at 4600K)	128
Ba (5535 \AA)	200 (at 940K)	148 ± 18 (at 4100K)	149

4.3 Emission measurement for Ca^+ -Ar pair

4.3.1 Introduction

As described in Chapter 1, many broadening experiments have been performed on alkali-rare-gas pairs since they are experimentally convenient and the hydrogen-like structure of alkalis are amenable to theoretical treatments. The isoelectronic singly-ionized alkaline-earth elements have received much less attention although they are important for an understanding of stellar spectra in which their lines are often the most prominent absorption features.

In the neutral-neutral collisions, the leading term of the long-range force is the van der Waals interaction which varies as R^{-6} , whereas in the ion-neutral collision it is the polarization force which varies as R^{-4} . However, it is the difference potential between the upper and the lower states of the transition that practically affects the broadening. So the view exists that the difference between the polarization force and the van der Waals force might not be appreciable (Bottcher et al 1975, Giusti-Suzor and Roueff 1975). On the other hand, the electrical charge on the ion makes the atomic radius of ions smaller than that of the corresponding neutral alkali metal atom, which may cause the reduction of the optical cross section.

In this experiment we study the Ca^+ resonance line doublet ($4s\ ^2\text{S}_{1/2} - 4p\ ^2\text{P}_{1/2,3/2}$) at 3968 and 3933\AA broadened by Ar. This pair was investigated before at low temperatures by Bowman and

Lewis (1978) and Giles and Lewis (1981), and only for the 3968\AA line at high temperatures by Holmes et al (1969) and Baur and Cooper (1977). Although we use almost the same shock tube as the previous study, some minor changes are made to observe the spectra in higher-temperature atmosphere. For example, a reflector is placed 5mm downstream from the observation window and spectral lines are observed from the reflected-shock region (namely ⑤ in Fig. 4.1). Next we outline the experimental setup and the method of analysis, and give results and discussions in the following sections.

4.3.2 Experimental setup

Fig. 4.6 shows the block diagram of the measuring apparatus. The apparatus to make the hook measurement (N_2 -laser excited dye laser, Mach-Zehnder interferometer, and 3.4m Ebert-Fastie spectrograph) is the same as the previous study. A greatly different point is that the spectral profile was measured by a rapid-scanning spectrometer with a synchronized rotating mirror (for details, see Urano et al 1971). The previous method (image sensor) was not feasible for this experiment, because our image sensor has low sensitivity in the relevant spectral region, and in addition its resolution is not high enough for this study. The spectrometer with the rotating mirror has a focal length 50cm, and a reciprocal linear dispersion of $16.6\text{\AA}/\text{mm}$ with a 1200 grooves/mm grating in the first order. The output signal from the spectrometer is recorded in a wave memory (NF, type WM-852) and then displayed on an XY-recorder and/or punched on a paper tape. The punched data are processed by a computer. Fig. 4.7 shows an example of the measured profile.

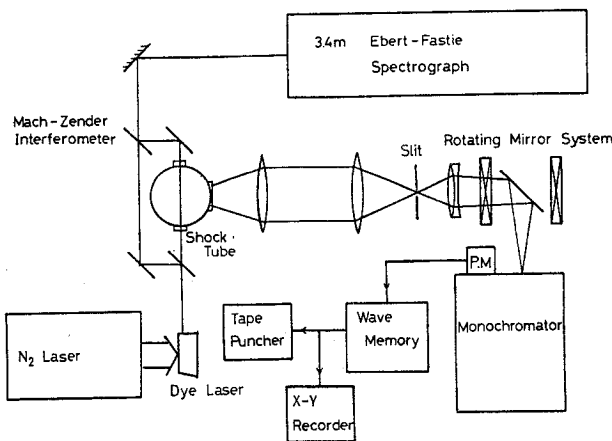


Fig.4.6 Block diagram of the meaning apparatus.

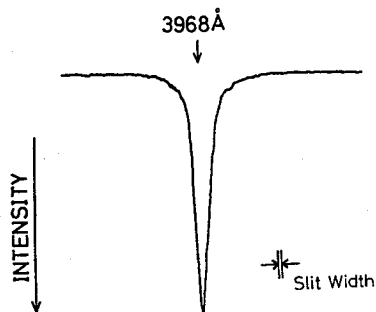


Fig.4.7 Measured profile of Ca^+ resonance line at 3968\AA .

Temperature of argon gas: 7960K.

Argon density: $[\text{Ar}] = 4.77 \times 10^{18} \text{ cm}^{-3}$.

Optical thickness of emitting gas: $\log \tau(0) = 3.1$.

Scanning speed of wavelength: $0.8\text{\AA}/\mu\text{s.}$

Slit width of spectrometer: 0.4\AA .

4.3.3 Method of analysis

A new method of measuring the small width of a collisionally broadened line using a low-resolution spectrometer has been developed. This method takes the advantage of the self absorption of the emitting layer.

If the optical thickness, i.e. the product of the absorption coefficient and the absorption length, of the emitting layer is large, the measured profile may be quite different from the true profile. Baur and Cooper (1977) considered this problem in the case when the optical thickness at the line center is $\mathcal{T}(0) \lesssim 1$. In the present case we treat $\mathcal{T}(0)$ two to three orders of magnitude larger than that. This is because we had to prepare dense ($10^{13} \sim 10^{14} \text{ cm}^{-3}$ in the ground state density) calcium vapor, to make the light intensity large enough for the small aperture of our spectrometer.

We firstly assume that the true line profile $I_t(\Delta\omega)$ is given by a Voigt function

$$I_t(\Delta\omega) = (a/\pi) \int_{-\infty}^{\infty} \exp(-y^2) / [a^2 + (\Delta\omega - y)^2] dy, \quad (4.20)$$

where a is given by

$$a = \sqrt{\ln 2} \gamma_L / \gamma_D. \quad (4.21)$$

$\gamma_{L(D)}$ denotes the Lorentzian (Doppler) width of the line in HWHM. We can easily show that the measured profile $I_m(\Delta\omega)$ is given by the optical thickness $\mathcal{T}(\Delta\omega)$ as

$$I_m(\Delta\omega) = \frac{1 - \exp[-\mathcal{T}(\Delta\omega)]}{\mathcal{T}(\Delta\omega)} \cdot I_t(\Delta\omega). \quad (4.22)$$

Here according to our assumption, $\mathfrak{T}(\Delta\omega)$ is given by

$$\mathfrak{T}(\Delta\omega) = \mathfrak{T}(0) I_t(\Delta\omega) / I_t(0). \quad (4.23)$$

By defining the width γ (HWHM) of $I_m(\Delta\omega)$ we get from (4.22) and (4.23)

$$\frac{I_m(\gamma)}{I_m(0)} \left(= \frac{1}{2} \right) = \frac{1 - \exp [-\mathfrak{T}(0) I_t(\gamma) / I_t(0)]}{1 - \exp [-\mathfrak{T}(0)]}, \quad (4.24)$$

which may be rewritten as

$$\frac{I_t(\gamma)}{I_t(0)} = \frac{\ln 2 - \ln (1 + \exp [-\mathfrak{T}(0)])}{\mathfrak{T}(0)}. \quad (4.25)$$

Fig. 4.8 shows the relation between $\mathfrak{T}(0)$ and γ which satisfying (4.25) for various values of a . If $\mathfrak{T}(0)$ and γ are simultaneously measured we can determine the value of a in Fig. 4.8 as the intersection of lines corresponding to these values.

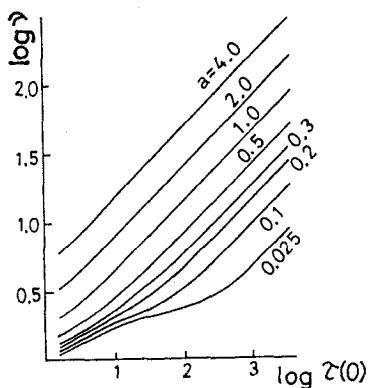


Fig.4.8

Apparent half-width γ versus the logarithm of optical thickness for various values of a (the Voigt parameter). For convenience, γ is measured taking γ_D as the unit.

$\tau(0)$ is calculated by the relation (Mitchell and Zemansky 1971)

$$\tau(0) = \sqrt{\pi \ln 2} r_e c f \ell [Ca^+] / \gamma_D , \quad (4.26)$$

where $[Ca^+]$ (the ground-state density of Ca^+) is obtained from the hook measurement, and γ_D is calculated from the temperature of the shock-heated region.

γ is known from the measured profile $I_m(\Delta\omega)$. Since the profile is distorted by the instrumental function, we have to remove the effect by deconvolution calculation in advance. We have measured the instrumental function by illuminating the spectrometer by the He-Ne laser line at 6328\AA .

4.3.4 Results and discussions

Like the discussion in 4.2.4(a), γ_L is the sum of many Lorentzian components (see eq. (4.17)). First we discuss γ_s (Stark broadening). Although ionization degree of argon is very small ($\sim 10^{-3}$) at the present temperature ($\sim 7700\text{K}$), the ejected electrons from argon may have a non-negligible contribution to γ_s , since the argon-gas pressure is relatively high. We have calculated electron densities by the Saha equation and estimated γ_s to be $20 \sim 30 \times 10^{-3} \text{ cm}^{-1}$ using the value of Baur and Cooper (1977). By subtracting γ_s (other factors are negligibly small) from γ_L we get the broadening by argon γ_F . Fig.4.9 shows the measured γ_F values (•) together with γ_D (○). The straight lines are obtained by the least-squares fit to γ_F .

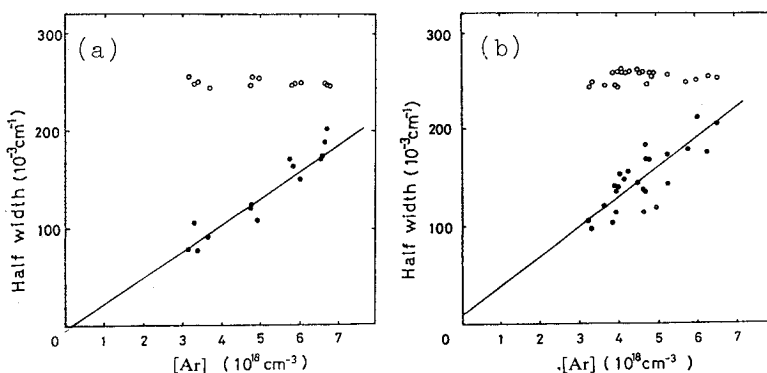


Fig.4.9

Half width τ_F (•) and τ_D (○) of Ca^+ resonance lines at 3968\AA (a) and 3933\AA (b), versus argon density.

Table 4.4 Comparison of the broadening coefficients ($10^{-20}\text{cm}^{-1}/\text{cm}^{-3}$).

Experiment				
Temperature	$765 \pm 80\text{K}$	$7466 \pm 800\text{K}$	$7630 \pm 350\text{K}$	$7700 \pm 400\text{K}$
3968\AA	1.57 ± 0.04^a	2.97 ± 0.67^b	2.60 ± 0.81^c	—
3933\AA	1.62 ± 0.08^a	—	—	2.84 ± 0.85^c
Theory	1.11^a	2.20^d	2.21^e	2.22^e

a: Bowman and Lewis (1978). b: Baur and Cooper (1977). c: Our results.

d: the value in Bowman and Lewis (1978) for this quantity seems to have a misprint. e: calculated by the hydrogenic model.

The slopes of the lines give the broadening coefficient $\tau_f/[\text{Ar}]$ ($= \bar{v} \alpha_r$ from (2.21), i.e. the product of the mean relative velocity and the cross section). They are given in Table 4.4 along with other observed data and calculated values by the classical impact formula (2.29). The temperature of Baur and Cooper (1977) is about the same as ours, and the agreement is fairly good. The calculated values are about 50% too small. This indicates a more elaborate quantal consideration is necessary.

Giusti-Suzor et al (1975) gave a theoretical value of $2.3 \times 10^{-20}\text{cm}^{-1}/\text{cm}^3$ for Ca^+ -He system. On the other hand, the observed value for K-Ar is about 50% larger than that for K-He system (Hindmarsh and Farr 1972). If this rule can be applied to

Ca^+ , broadening coefficient for Ca^+ -Ar will be about $3 \times 10^{-20} \text{ cm}^{-1}/\text{cm}^{-3}$, which is close to our value.

Giusti-Suzor et al also investigated theoretically the broadening for the isoelectronic systems Rb-He and Sr^+ -He. According to them, the collision broadening for Sr^+ -He is about 50% smaller than that for Rb-He. They attributed this difference to the reduction of the atomic radius, and consequently of the optical cross section. If the same reasoning can be applied to the present case, the broadening coefficient $3.76 \times 10^{-20} \text{ cm}^{-1}/\text{cm}^{-3}$ observed for K-Ar system (Hindmarsh and Farr 1972) will give a value close to ours for the Ca^+ -Ar system.

Similar discussions may be given based on the model potential of Baylis (1969a,b). Since Ca^+ has the hydrogen-like structure, we can apply his method to calculate the potential for Ca^+ -Ar pair. Our result is displayed in Fig.4.10 together with the Baylis' calculation for K-Ar for comparison. Here the difference potentials $\Delta V = V(^2\text{P}_{1/2}) - V(^2\text{S}_{1/2})$ at large interatomic distance are shown. In the classical discussion of Weisskopf (1933), long-range interactions near the Weisskopf radius (in this case $\rho_w \approx 10\text{\AA}$) essentially determine the broadening. We find the long-range attraction for Ca^+ -Ar is weaker than that for K-Ar. This indicates the small cross section for the former pair. Such an weak attraction is probably due to the compact valence-electron cloud of Ca^+ . Fig.4.11 shows the square of radial wavefunction for the valence-electron of Ca^+ and K. Since the valence electron of Ca^+ is more strongly bound to the core (charge of $+2e$) than that of K, it has a peak of charge distribution at a smaller distance from the core

than that of K. Finally we comment on the polarization force. The inset figure of Fig.4.10 shows the logarithmic plot of ΔV , from which we can deduce the power dependence of R. We have found the relation $\Delta V(R) \propto -R^{-5.1}$ holds at $10 \leq R \leq 20 \text{ \AA}$ for Ca^+ -Ar pair. This power dependence is between that of the van der Waals interaction (-6) and that of the polarization force (-4).

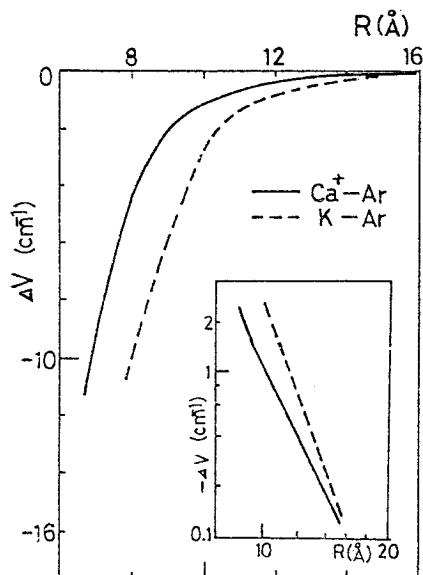


Fig.4.10

Difference potentials for Ca^+ -Ar and K-Ar pairs by Baylis' model potential. The inset figure is the logarithmic plot.

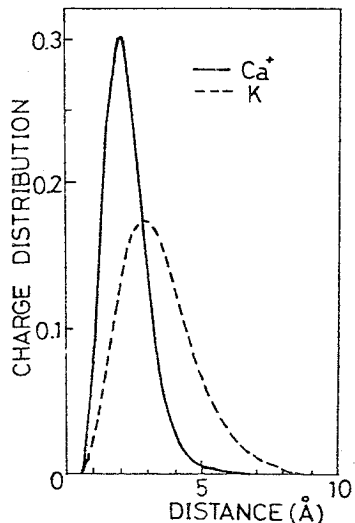


Fig.4.11

Charge distribution of the 4p electron of Ca^+ and K.

Chapter 5. Heat-pipe cell experiment

5.1 Introduction

In the preceding chapter we have investigated the line-core region of the resonance lines and discussed mainly the long-range interactions from the result. In this chapter we present absorption measurements for the wing region and discuss relatively short-range interactions.

We have seen in the first chapter that data of wing region is quite scarce for alkaline-earth-rare-gas systems, and this comes partly from experimental difficulties. The related experiments may be listed only as follows: at low rare-gas densities where the binary interaction between these atoms dominates the collision process, strontium resonance line broadened by helium and argon (Farr and Hindmarsh 1971), barium principal series broadened by xenon (Kielkopf 1978), and magnesium and barium resonance lines broadened by rare gases (Zhuvikin et al 1979).

Here we measure wing spectra of the resonance lines of strontium and barium broadened by various rare gases.

In the meaning that ① the absorption coefficients are given in "absolute unit" (the definition is given in the next section) and ② the measured spectral range is much wider than previous measurements, we believe the present result will be the first extensive study for these lines.

From the result we can make detailed discussions on the interatomic potentials for Sr (or Ba)-rare-gas pairs. Here we use two line-broadening theories, namely the classical phase-shift theory (both the general- and the quasi-static-treatments) and the UFC quantum treatment. Sophisticated calculations of the interatomic potentials between alkaline earth-rare gas have been reported on very limited pairs; Ca, Mg-He, Ne (Malvern 1978) and Mg-He (Bottcher et al 1975). Therefore, the present empirical potentials will be a very useful guide for future comparisons with theoretical calculations.

We notice that the alkaline-earth singlet lines have recently received much attention in connection with the collisional redistribution of radiation. From this viewpoint, collision-induced fluorescence spectra in the wing region have been reported for Sr-Ar (Carlsten et al 1977) and Ca-Ar pairs (Corney and McGinley 1981). For Sr-Ar pair, Thomann et al (1980) made a polarization measurement of the fluorescence spectra, and Julienne (1981, 1982) have explained the spectra based on his calculated potentials.

In the next section we describe the detail of the absorption cell, the optical arrangement, and the data-reduction method. These are almost common to the experiments for Sr-rare-gas and Ba-rare-gas pairs. Then we show the results and discussions separately on these two cases.

5.2 Experiment

5.2.1 Absorption cell

In making spectroscopic measurements on metal-vapor-rare-gas systems in a confined cell, the following conditions must be satisfied: ① the metal and rare-gas atoms mix uniformly ② in a well-defined region, ③ the temperature and vapor densities are accurately known, and ④ the observation windows are kept free of metal deposit. A conventional type of cell (see, e.g. Pollock and Jensen 1965) which uses two separate cells can well define the vapor region by the length of the inner cells, but does not fulfill the condition ④.

The heat-pipe cell developed recently by Vidal and Cooper (1969) ideally satisfies ②, ③ and ④, since it confines a metal vapor in the central region by the rare-gas pressure (see the schematic figure in Fig.5.1(a)). Thus, this operates well when the metal-vapor pressure is high enough to equilibrate with that of rare gas (typically ~ 10 Torr). It has a woven mesh in its inside, which acts as a wick to return the metal condensate back to the center by the capillary force. However this type of cell is not necessarily suitable for the present purpose. This is because, in the first place, the metal and rare-gas atoms mix mainly in the boundary layer (the hatched area) and we can not observe only this mixed region if we look at the cell through the axis. The second reason is that the present metal-vapor pressure is low ($10^{-2} \sim 10^{-1}$ Torr, at $T \sim 1000K$), so that we can not equilibrate the pressure

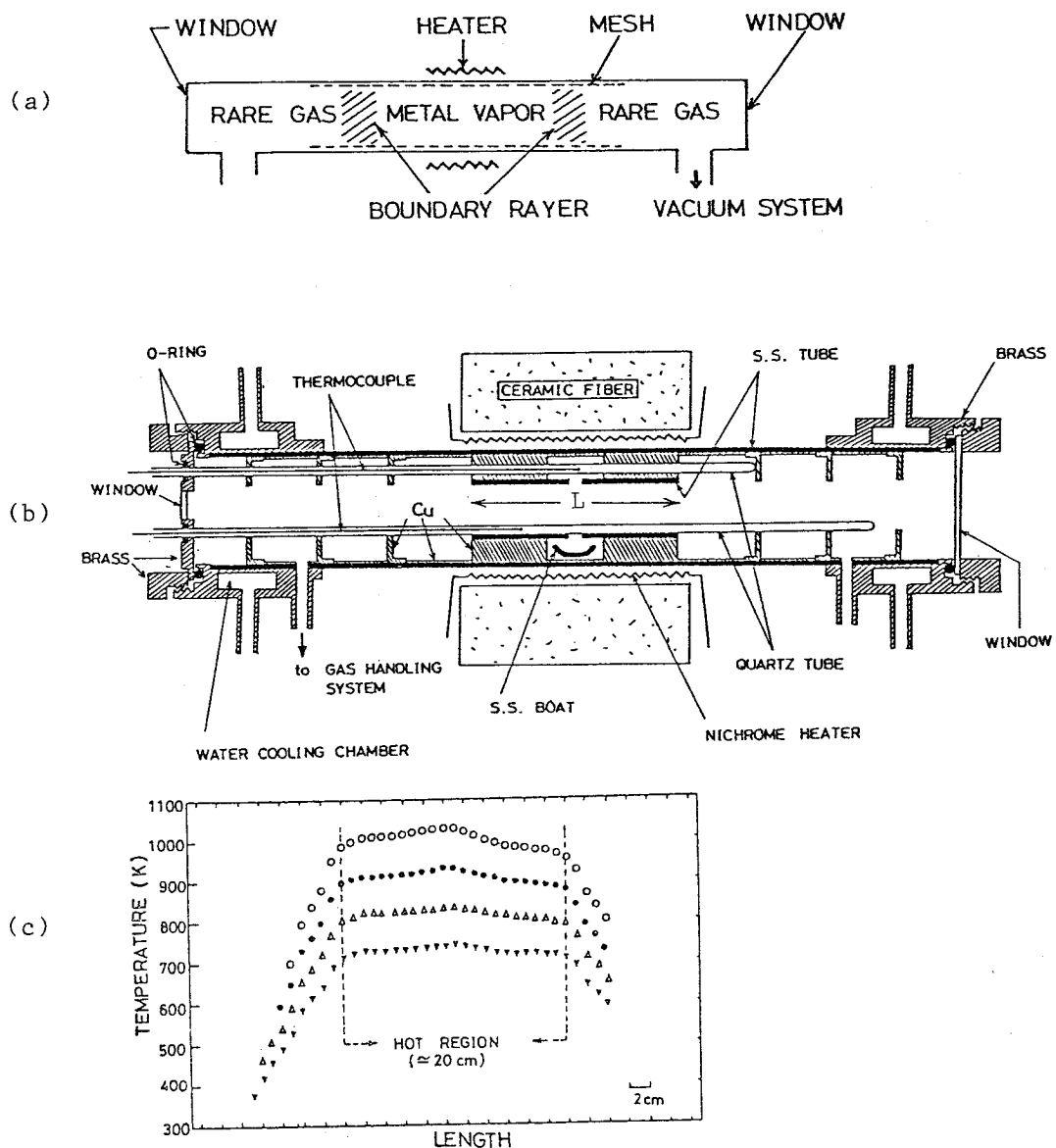


Fig.5.1 Schematic arrangement of the heat-pipe cell (a), the present cell (b) with $L = 20\text{cm}$, and the temperature distribution (c).

with that of the rare gas.

Our cell design is shown in Fig.5.1 (b). There is no mesh inside the tube, and the metal-vapor region is defined by the temperature distribution of the cell. It was made according to the design of McCartan and Farr(1976) with some modifications. It is made of a stainless-steel tube of inner diameter 3 cm and length 50 cm with a water-cooled quartz window at each end. Its central portion has copper baffles and is heated by an external nichrome heater for about 20 cm of its length. The metal is vaporized and mixed with rare gas in this region and the windows are kept almost free of metal deposit. Rare gas is introduced into the cell through a gas-handling system incorporating pressure gauges.

Temperature distributions along the cell axis are measured by a thermocouple in an inserted quartz tube. Another thermocouple is connected to a temperature-controlling system. The measured temperature distribution in Fig.5.1 (c) shows well-defined hot regions. Since the rare-gas pressure is a few orders of magnitude higher than that of the metal, the metal vapor is well diluted with rare gas in this region. Though the metal density may have a gradient along the cell axis due to diffusion, we can neglect this effect in our analysis because we make the hook measurement and integrate the density along the axis. For Ba-rare-gas system we somewhat simplified the cell structure, since barium is highly reactive at high temperatures and attack the cell elements made of copper.

Though our cell is slightly different from the usual heat-pipe cell, it has a similar mechanism to that in confining the metal vapors by rare gases and keeping the windows free of metal deposit. In the present study, we will call ours simply as a heat-pipe cell for convenience.

5.2.2 Optical arrangement and data reduction

Fig. 5.2 shows the schematic diagram of the experiment. Light from a 30 W tungsten filament lamp is split into two beams. The sample beam which traverses an absorption cell and the reference beam which traverses the ambient atmosphere are chopped at different frequencies, 150 and 210 Hz respectively, by a mechanical chopper which has a rotating wheel with double-beam windows at different radii. The two beams are focused on the entrance slit about 40 μ m wide of an Ebert-type scanning monochromator of focal length 50 cm. Using a grating of 1200 grooves/mm in the first order, the monochromator has a dispersion of about 16.6 $\text{\AA}/\text{mm}$ in the measured spectral region. To check the instrumental function, the profile of the He-Ne laser line at 6328 \AA was measured. It is a Gaussian-like shape of FWHM about 1 cm^{-1} with a slight tail to the red side. The signal from a photomultiplier is led to two lock-in amplifiers and is then separated into the intensity of the sample beam (I) and the reference beam (I_0) by synchronizing with gate signals from the chopper. I/I_0 is obtained by a divider (Teledyne Philbrick 4452) and is recorded on a strip chart. Our mirror/beam-splitter system is arranged as a Mach-Zehnder interferometer, therefore it is also used to measure the metal-vapor density by the hook method (Marlow 1967). The hook spectra were obtained using a 1 m-focal length Czerny-Turner-type spectrograph with an N_2 laser-excited dye laser as a light source.

The absolute absorption coefficient is defined as the measured absorption coefficient divided by the product of the

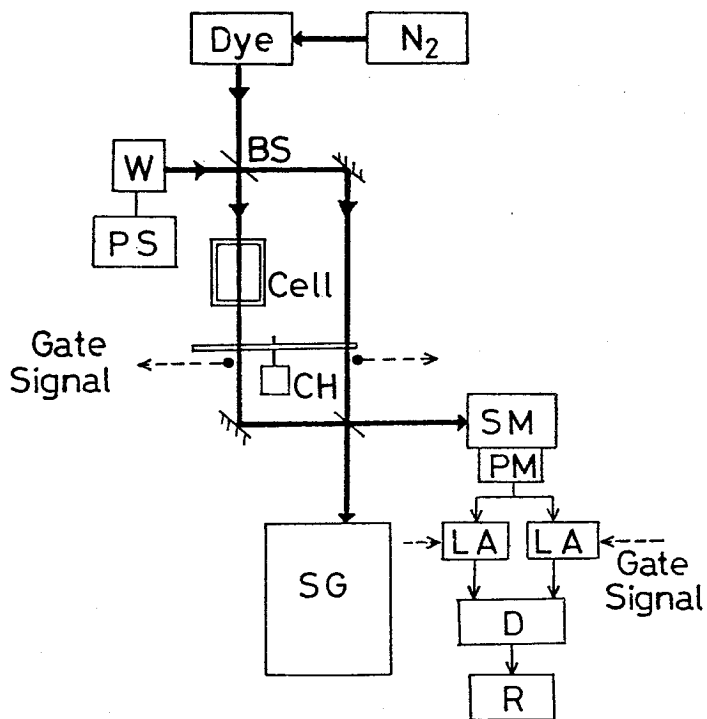


Fig.5.2 Schematic diagram of the experiment.

Full arrows show the optical path.

W:W lamp. PS:Power stabilizer. BS:Beam splitter.

CH:Chopper. SM:0.5m scanning monochromator.

PM:Photomultiplier. LA:Lock-in amplifier.

D:Signal divider. R:Chart recorder.

N_2 and Dye: N_2 -laser-excited dye laser.

SG:1m spectrophotograph.

metal vapor and rare-gas densities. This is deduced as follows.

Assuming the usual absorption law (4.9)

$$I(\Delta\omega) = I_0(\Delta\omega) \exp [-k(\Delta\omega) \ell], \quad (5.1)$$

where k is the absorption coefficient at $\Delta\omega$ and ℓ is the absorption length, it is given in cm^5 by

$$\frac{k(\Delta\omega)}{[M][R]} = \frac{\ln [I_0(\Delta\omega) / I(\Delta\omega)]}{\ell [M][R]}, \quad (5.2)$$

where $[M]$ and $[R]$ are the densities of the metal vapor and rare gas respectively.

$I_0(\Delta\omega) / I(\Delta\omega)$ is obtained from the transmission measurement. $\ell[M]$ is obtained by the hook method as (4.15) (Marlow 1967), i.e.

$$[M]\ell = \frac{\pi K \Delta^2}{r_e f \lambda_0^3}, \quad (5.3)$$

where K and Δ are the interference-fringe order and the hook separation, r_e is the classical electron radius, λ_0 is the resonance-line wavelength, and f is the oscillator strength (we used the value $f = 1.9$ for Sr (Kelley et al 1974), and $f = 1.6$ for Ba (Miles and Wiese 1969)). We measured $[M]\ell$ before and after each scan of the profile. $[R]$ (cm^{-3}) is known from the ideal-gas relation

$$[R] = 9.66 \times 10^{18} p/T, \quad (5.4)$$

where p is the rare-gas pressure in Torr and T is the cell temperature in Kelvin.

5.3 Results and discussions

5.3.1 Sr - rare gas

(a) Observed profile

Fig. 5.3 shows typical transmission spectra of the Sr resonance line broadened by (a) Ar at 938K and (b) Xe at 1011K for various pressures below one atmosphere. They are plotted against the wavenumber separation from the line center $\Delta\nu = \nu - \nu_0$ (cm⁻¹), which is converted to $\Delta\omega$ (radian·sec⁻¹) by $\Delta\omega = 2\pi c \Delta\nu$ (c is the light speed). In both cases they have asymmetric wings to the red ($\Delta\nu < 0$) side, which become apparent as the rare-gas pressure increases. In the case of Xe, a prominent satellite or shoulder appears at about -50 cm⁻¹ superimposed on a strong tail and its position does not change with the Xe pressure.

Fig. 5.4 shows the absolute absorption coefficients on a logarithmic scale. To cover the whole range of data, $\ell[\text{Sr}]$ was varied between 2×10^{14} and 2×10^{16} cm⁻² by changing the cell temperature between 817 and 1011K and the rare-gas pressure was varied between 50 and 700 Torr. The data near the line center were obtained at relatively small values of $\ell[\text{Sr}]$ (therefore at low cell temperatures) and $[\text{R}]$, while for the outer region they were obtained at relatively large values of $\ell[\text{Sr}]$ and $[\text{R}]$.

The results under these various conditions converged well within our experimental error limit and were linked smoothly to each other (this figure shows only typical examples for clarity). This fact means, firstly, that the proportionality between the absorption coefficient and the product of Sr and rare-gas densities holds well in the measured spectral range, and secondly, that the present temperature variation has a negligible effect on the profile.

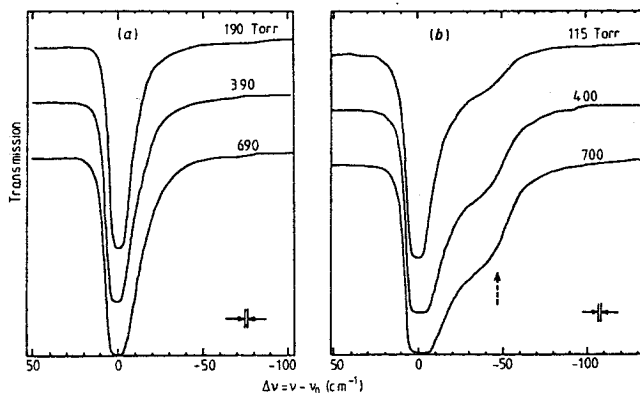


Fig.5.3 Typical transmission spectra of Sr-Ar at 938K (a), and Sr-Xe at 1011K (b). The FWHM of the instrumental function is shown by the full arrows. The broken arrow shows the satellite position.

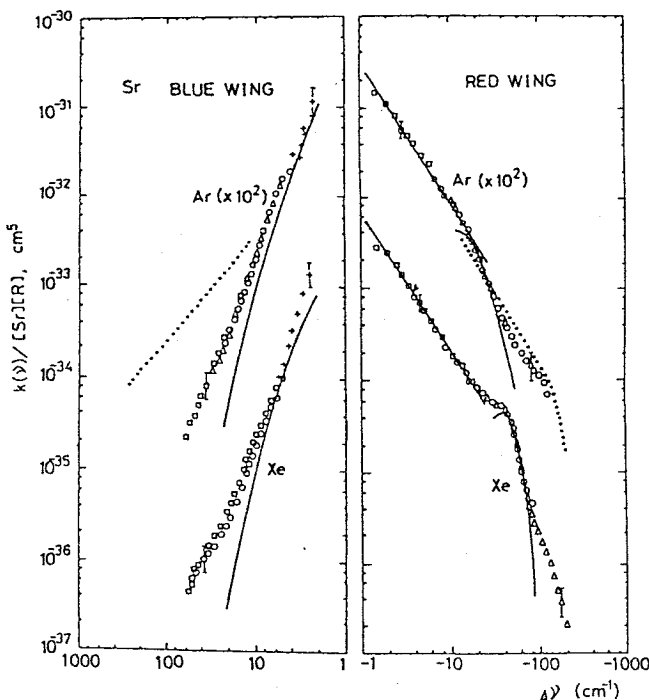


Fig.5.4 Δv dependence of the absolute absorption coefficients. The solid lines are the best fit to the profile by the UFC theory. The dotted lines are calculated by Julienne (1981, 1982) based on his potentials.

The former point indicates that the absorption coefficient is determined by the binary collision between a Sr atom and a rare-gas atom. This is, as seen in Chapter 2, the basic assumption of the line-broadening theories used in the present work. The latter point (small temperature effect) will be discussed later.

In the first place, we discuss the red-wing ($\Delta\nu < 0$) profiles. For both Ar and Xe, an approximate $-3/2$ power dependence appears at $2 \leq |\Delta\nu| \leq 10 \text{ cm}^{-1}$. The same dependence has been found for Sr-Ar pair at Ar pressures below one atmosphere by Farr and Hindmarsh (1971), and at several tens of atmosphere by Chen and Wang (1978). A prominent shoulder appears near -50 cm^{-1} for Xe, while for Ar a very diffuse structure appears near -20 cm^{-1} . Next we see the blue-wing ($\Delta\nu > 0$) profiles. Both profiles vary rapidly with an approximate -3 power dependence and have rather slight tails. This is a more rapid variation than that of the $-7/3$ power dependence first predicted by Lindholm (1945) based on a simple quasi-static theory (we can not derive this dependence within the framework of the present theoretical treatments). A similar dependence has been found in many alkali-rare-gas systems (for example, Chen and Phelps 1973) or in other systems such as Tl-rare-gas (Cheron et al 1977).

From the measured instrumental function of the monochromator, the profiles are believed to be free of distortions at $|\Delta\nu| \gtrsim 3 \text{ cm}^{-1}$, yet the data have some experimental uncertainty coming from three sources (see (5.2)), namely the evalution of $\ln(I_0/I)$, $\ell[\text{Sr}]$ and $[\text{R}]$. The third makes a negligible contribution compared with others in our experiment. The first makes the largest contribution in the outer region, while the second makes the largest contribution near the line center. we estimate the uncertainty limit to be roughly 60% at $|\Delta\nu| \gtrsim 100 \text{ cm}^{-1}$, 30% at $|\Delta\nu| \leq 10 \text{ cm}^{-1}$ and 10% elsewhere.

(b) UFC analysis

We have seen in 2.2.2 and 2.3 that both the classical (2.39) and the UFC (2.69) formulae predict that a satellite appears at $\Delta\omega$ if

$$\hbar \frac{d\Delta\omega}{dR} = \frac{d\Delta V(R)}{dR} = 0 \quad . \quad (5.5)$$

However we can not use the classical formula for quantitative discussions of the line intensity, because (2.39) goes to infinity at the satellite position. We start from the UFC wing formula (2.73), i.e.

$$I(\Delta\omega) = 4\pi[R] \sum_c \frac{(Re R_c)^2 \exp[-V_l(Re R_c)/kT]}{\left|\Delta V'(R_c)/\hbar\right|} \left|36\pi Z_c\right|^{1/2} L(Z_c), \quad (5.6)$$

where kT is the thermal energy, and the summation is over all Condon points R_c with positive values of $Re R_c$. The values R_c are complex in general and are evaluated as solutions of the equation

$$\hbar\Delta\omega = \Delta V(R), \quad (5.7)$$

where $\Delta V(R)$ is the difference between the interaction potentials of the upper (V_u) and lower (V_l) states at interatomic distance R , namely

$$\Delta V(R) = V_u(R) - V_l(R) \quad . \quad (5.8)$$

Z_c and $L(Z_c)$ are given by $\Delta V'(R_c)$ and $\Delta V''(R_c)$ as (2.70) through (2.72).

To compare $I(\Delta \omega)$ with the observed quantity $k/[Sr][R]$, we use the well-known relation (4.9) (Mitchell and Zemansky 1971) which describes the total integrated strength of the absorption coefficient

$$\int_0^\infty k(\Delta \omega) d\omega = 2\pi^2 c r_e f [Sr] , \quad (5.9)$$

where r_e is the classical electron radius. Since $I(\Delta \omega)$ is normalized as

$$\int_0^\infty I(\Delta \omega) d\omega = 1 , \quad (5.10)$$

$I(\Delta \omega)$ and $k(\Delta \omega)/[Sr][R]$ can be equated as follows if the theory explains the observed spectra:

$$\frac{I(\Delta \omega)}{[R]} 2\pi^2 c r_e f = \frac{k(\Delta \omega)}{[Sr][R]} . \quad (5.11)$$

For $\Delta V(R)$ two types of functions are assumed; the first is the van der Waals potential

$$\Delta V(R) = -\Delta C_6 R^{-6} , \quad (5.12)$$

where $\Delta C_6 (>0)$ is the van der Waals coefficient. As we have seen in 2.3, if R_c is real and $Z_c \gg 1$ the UFC profile is reduced to the classical quasi-static formula (2.39), and it is easy to calculate:

If we put $p = 6$ in (2.40) we get

$$I(\Delta \omega) = \frac{2\pi}{3} [R] \left(\frac{\Delta C_6}{\hbar} \right)^{1/2} \Delta \omega^{-3/2} , \quad (5.13)$$

for the red (we find from (2.36) that $\Delta\omega < 0$) wing. This result coincides with the observed power dependence. If we assume appropriate values for ΔC_6 (given in Table 5.1), (5.13) gives a good fit to part of the observed red-wing profile (see the straight lines in Fig. 5.4 at $-10 \lesssim \Delta\nu \lesssim -2 \text{ cm}^{-1}$). If R_c is complex and $z_c \ll -1$, (5.6) predicts the blue-wing profile (Szudy and Baylis 1975)

$$I(\Delta\omega) = \sqrt{2}\pi \left(\frac{\Delta C_6}{\hbar} \right)^{1/2} \Delta\omega^{-3/2} \exp[-K' \Delta\omega^{5/9}], \quad (5.14)$$

where K' is a constant related to ΔC_6 and the mean relative velocity. By substituting the above ΔC_6 values we obtain the rapidly decreasing curves at $\Delta\nu > 0$ in Fig. 5.4. They show a similar dependence to the data at $4 \lesssim \Delta\nu \lesssim 10 \text{ cm}^{-1}$. However for Xe, there is a systematic discrepancy of a factor ~ 2 which is greater than the present experimental error limit. The discrepancy observed in the tails clearly increases as $\Delta\nu$ increases for both Ar and Xe. A similar discrepancy has been reported by Cheron et al (1977) for Tl-Xe system.

The second assumption for $\Delta V(R)$ is a quadratic function

$$V(R) = -\mathcal{E} + \frac{36\mathcal{E}}{R_0^2} (R - R_0)^2, \quad (5.15)$$

where $\mathcal{E} (> 0)$ and R_0 are the potential parameters which mean the well depth and radius respectively. We see this is obtained by expanding the well-known Lennard-Jones potential

$$V(R) = \mathcal{E} \left[\left(\frac{R_0}{R} \right)^{12} - 2 \left(\frac{R_0}{R} \right)^6 \right] \quad (5.16)$$

in Taylor series about $R = R_0$. Since we know from (5.5) that a satellite appears at $\Delta\omega$ in a red-wing if $\Delta V(R)$ has a well of depth $\hbar\Delta\omega$, the quadratic assumption (5.15) is useful to determine the well parameters by a fitting procedure. The resultant UFC profile is (Szudy and Baylis 1975)

$$I(\Delta\omega) = \frac{2\pi}{3} [R] \frac{R_0^3 |36\pi z_c|^{1/2} L(z_c)}{\epsilon^{1/2} |\epsilon + \Delta\omega|^{1/2}} \left\{ 1 + \frac{\delta}{36} \left(1 + \frac{\Delta\omega}{\epsilon} \right) \right\}, \quad (5.17)$$

where δ is a numerical factor taking $\delta = 0$ if $\Delta\omega < -\epsilon$, or $\delta = 1$ if $\Delta\omega > -\epsilon$. The best fit calculations to our data are shown in Fig.5.4 by the curves at $-100 \lesssim \Delta\nu \lesssim -20 \text{ cm}^{-1}$. Their well parameters are $\epsilon = 20 (50) \text{ cm}^{-1}$ and $R_0 = 5.9 (6.7) \text{ \AA}$ for Sr-Ar (Sr-Xe). We find the theory can explain a limited spectral region near the satellite in both cases.

From the standpoint of the UFC treatment, it is expected that a small temperature variation has little effect on the profile. The general expression (2.69) predicts a temperature dependence of the theoretical profile $I(\Delta\omega)$ near a shoulder such as $I(\Delta\omega) \propto T^{-1/6} \exp(-V_\ell / kT)$. Using a representative value for V_ℓ , this gives a temperature dependence of $I(\Delta\omega)$ of less than 10% for the present temperature variation between 817 and 1011K.

(c) Interatomic potentials

The deduced potentials are compared with other data and discussed in this section.

ΔC_6 values are compared in Table 5.1 with others from line-core measurements. The last column gives a theoretical estimate by the hydrogenic model (3.10). We have seen in 2.2.1 the line-core result is related to $\Delta V(R)$ at relatively large values of R , typically the Weisskopf radius ρ_w . In the present case, the result is valid near ρ_w or slightly smaller values of R , since it was obtained from a wing region which is adjacent to the line-core region. Therefore our result is expected to be comparable in magnitude with the line-core results. For Ar, our result agrees relatively well with others, except for that of Chen and Wang (1978). For Xe, our result is comparable with the theoretical estimate while that of Wang and Chen (1979) is quite large. There are two possible causes for the large discrepancy between the results of Wang and Chen and others for both Ar and Xe. The first is that classical impact analysis depends critically on the forms of $\Delta V(R)$ assumed.

Table 5.1 Comparison of ΔC_6 (10^{-58} ergcm $^{-6}$). The last row shows the assumed forms for $\Delta V(R)$. For example, $C_6 C_8 C_{12}$ means $\Delta V(R) = \Delta C_{12} R^{-12} - \Delta C_8 R^{-8} - \Delta C_6 R^{-6}$. The value with (*) is calculated by us using the hydrogenic model.

	Penkin et al (1968)	Farr et al (1971)	Chen and Wang (1978)	Wang and Chen (1979)	Present work	Theory
Ar	1.72	2.8	10.2	—	2.0	2.6
Xe	—	—	—	44.4	8.9	6.4*
C_6	$C_6 C_8 C_{12}$	$C_6 C_{12}$	$C_6 C_{12}$	—	—	—

For example, Hindmarsh et al (1970) have reported that ΔC_6 can be greatly reduced if an additional attractive term ΔC_8 is introduced into the Lennard-Jones potential. The second possible cause of the discrepancy is that Wang and Chen obtained the result at high rare-gas pressures (in density up to 10^{20} cm^{-3}), where the binary-collision assumption becomes doubtful.

Fig.5.5 shows $\Delta V(R)$, the van der Waals and quadratic potentials obtained, by full heavy curves, the Lennard-Jones potentials of other authors from line-core measurements are shown by full thin curves. Our result for Sr-Ar shows a agreement with that of Farr and Hindmarsh (1971), but shows clear discrepancies with those of Chen and Wang (1978) and Wang and Chen (1979). The latters seem to overestimate the short-range repulsive term as a result of the high rare-gas pressures used.

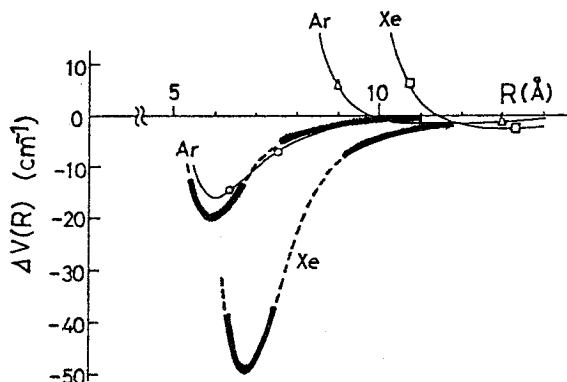


Fig.5.5 Interaction potentials obtained by us (full heavy curves), Chen and Wang (1978) (Δ), Wang and Chen (1979) (\square), and Farr and Hindmarsh (1971) (\circ). The broken curves are drawn to connect our results for the van der Waals and quadratic potentials smoothly.

Julienne (1981, 1982) has recently calculated the interatomic potentials for Sr-Ar by ab initio UFC calculations and the damped dispersion interaction (see 3.3.1), and compared his theoretical absorption coefficients with our observations. His potentials appear in Fig.5.6 (a). In the collision with a rare-gas atom in the ground state, the atomic 1P_1 state of Sr splits into two molecular states (see Fig.5.7 for reference). One is the $^1\Sigma$ state (in the notation of Hertzberg 1950) which is purely repulsive, because the valence electron of Sr has a $p\alpha$ orbital and overlaps the noble gas at large interatomic distance R . The other is the $^1\Pi$ state which is weakly attractive at large R , because the valence electron has a $p\pi$ character along the internuclear axis. The atomic ground state 1S_0 of Sr makes only the $X^1\Sigma$ state, which is very weakly attractive at large R . Since $\Delta V(R)$ is defined by (5.8) as the difference of the interatomic potentials for these states, $\Delta V(R)$ may be equal to $V(^1\Pi) - V(X^1\Sigma)$ or $V(^1\Sigma) - V(X^1\Sigma)$. These difference potentials are shown in Fig.5.6 (b). The difference $V(^1\Pi) - V(X^1\Sigma)$ of Julienne's potential shows a similar R dependence to our result at $R \gtrsim 6\text{\AA}$, but has no wells. Therefore with his potential we can not predict the red-wing satellite as is observed (see the dotted line in Fig.5.4, which shows Julienne's prediction of profile). However a good agreement has been obtained with our data in the outer region $-\Delta\nu \gtrsim 20\text{ cm}^{-1}$. Julienne also calculated the blue-wing profile based on his difference potential $V(^1\Sigma) - V(X^1\Sigma)$ but the agreement is quite poor. These discrepancies indicate that the ab initio calculations should be further refined in the future.

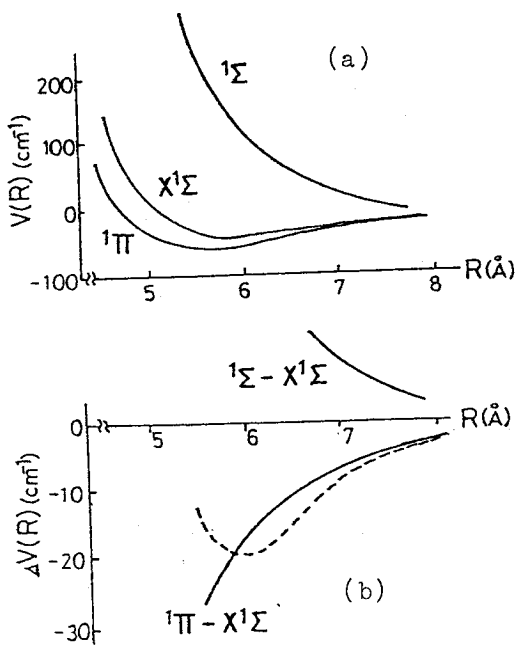


Fig.5.6

Calculated interatomic potentials for Sr-Ar
 (a) (Julienne 1981,1982),
 and their difference (b).
 The dotted curve shows
 our result (see Fig.5.5).

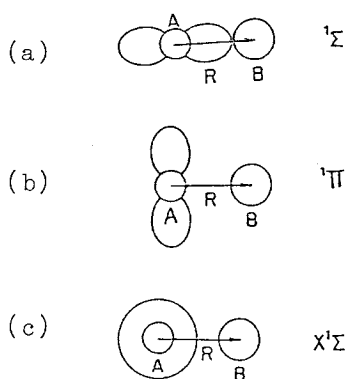


Fig.5.7

Schematic representation of the electron distribution for the states 1Σ (a), 1Π (b), and $X^1\Sigma$ (c).
 A and B denote the alkaline-earth
 and the rare-gas atom respectively.

5.3.2 Ba-rare-gas

(a) Observed profile

Fig.5.8 shows the $\Delta\nu$ dependence of the absolute absorption coefficient $k(\Delta\nu)/[Ba][R]$ for $R = He, Ne, Ar, Kr$ and Xe . To cover the whole range of data, $l[Ba]$ was varied between 4×10^{15} and $2 \times 10^{16} \text{ cm}^{-2}$ by changing the cell temperature between 1050 and 1150K and the rare-gas pressure was varied between 50 and 700 Torr. Since the profiles behave rather differently depending on the rare-gas species, we describe the details in two parts, namely Ba-Xe, Kr and Ar (the heavy rare-gases) and Ba-Ne and He (the light rare-gases) in the followings.

In the first place, we see the detail of the profiles for heavy rare-gases. The red wings have structures like satellites or shoulders at $10 < |\Delta\nu| < 100 \text{ cm}^{-1}$. From Xe to Ar the satellites shift the position toward the line center and become less prominent; for Ar it appears only as a gradual change of the slope at $-\Delta\nu \approx 10 \text{ cm}^{-1}$. Inside the shoulders the profiles have straight regions, which may be well represented by a power dependence of -1.2 for Xe and Kr, and -1.5 for Ar. The blue wings fall off very rapidly at $|\Delta\nu| \leq 10 \text{ cm}^{-1}$ with roughly -3 to -4 power dependence. They seem to become steeper from Ar to Xe. Very diffuse shoulders appear in the tail at $|\Delta\nu| > 30 \text{ cm}^{-1}$. Their position shifts, in the opposite way to the red side, outwards from Xe to Ar.

Zhuvikin et al (1979) reported similar red-wing shoulders, yet their absolute absorption coefficients are about 10 to 30% smaller

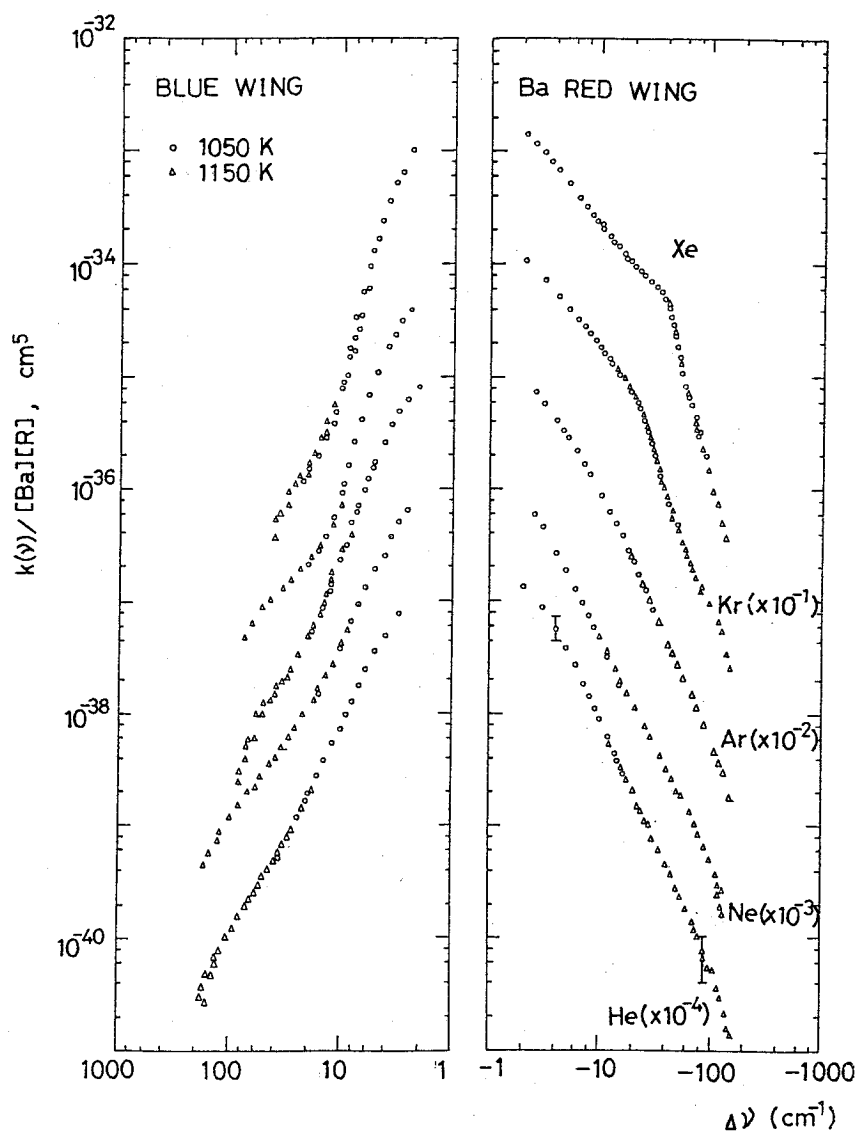


Fig. 5.8 $\Delta\nu$ dependence of the absolute absorption coefficient for the Ba-rare-gas systems.

than our result and the power dependence of the straight region is -1.5 for all cases of these heavy rare gases. These discrepancies may come from some systematic error; we suspect Zhuvikin et al underestimated the background intensity I_0 of the transmission data.

Corney and McGinley (1981) observed both wings ($1 \leq |\Delta\nu| \leq 30 \text{ cm}^{-1}$) for Ca-Ar pair. They found a -1.6 power dependence for the red-wing with an undulatory pattern at the shoulder position, while the blue-wing falls off with -2 power dependence near the line center and more steeply in the outer region. Our previous measurement of Sr-Xe, Ar shows very similar profiles to the present result of Ba, except that in this case the red-wing power dependence was -1.5 for Xe.

Tables 5.2 and 5.3 are summaries of the observed features of Ba, which also include the result for light rare-gases.

Table 5.2 gives the effective power dependence n of the absolute absorption coefficients in $k/[Ba][R] \propto |\Delta\nu|^{-n}$ together with the fitted spectral region. There is a region in each wing where a power law gives a good fit across one to two decades in intensity. The fitting procedure typically determines n with about ± 0.1 accuracy. Table 5.3 gives the estimated satellite positions. In many cases the structures are so severely smeared out that they are mere inflections whose centers are ill defined.

Finally we see the detail of the profiles for light rare-gases. In this case the profiles are nearly symmetric with a power dependence of approximately -2 but they deviate from this straight dependence in the outer region; in the red-wing roughly at $|\Delta\nu| \simeq 100 \text{ cm}^{-1}$ for both Ne and He, while in the blue-wing at $|\Delta\nu| \simeq 30$ and 60 cm^{-1} for Ne and He respectively. As with the heavy rare-gas cases, the blue-wings have very diffuse satellites or shoulders at $|\Delta\nu| \gtrsim 80 \text{ cm}^{-1}$.

Table 5.2 Wing power dependence $k(\Delta\nu)/[Ba][R] \propto |\Delta\nu|^{-n}$.

Atom	Blue wing		Red wing	
	n	(cm ⁻¹)	n	(cm ⁻¹)
He	2.0	4-60	2.1	4-90
Ne	2.0	3-30	2.0	4-110
Ar	2.7	4-18	1.5	3-10
Kr	3.4	4-14	1.2	3-12
Xe	4.2	3-13	1.2	3-20

Table 5.3 Satellite position $\Delta\nu$ (cm⁻¹).

Atom	Blue wing	Red wing
He	120 ± 50	—
Ne	100 ± 30	—
Ar	50 ± 20	13 ± 5
Kr	40 ± 15	24 ± 5
Xe	30 ± 15	45 ± 5

(b) UFC and AC analysis

In the preceding analysis for Sr, we used the UFC-profile formula (5.6) together with two trial potentials, i.e. the van der Waals type (5.12), and the quadratic type (5.15). We have seen the former predicts -1.5 power dependence (5.14) near the line center of the red-wing. However in the present case for Ba-Xe and Kr they have not such a dependence (i.e. -1.2, see Table 5.3), thus van der Waals type is not necessarily suitable for the profile analysis. Here we use two types of potential form for $\Delta V(R)$; the first one is the Lennard-Jones function

$$\Delta V_{LJ}(R) = \epsilon \left[\left(\frac{R_0}{R} \right)^{12} - 2 \left(\frac{R_0}{R} \right)^6 \right], \quad (5.18)$$

where $\epsilon (> 0)$ and R_0 are the fitting parameters (the well depth and radius respectively), and the second one is the quadratic function such as

$$\Delta V_{Q\pm}(R) = \pm \epsilon \left[1 + \frac{\kappa}{2R_0^2} (R - R_0)^2 \right], \quad (5.19)$$

where the additional factor κ is a dimensionless parameter called the reduced curvature. Previously to consider the well parameters from the red-wing satellites, we have assumed a special case of (5.19), namely by putting $\kappa = -72$ for ΔV_{Q-} we obtained (5.15). In this case we use ΔV_{Q+} with large values of $-\kappa$ to obtain parameters of "reversed" parabolic well from the diffuse blue-wing satellites. Fig. 5.9 shows a schematic drawing of ΔV_{LJ} and $\Delta V_{Q\pm}$. We see

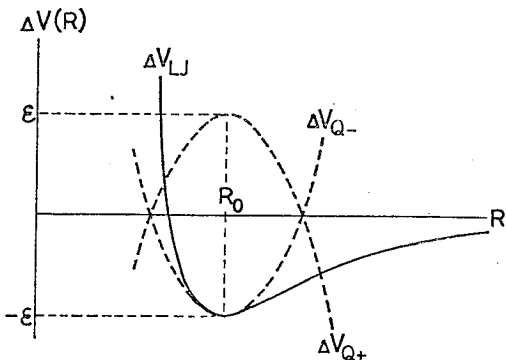


Fig. 5.9 Schematic drawing of ΔV_{LJ} and ΔV_{Q-} with $\kappa = -72$.

that (5.19) can represent either the "usual" parabolic well by ΔV_{Q-} or the "reserved" one by ΔV_{Q+} . As previously mentioned, ΔV_{Q-} with $\kappa = -72$ represents the asymptotic formula for ΔV_{LJ} near the well. We have generalized the UFC profile (5.17) for $\kappa = -72$ (Szudy and Baylis 1975) to arbitrary values of κ . The best fit to the observed profile is found by sequentially iterating the parameters ϵ , R_0 and κ . This procedure is straightforward since each parameter controls a well-defined aspect of the profile, namely ϵ determines the spectral position of a satellite, R_0 determines the intensity of the UFC profile near the satellite, and κ changes the sharpness of the satellite structure.

In addition to the UFC treatment, we use here the general treatment by the classical phase-shift theory (see section 2.2.3, hereafter we will call this method as the auto-correlational, abbreviated as AC, analysis). We start from the formula (2.49) of Kielkopf (1981), i.e.

$$I(\Delta\omega) = \frac{1}{\pi \bar{v}} \int_0^\infty \exp[-\alpha(u)] \cos \left[\Delta\omega \frac{u}{\bar{v}} - \beta(u) \right] du , \quad (5.20)$$

where \bar{v} is the mean relative velocity and $\exp(\alpha + i\beta)$ gives the auto-correlation function. Here we take the correlation delay in spatial unit $u = vt$ rather than time t . $\alpha(u)$ and $\beta(u)$ are defined by (2.46) through (2.48). $I(\Delta\omega)$ must be calculated numerically since it is not analytic in general.

Following Kielkopf's procedure to account for a wide range of satellite profiles, we assume that $\Delta V(R)$ is described by two analytic functions

$$\Delta V_<(R) = \Delta B_0 + \Delta B_2 R^2 + \Delta B_4 R^4 , \quad (5.21)$$

and

$$\Delta V_>(R) = -\Delta C_6 R^{-6} , \quad (5.22)$$

corresponding to small and large values of R , respectively. The three factors B_0 , B_2 and B_4 produce a set of potential curve parameters, namely the potential extremum ϵ (we should note in this definition that ϵ can have either positive or negative sign, and if it is negative this means usual well), its radius R_0 and the reduced curvature $K = R_0^2 \Delta V''(R_0) / \epsilon$, so that ϵ , R_0 and K can be uniquely determined by fitting to the observed satellite profiles. If they are fixed, ΔC_6 is determined by these values, since $\Delta V_>$ is supposed to connect smoothly with $\Delta V_<$ at $R = R_m (> R_0)$ by the conditions

$$\Delta V_>(R_m) = \Delta V_<(R_m) , \quad \Delta V'_>(R_m) = \Delta V'_<(R_m) . \quad (5.23)$$

(c) Interatomic potentials

Fig. 5.10 shows the comparison of the observed profiles with the best-fit calculations by the UFC and the AC analysis for Ba-Xe and Ba-He as representative cases. The potential forms are shown in Fig. 5.11 and the parameters deduced from the AC analysis are summarized in Table 5.4.

We see in Fig. 5.10 (b) that the observed red-wing for Xe is well explained by the Lennard-Jones potential or slightly-modified one, except for two serious discrepancies. The first is the undulation of the UFC profile near the shoulder. This is a characteristic feature of the UFC profile (see (2.65) and the following explanation), and will vanish if the profile is averaged over a Maxwellian velocity distribution (Szudy and Baylis 1975). The second discrepancy appears in the tail, where calculated profiles fall off too rapidly. From the UFC viewpoint this tail region is called the anti-static wing where only complex Condon points R_c contribute to the intensity, and to increase the intensity drastically as the observed profile, real Condon points are needed (we can find $L(Z_c)$ in (2.69) becomes very small for a complex value of R_c). Real R_c might be obtained if e.g. $\Delta V(R)$ decreases again at some small R ($\lesssim 5\text{\AA}$, see Fig. 5.11(a)) and does not continue to rise monotonically from the potential well.

In the blue wing for Xe, unlike the red wing, the UFC and AC profiles differ markedly from each other, and neither of them shows a good agreement with the observation. This implies we should make some more realistic assumption for $\Delta V(R)$ on the repulsive side;

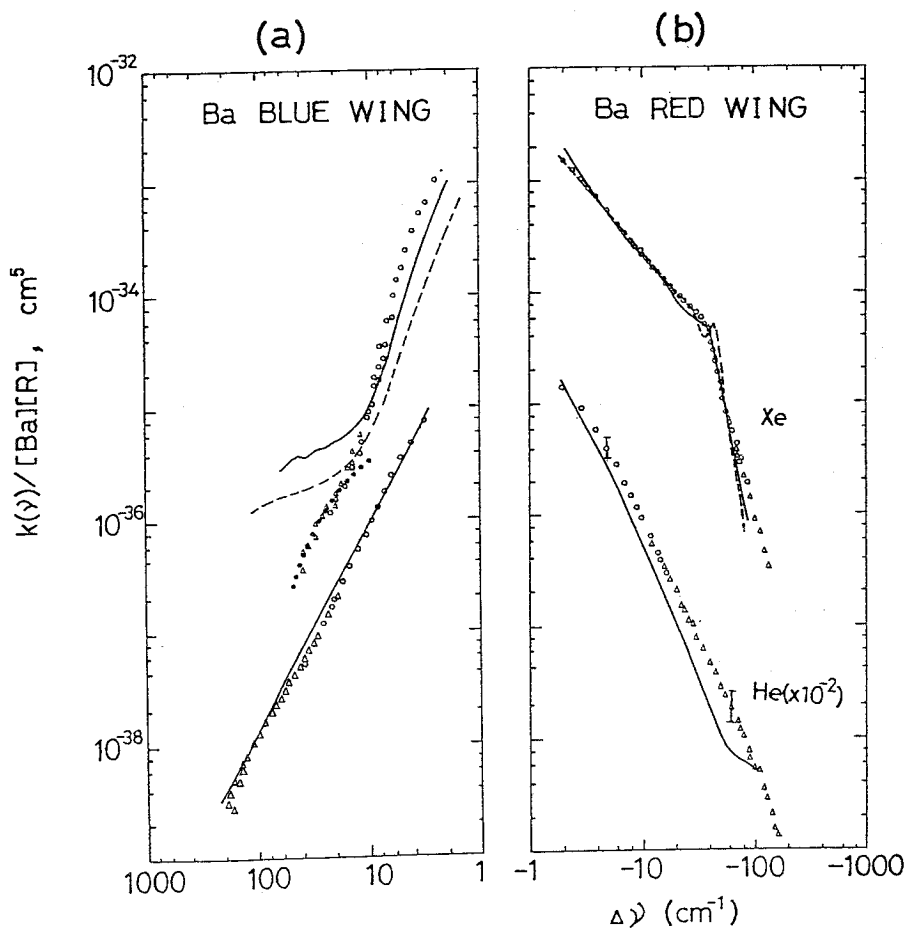


Fig. 5.10 Comparison of the calculated profile with the observations for Xe and He.

The full curves corresponds to the AC analysis, while the dashed and dotted curves (the latter appears in (a) for Xe) correspond to the UFC analysis with ΔV_{LJ} and $\Delta V_{\text{Q+}}$, respectively.

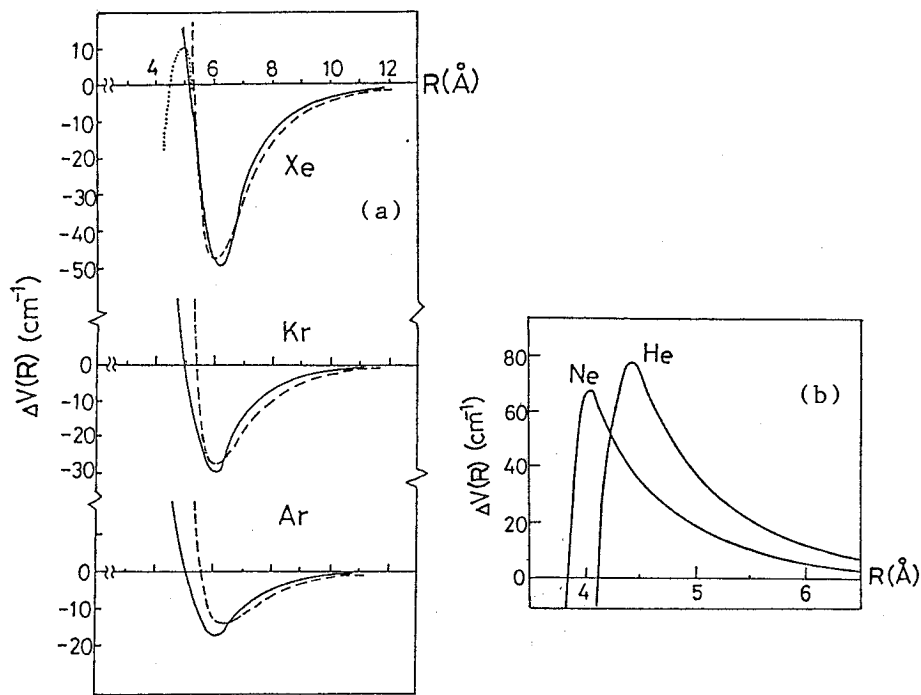


Fig. 5.11 The potentials $\Delta V(R)$ deduced for Ba-Xe, Ba-Kr and Ba-Ar (a) and Ba-Ne and Ba-He (b). The full curve corresponds to the AC analysis, while the broken and the dotted (for Xe) curves correspond to the UFC analysis with ΔV_{LJ} and $\Delta V_{\text{Q+}}$, respectively.

Table 5.4 Potential parameters deduced from the AC analysis.

Parameter	Xe	Kr	Ar	Ne	He
$\epsilon (\text{cm}^{-1})$	-50	-30	-18	70	80
$R_0 (\text{\AA})$	6.2	6.2	6.2	4.0	4.4
κ	-80	-80	-90	-800	-400

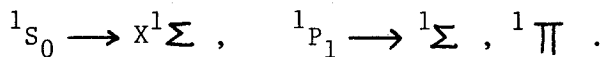
for example the strong tail of the UFC profile at $10 < \Delta \gamma < 40 \text{ cm}^{-1}$ is greatly improved by introducing ΔV_{Q+} (see the dotted curve). If we use a steeply rising function $\Delta V(R)$, like the Lennard-Jones form, the intensity of this tail region is mainly determined by real Condon points of $R_c \approx 5 \text{ \AA}$. In contrast, with ΔV_{Q+} the intensity is determined only by complex Condon points, which is the reason of the weak intensity. We find in Fig.5.11 (a) that ΔV_{Q+} is smoothly connected to the attractive side of $\Delta V(R)$.

For Ba-He we made only the AC analysis with a repulsive potential with a sharp peak near $R = 4.5 \text{ \AA}$ to explain the diffuse blue-wing. This potential fails to explain the red-wing profile. This may indicate, like the above discussion for Xe, that the potentials should be further refined in the future.

For Ba-Ar, we have measured the van der Waals coefficient ΔC_6 from the impact analysis for the line-core region (see Table 4.2). As previously described, classical impact analysis yields long-range interactions near Weisskopf radius (typically $\rho_w \sim 10 \text{ \AA}$ for Ba-Ar). The present AC analysis is based on the same potential form for the long-range interaction at $R_m \leq R$, therefore we may expect the ΔC_6 value has a comparable magnitude with the above result. From the deduced parameter in Table 5.4 for Ar and the relations (4.16), we obtain $\Delta C_6 = 2.3 \times 10^{-58} \text{ erg} \cdot \text{cm}^6$, which is comparable to the value $1.4 \times 10^{-58} \text{ erg} \cdot \text{cm}^6$ deduced from the impact analysis. The slight difference may be understood if ΔC_6 value from the AC analysis is affected by the short-range interaction, since $R_m (\sim 6.5 \text{ \AA})$ is smaller than ρ_w .

Finally we discuss how the deduced $\Delta V(R)$ is related to the

molecular potentials in a simple manner taking Ba-Xe and Ba-He pairs as examples. Like the previous discussion for Sr, the atomic states 1S_0 and 1P_1 of Ba generate three molecular states in the collision with a rare-gas atom.



$\Delta V(R)$ is defined as the difference of interatomic potentials for these states. We can show as follows that for Ba-Xe the $\Delta V(R)$ may be attributed to $V(^1\Pi) - V(X^1\Sigma)$ on the analogy of alkali-rare-gas potentials.

To consider the R dependence of these potentials, we firstly make a rough estimate of the interatomic distance R' where these states show a strongly repulsive character due to the electronic-charge overlap. Baylis (1969 b) gives an estimate for alkali-rare-gas pairs as follows;

$$\begin{aligned} R' &= \sqrt{\langle r_S^2 \rangle} + \sqrt{\langle r_R^2 \rangle} && \text{for } S\Sigma, \\ &= \sqrt{0.6 \langle r_P^2 \rangle} + \sqrt{\langle r_R^2 \rangle} && \text{for } P\Pi, \\ &= \sqrt{1.8 \langle r_P^2 \rangle} + \sqrt{\langle r_R^2 \rangle} && \text{for } P\Sigma. \end{aligned} \quad (5.24)$$

Here $\langle r_S^2 \rangle$ and $\langle r_P^2 \rangle$ are the mean squared radii of the valence electron in s and p orbitals respectively, which are calculated by the Bates-Damgaard-type wavefunctions (Bates and Damgaard 1949). The mean squared radius of the outer most electron of the rare-gas atom, $\langle r_R^2 \rangle$, is calculated by the Gombas' wavefunction (Gombás 1967). If we can use (5.24) for Ba-Xe, R' is calculated to be 3.4, 3.7 and 5.7 Å for the $X^1\Sigma$, $^1\Pi$ and $^1\Sigma$ states respectively.

On the contrary at large R , these states show a somewhat attractive character due to the electrostatic interaction, so that they have wells at some intermediate R . The ground state of Cs-Xe has a well of depth $\sim 110 \text{ cm}^{-1}$ at $R \sim 5 \text{ \AA}$ (Buck and Pauly 1968). Since there is not a great difference between Ba and Cs for the size of the electronic wavefunction in the ground state, we may assume by analogy that the $X^1\Sigma$ state of Ba-Xe has a similar potential well. Since $^1\Sigma$ state is strongly repulsive at $R \gtrsim 5 \text{ \AA}$, the $^1\Pi$ state is the only candidate to have a weakly attractive character like $X^1\Sigma$ state in this R region (see the schematic drawing in Fig.5.12 (a)). To explain the deduced $\Delta V(R)$ for Ba-Xe in Fig.5.11, the $^1\Pi$ state must have a deeper potential well than that of $X^1\Sigma$ state at $R \approx 6.2 \text{ \AA}$. The low positive peak of ΔV (the dotted curve in Fig.5.11) introduced to explain the diffuse blue-wing shoulder, may be understood if double crossing of these curves occur at $R \sim 5 \text{ \AA}$. (see Fig.5.12(b)). Cheron et al (1977) gave a similar explanation for the shoulders observed in both wings of $Tl 3776 \text{ \AA}$ line perturbed by Xe.

The repulsive potential for Ba-He (Fig.5.11 (b)) may be similarly discussed. In this case, due to the small polarizability of rare gases, the potentials are estimated to be purely repulsive or only weakly attractive. If the $X^1\Sigma$ state is less repulsive at large R than the upper state ($^1\Sigma$ or $^1\Pi$, not specified) and a crossing occur at $R \sim 4 \text{ \AA}$ as shown in Fig.5.12 (c), the potential difference will show a similar character to that deduced.

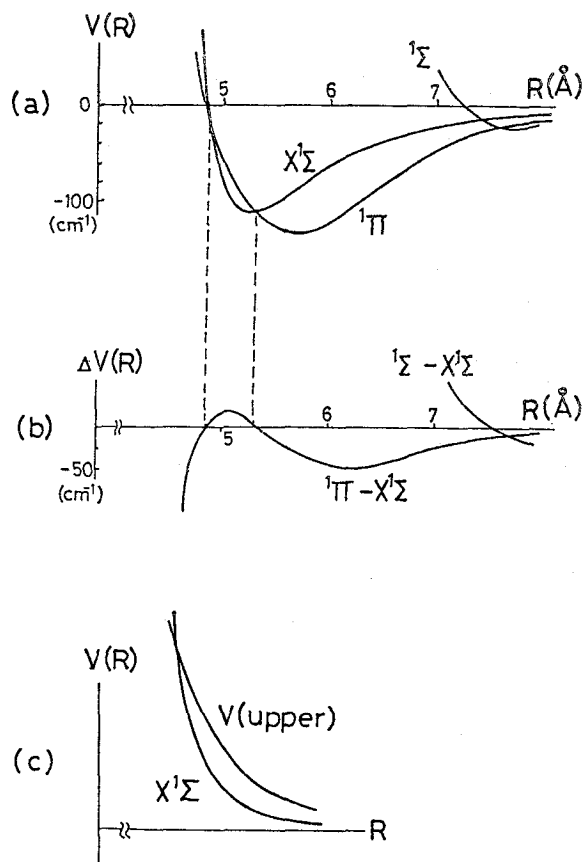


Fig.5.12 Schematic figures of the interatomic potentials for (a) Ba-Xe, (b) their difference, and (c) the interatomic potentials for Ba-Ne and Ba-He.

Chapter 6. Discharge-cell experiments

6.1 Introduction

In this chapter we present an absorption measurement of Ar-Ar pairs using a discharge cell. In various kinds of discharges in rare gases, including recently developed excimer lasers, the lowest excited states play important roles as the energy pooling states due to their high population densities. For the measurements of the population densities of these states using the absorption and the laser-induced fluorescence techniques, precise knowledge of the broadening and shift of spectral lines terminating upon these levels is required.

When the colliding atoms are identical, resonance interaction becomes important, since there is a finite probability of energy exchange between these atoms (see 3.2.1 for the line-broadening mechanism). This type of interaction becomes effective when the upper or lower state of a spectral line has a large dipole-transition probability to the ground state (here we assume the perturbers are in the ground state). In the present experiment we investigate three atomic lines of argon at 8115, 8104 and 8404°A . Relevant energy levels (Moore 1971) are shown in Fig.6.1, where we find the 8104 and 8404°A lines terminate upon the resonance states $1s_4$ (Paschen notation) and $1s_2$ respectively which are strongly connected to the ground $1p_0$ by dipole transition (namely the resonance transitions). Therefore these lines are expected to be broadened largely by resonance interaction.

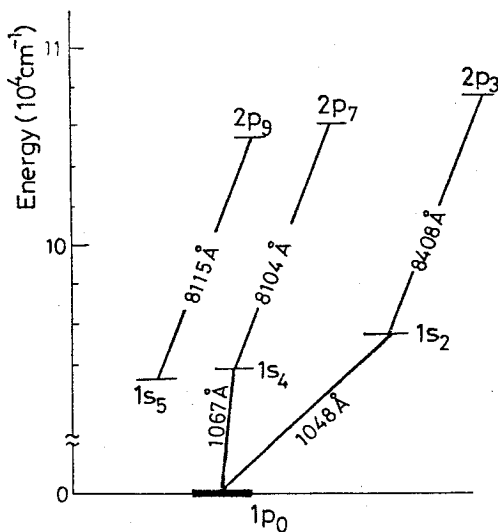


Fig. 6.1

Relevant energy level diagram of argon (in Paschen notation).

In this case these lines will show only the collision shift which is proportional to argon density and no shift (see (2.27) and (3.5)). On the other hand the 8115 \AA line terminates upon the lowest metastable state $1s_5$, so that the resonance interaction gives no contribution to the broadening. In this case the van der Waals interaction becomes important as the foreign-gas broadening and, according to the classical theory (2.29), we may observe a collision shift for this line.

Most of the previous measurements of Ar-Ar pair at low pressures have been carried out on the emission lines using a high resolution Fabry-Perot interferometer (e.g. Hindmarsh and Thomas 1961). In the present study we use a tunable diode laser as a light source for the absorption measurement. This method is effective for the lines which are suffered from the difficulties of self absorption in the emission measurements. Moreover in this method, we can expect a very small instrumental width, which

is determined by the laser spectral width $\sim 1\text{MHz}$ (see Takakura et al 1980 and references therein). Though there are some examples of using infrared diode lasers for the line-profile measurements of simple molecules (see e.g. Varghese and Hanson 1981), there is no example to the author's knowledge of using near-infrared diode lasers for spectroscopy of rare gases except for the measurement of the decay of excited kripton atoms in the afterglow of a pulsed discharge (Ku et al 1973). In the next section we show the experimental setup and the method of deconvolution of the observed profile, and give the results and discussions in the following sections.

6.2 Experiment

Fig.6.2 shows the experimental arrangement. A TS-type GaAlAs diode laser (Sugino et al 1979) operating at room temperature was mounted in a box, whose temperature was stabilized using a thermo-electric element. Two different diode lasers were used for the wavelength regions of around 8100 and 8400\AA . Coarse wavelength tuning was performed by controlling the temperature, while fine tuning was done by varing the injection current. The stability of the operating temperature was about $\pm 5 \times 10^{-4}\text{K}$, which corresponds to $\pm 14\text{MHz}$ in frequency scale, within a typical measuring time of 10 minutes. The frequency of the laser was swept over the absorption line profile by applying a sawtooth pulse to the injection current. Typical frequency-sweep range was 10GHz . A frequency mark was obtained at every 500MHz by a hemispherical etalon whose spacing is

15 cm. The main longitudinal mode was separated from the small additional longitudinal modes by a monochromator of focal length 50 cm. The transverse mode was ascertained to be single. The laser power was reduced to less than 0.1 mW mm^{-2} by neutral density filters in front of the absorption tubes to avoid the disturbances due to the pumping effects.

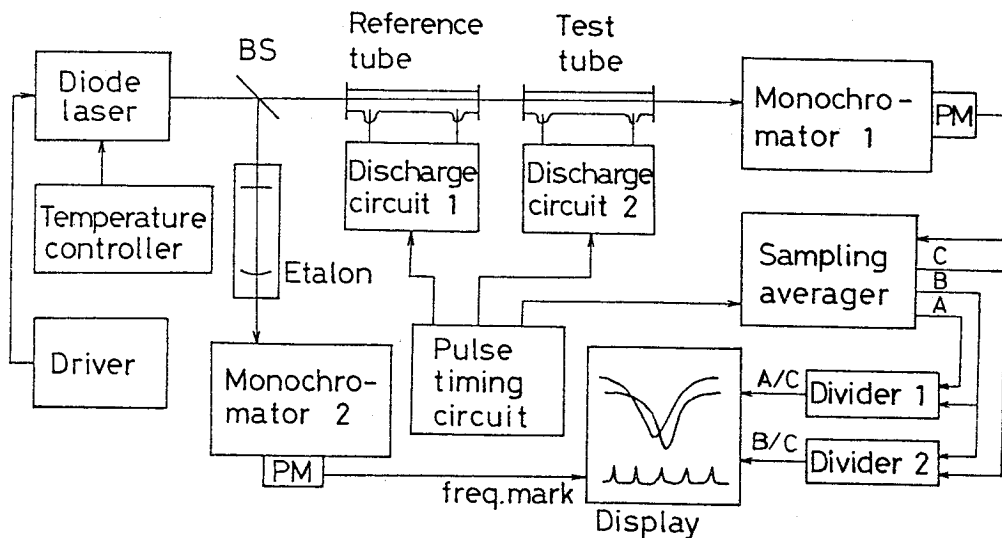


Fig.6.2 Schematic diagram of the experimental arrangement.

Two discharge tubes were used; one for the fixed-pressure reference tube of 20 mm inner diameter and the other for the variable-pressure test tube of 8 mm inner diameter. Absorption was measured through the uniform positive column of 20 cm in length in each tube. Discharge current was adjusted so that the absorption

was well below saturation, say less than 70 %. Typical values of the discharge current were 0.2 mA for the measurement of 8115\AA line, 0.2 to 1 mA for the 8104\AA line, and 1 to 10 mA for the 8408\AA line respectively. The filling-gas pressure was varied from 1 to 40 Torr for the test tube, while that of the reference tube was fixed at 1 Torr.

Two different measurement procedures were used. In the first method (see Fig.6.2), the three signals A, B and C which correspond respectively to the signal absorbed by the reference tube, that by the test tube, and the background signal without absorption were sampled by a three-channel sampling averager from the same laser beam according to the time chart shown in Fig.6.3.

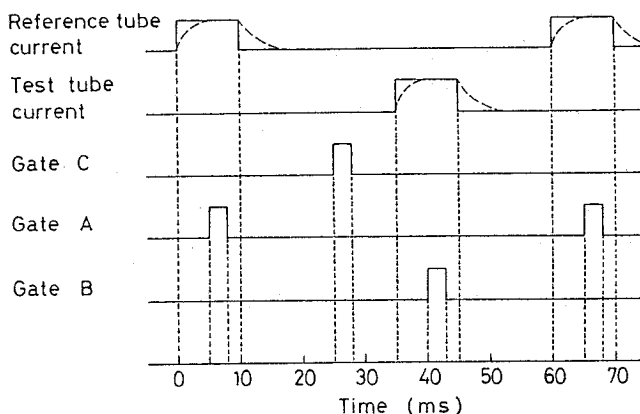


Fig.6.3 Time chart for the absorption measurement.

Typical waveforms for the long-lived excited-state density are shown by the dashed lines. Gates A and B are opened when the quasi-steady states are reached and C is opened when the excited-state density is zero.

The frequency-sweep time was 5 to 10 minutes with an averaging time constant of 0.1 sec.. In the second method a waveform of the transmitted intensity was sampled at 200 points within one frequency sweep (the sweep time was 0.1 sec.). Ten successive sweeps were additively superposed. The three waveforms corresponding to the three signals mentioned above were measured successively and stored in a memory of a micro-computer. The acquisition time for a complete set of data was about 2.5 minutes in this case, which is shorter than that in the first method. When the absorbed signals were divided by the corresponding background signal, the change in the laser output power due to the frequency sweep was compensated and the absorption profiles were obtained on flat backgrounds. The fact that the results obtained by the above two methods agree with each other shows that the stability of the reproducibility of the injection current in the second method were good enough.

Fig.6.4 shows an example of the absorption profiles for the 8104\AA line obtained by the second method, where the frequency scale was linearized by the frequency marks. The absorption profile for the reference tube (hereafter referred to as the reference profile) shows small shoulders on both sides at a frequency displacement of ~ 1 GHz from the line center, though these are not clear for the profile for the test tube (test profile) because of the large broadening. The reason for this profile can be understood if we assume that the spectral structure of the laser is composed of a main peak and small subpeaks on both sides. This kind of structure has been observed in various types of diode lasers (Umeno et al

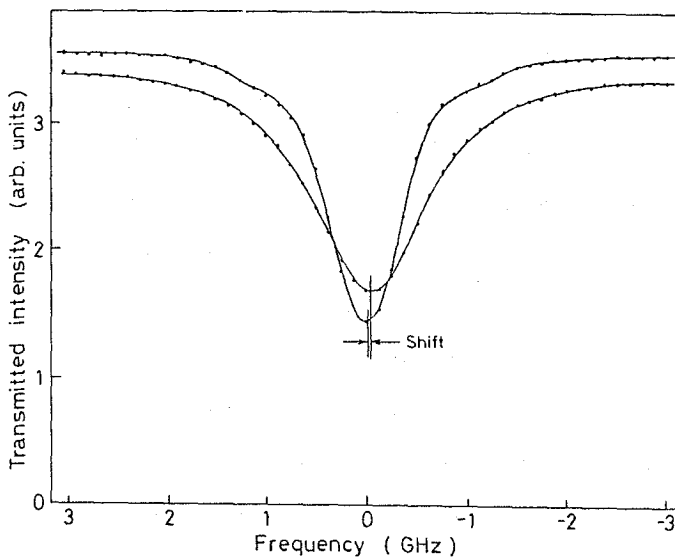


Fig.6.4 Typical transmission profiles for the 8104\AA line.
Upper trace: reference profile (the argon pressure is 1 Torr). Lower trace: test profile (23 Torr).

unpublished). The amplitude and the displacement of the subpeaks depend on the structure of the diode laser itself and also on the operating condition. One possible reason may be a resonance amplification of noise in the active region. There is no data so far on the width of the subpeaks, however an assumption that the width is the same as that of the main peak (~ 1 MHz) would not produce appreciable errors in the final results because of the smallness of the subpeaks. Actually, we can obtain a satisfactory fit to the measured reference profile in Fig.6.4 in a way described below, if we take a value of 5 % as the amplitude ratio of the subpeaks to the main peak, and a value of 1 GHz as the frequency displacement from the main peak.

We assume that the observed (both test and reference) transmission profiles are composed of three components, namely those of the main peak ($i = 1$) and the above two subpeaks ($i = 2$ and 3), thus

$$I(\Delta\omega) = \sum_{i=1}^3 I_0 g_i \exp[-k_i(\Delta\omega) \ell]. \quad (6.1)$$

Here I_0 is the normalized background intensity, g_i and k_i are respectively the weight factor and the absorption coefficient at a frequency distance $\Delta\omega$ from the line center, and ℓ ($= 20 \text{ cm}$) is the absorption length. We further assume $k_i(\Delta\omega)$ is given by a Voight function (4.20) centered at ω_i from the main peak (we put $\omega_1 = 0$)

$$k_i(\Delta\omega) = k_0 \frac{a}{\pi} \int_{-\infty}^{\infty} \frac{\exp(-y^2)}{a^2 + (\Delta\omega - \omega_i - y)^2} dy, \quad (6.2)$$

where k_0 is the absorption coefficient at the line center, and a is the ratio of the Lorentz width τ_L to the Doppler width τ_D . In practice we used an approximate formula for (6.2) of Whiting (1968) (details of the analysis is described by Tachibana et al 1982). The relative frequency shift (see Fig.6.4) is obtained from the difference of line centers for the test and reference profiles.

6.3 Results and discussions

Fig. 6.5 shows the obtained broadening $2\gamma_L$ and shift β for the 8115\AA line. We find they are proportional to the argon density and the straight lines which give good fits to the data go through the origin. This indicates that the observed broadening and shift are determined by the binary collision between argon atoms, and other mechanisms which also yield Lorenzian broadenings, such as natural or Stark broadening, can be neglected in the present case. Since the resonance interaction gives no collision shift, the dominant interaction is not this type. The most probable interaction is the van der Waals type. This is supported by the following consideration on the temperature dependence of the broadening and shift.

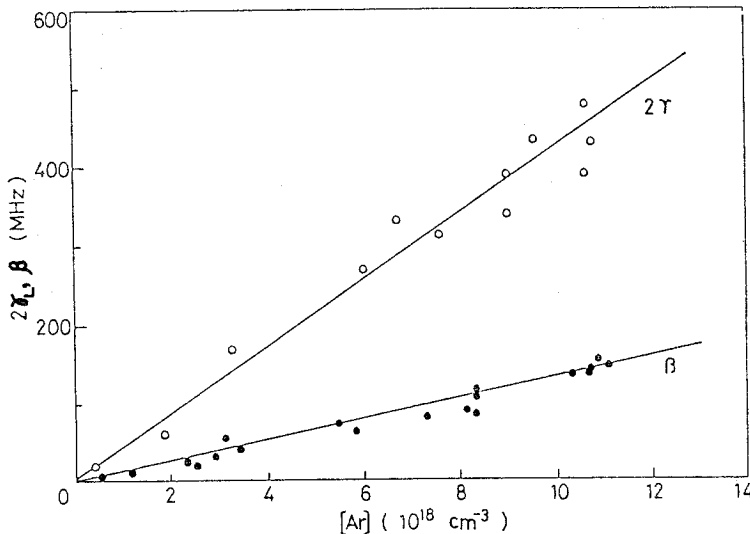


Fig. 6.5 Broadening and shift for the 8115\AA line as functions of the argon density.

Table 6.1 gives the observed broadening- and shift-coefficients, $2\gamma_L/[\text{Ar}]$ and $\beta/[\text{Ar}]$, together with other data for comparison. For the 8115\AA line, high temperature data are reduced to the present condition ($\sim 300\text{K}$) using the relations

$$2\gamma_L/[\text{Ar}] , \quad \beta/[\text{Ar}] \propto T^{0.3} . \quad (6.3)$$

These relations can be derived from the classical impact result for the van der Waals interaction (2.29), i.e. $\gamma_L, \beta \propto \bar{v}^{3/5}$ and the definition of the mean relative velocity $\bar{v} = (8kT/\pi\mu)^{1/2}$, where k and μ are the Boltzmann constant and the reduced mass respectively. We find our broadening coefficient $2\gamma_L/[\text{Ar}]$ agrees fairly well with the reduced value of Vallee et al (1977). As for the shift coefficient $\beta/[\text{Ar}]$, our result agrees well again with that of Vallee et al, while those of Aeschliman et al (1976) and Copley and Camm (1974) are about two times as large as ours. Since these authors did not measure the broadening coefficient because of the self-absorption difficulties, we can not discuss this difference from the viewpoint of $2\gamma_L/\beta$, i.e. the broadening-to-shift ratio. This gives a measure of the consistency of the measurements. If we assume the van der Waals interaction is dominant between the colliding atoms, we get $2\gamma_L/\beta = 2.8$ from the classical impact theory (2.29). Although our result ($= 3.2$) is slightly larger than this value, this difference may be understood if we introduce a higher order term into the interaction. For example, for the Lennard-Jones potential $\Delta V(R) = \Delta C_{12}R^{-12} - \Delta C_6R^{-6}$, we get (see Hindmarsh et al 1967 for the derivation)

$$2\gamma_L/\beta = 4 B(\alpha) / S(\alpha) . \quad (6.4)$$

Table 6.1 Broadening and shift coefficients.

		temperature		
		3900K ^a	1130K ^b	300K ^c
8115 ^o	2.9±0.3	—	—	1.42±0.14
$2\gamma_L/[\text{Ar}]$	(1.3±0.1)			
$(10^{-20} \text{ cm}^{-1} \text{ cm}^{-3})$	8104 ^o	4.0±0.4	4.30±0.18	3.72±0.76
	8408 ^o	10.1±1.3	16.2±1.0	—
8115 ^o	9.6±1.1	12.2	7.18±0.38	4.4±0.4
$\beta/[\text{Ar}]$	(4.4±0.5)	(8.2)		
$(10^{-21} \text{ cm}^{-1} \text{ cm}^{-3})$	8104 ^o	7.4±1.1	—	3.43±0.15
	8408 ^o	0.5±0.5	—	0.0±0.5

a: Vallee et al (1977).

b: Copley and Camm (1974).

c: Aeschliman et al (1976).

d: Our result.

The () denote reduced values to 300K by the $T^{0.3}$ dependence.

Here B and S are functions of $\alpha = K \bar{v}^{1.2} \Delta C_{12} \Delta C_6^{-2.2}$ (K is a constant) and tabulated by Hindmarsh et al. We find from their result that if we take $\alpha \sim 0.7$, we get our result $2\gamma_L/\beta = 3.2$.

Fig. 6.6 shows the broadening of the 8104 and 8408Å lines. For the 8408Å line no appreciable shift was observed. This implies that the resonance interaction is predominant in this case. This is supported by the fact that the broadening coefficient in Table 6.1 has no clear temperature dependence as predicted by (3.5). In this case we can calculate the oscillator strength f of the resonance line at 1048Å ($1p_0 - 1s_2$) from the measured coefficient and from (3.5).

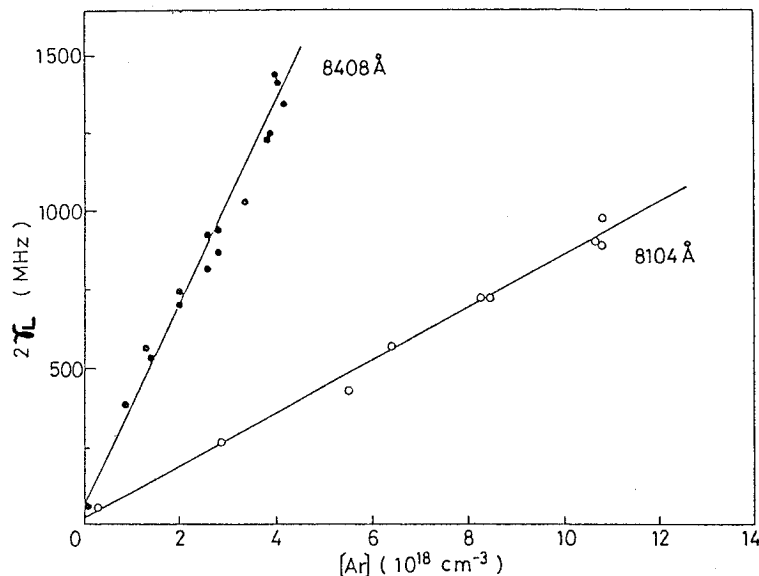


Fig. 6.6 Broadenings of the 8104 and 8408Å lines as functions of the argon density.

Using the value $k_{jj} = 1.45$ (Omont 1966, which is supported by the experiment of Vaughan 1966 for He), we get $f = (207 \pm 20) \times 10^{-3}$. For the 8104\AA line, a small red shift was observed, yet it has a very small temperature dependence for the broadening coefficient (see Table 6.1). This indicates that the main interaction for the 8104\AA line is the resonance interaction, but a small van der Waals interaction should be added to it. A mixing of these interactions is discussed by Lewis (1967). According to his theory, we estimate that about 4 % of the measured broadening coefficient is attributed to the van der Waals interaction, and also calculated the oscillator strength for another resonance transition at 1067\AA ($1p_0 - 1s_4$) to be $f = (49 \pm 5) \times 10^{-3}$. Westervelt et al (1979) give a comprehensive list of f values for these resonance transitions obtained by various methods. Experimental and theoretical values listed therein range from 0.098 to 0.083 for the 1067\AA line and from 0.170 to 0.350 for the 1048\AA line. Our values lie within these ranges, and we note a satisfactory agreement is obtained with the fluorescence decay data of Lawrence (1968) (0.059 and 0.228).

To conclude, absorption line profiles of argon spectral lines have been investigated using GaAlAs diode laser as a light source. For 8115\AA line, which terminates upon the metastable state $1s_5$, the measured broadening coefficient shows a good agreement with the theory if we assume the van der Waals interaction is dominant in the collision of argon atoms. However the measured broadening-to-shift ratio shows a slight discrepancy with a theoretical prediction. This indicates higher order terms such as ΔC_{12} repulsive term should be included into the interaction. For the

8408 Å^o line, which terminates upon the resonance state $1s_2$, no shift was observed. This indicates the resonance interaction essentially determines the broadening in this case. This is supported by the fact that the broadening coefficient shows no temperature dependence. For the 8104 Å^o line, which terminates upon another resonance state $1s_4$, a small red shift was observed, and the temperature dependence of the broadening coefficient was quite small. This indicates that the dominant factor is the resonance interaction, and the van der Waals interaction should be slightly added. From the latter two lines, the oscillator strength of the resonance transitions were evaluated. The result shows a good agreement with previous investigations.

Chapter 7. Conclusions

The results and conclusions obtained in the present work are summarized as follows.

In Chapter 1 we have made a brief review of the collision broadening experiments of atomic spectral lines and classified the broadening mechanism by the species of perturbers. In the collision of neutral atoms, the diatomic systems composed of alkali-, alkaline-earth- and rare-gas-atoms are the subjects of continual interest from the viewpoint of stellar-spectra analyses, and a possible source of future gas lasers. Among them, alkaline-earth-rare-gas pairs have not yet been studied in detail due to the experimental difficulties, and theoretical investigations on the interatomic potentials for these pairs are also scarce.

In Chapter 2 we have reviewed collision-broadening theories which are used in the present work for the profile analyses. We have seen that the theories are closely connected to the interatomic potentials of the colliding atoms. The theories are classified as follows:

- (1) the classical impact- and quasi-static-limits which are applicable respectively to the line-core- and wing-regions of the spectra,
- (2) the general theory which spans a bridge between these two limiting cases,
- (3) the quantum UFC theory in which the perturber's motion is represented by the WKB approximate wavefunction.

In Chapter 3 some representative methods to calculate the interatomic potentials have been introduced. By the perturbation

method which is applicable to long-range interactions we have seen that

- (1) when the colliding atoms are identical, the leading term of interaction is the resonance type, which varies with the interatomic distance R as R^{-3} ,
- (2) when the colliding atoms are different, it is the van der Waals type of interaction, which varies as R^{-6} .

For the calculation of the short-range interactions two approximate methods, the Gombás' pseudopotential and the Fermi potential, have been introduced. Both of them are valid when the charge overlap of colliding atoms is not significant. In this method we can calculate the interaction for a wide range of R .

In Chapter 4 we have described the shock-tube experiments. From the absorption measurement of Ca-Ar and Ba-Ar pairs, we have found that the long-range interactions between these atoms are dominated by the van der Waals interaction. The deduced van der Waals coefficients agree well with previous results obtained at relatively low temperatures. From the emmision measurement of Ca^+ -Ar pair we have found that the van der Waals interaction is important in this case too in the long-range interatomic distance. From the comparison between the results of Ca^+ -Ar and K-Ar pairs, where the latter one is measured by other authors, we have found that the Ca^+ -Ar pair has the larger broadening coefficient. We have discussed the difference based on the model potential of Baylis, and found it may be attributed to the compact valence-electron cloud of Ca^+ .

In Chapter 5 we have described the heat-pipe-cell experiments. We have found that when perturbers are heavy rare gases (Ar, Kr and Xe) the absorption profiles for both strontium and barium show strong asymmetries and have satellites in the red wing. From the profiles we have deduced empirical interatomic potentials. They have the following characteristics:

- (1) the long-range interactions (typically $R \gtrsim 10 \text{ \AA}^\circ$) are well described by the van der Waals type of potentials,
- (2) however, the short-range interactions (typically $R \lesssim 5 \text{ \AA}^\circ$) show strongly repulsive character due to the electronic-charge overlap,
- (3) and they have wells at some intermediate interatomic distance ($R \sim 6 \text{ \AA}^\circ$).

When perturbers are light rare gases (He and Ne) the potentials show mainly repulsive character. We have discussed how these empirical potentials are explained on the analogy of the Baylis' model potentials for alkali-rare gas.

In Chapter 6 we have described the discharge-cell-experiment for Ar-Ar pair. We have seen that for transitions whose lower state is the resonance state, the resonance interaction essentially determines the collision broadening and yields no shift in the line-core spectra. For a transition whose lower state is the lowest metastable state, we have found that the van der Waals interaction determines the collision broadening and shift.

In conclusion, we have investigated collisionally broadened spectra for some pairs including alkaline-earth and rare-gas atoms. In most combinations of atoms the long-range potentials are well

described by the van der Waals interactions. For some pairs the deduced interaction coefficients agree well with results of simple calculations based on the hydrogenic model of atoms. From the wing-region spectra we have deduced empirical potentials in the relatively short interatomic distance. We can not predict these potentials at present by ab initio calculations, e.g. the SCF method. This is a remaining problem. However we believe, as the final comment, that the present results will be used in analysing various experimental observations of atomic collisions including these elements.

Acknowledgement

The author would like to express his sincere appreciations to the staff members of the Urano Laboratory, Department of Electronics, Kyoto Technical University; Professor Y.Urano helped the author with experiments, made lots of stimulating discussions, carefully read the manuscript, and gave him continuous encouragement. Professor K.Tachibana helped the author with experiments, made fruitful discussions and gave him helpful advice. Mr.S.Oshima helped the author to provide various experimental equipments.

Special thanks are due to Professors S.Fujita, A.Mitsuishi and S.Minami of Department of Applied Physics, Osaka University for the critical reading of the thesis and important suggestions. Thanks are also due to Professor S.Nakashima of Department of Applied Physics for the encouragement.

The author is very greatful to Professor J.F.Kielkopf of University of Louisville, USA, who kindly instructed the author in the detail of the AC analysis of the line shape and freely made available his excellent program used in Chapter 5. He is also indebted to Professor D.G.McCartan of University Newcastle upon Tyne, England, who gave him valuable advice in constructing the absorption cell used in the experiments in the same chapter. Thanks are also due to Dr.P.Julienne of NBS, Washington, USA, who made valuable discussions on the Sr-Ar potential, and showed the author his calculations prior to publication.

Finally, the author is deeply grateful to his wife, Kayo, for the continuous encouragement and the skillful typing.

References

Aeschliman D P, Hill R A and Evans D L 1976 Phys. Rev. A 14 1421-7

Anderson P W 1952 Phys. Rev. 86 809

Ayres T R 1977 Astrophys. J. 213 296-308

Baranger M 1958 Phys. Rev. 111 481-93

Baranger M 1962 Atomic and Molecular Process , edited by D R Bates (New York: Academic Press)

Bates D R and Damgard A 1949 Phil. Trans. Roy. Soc. London A242 101-22

Baur J F and Cooper J 1977 J. Quant. Spectrosc. Radiat. Transfer 17 311-22

Baylis W E 1969a J. Chem. Phys. 51 2665-79

— 1969b JILA Report No 100 , University of Colorado, Boulder, Colorado

Bottcher C, Cocken K K and Dalgarno A J. Phys. B: At. Mol. Phys. 8 1756-64

Bowman N J and Lewis E L 1978 J. Phys. B: At. Mol. Phys. 11 1703-11

Breene R G 1961 The Shift and Shape of Spectral Lines (Oxford: Pergamon)

— 1981 Theories of Spectral Line Shape (New York: John Wiley & Sons)

Buck U and Pauly H 1968 Z. Phys. 208 390-417

Carlsten J L, Szöke A and Raymer M G 1977 Phys. Rev. A 15 1029-45

Chen S Y and Lonseth A T 1971 Phys. Rev. A 3 946-50

Chen C L and Phelps A V 1973 Phys. Rev. A 7 470-9

Chen S Y and Takeo M 1957 Rev. Mod. Phys. 29 20-73

Chen S Y and Wang S Y 1978 Acta Phys. Pol. A 54 721-8

Cheron B, Scheps R and Gallagher A 1977 Phys. Rev. A 15 651-60

Cooper J 1967 Rev. Mod. Phys. 39 167-77

Copley G H and Camm D M 1974 J. Quant. Spectrosc. Radiat. Transfer 14 899-907

Corney A and McGinley J V M 1981 J.Phys. B: At. Mol.Phys. 14 3047-67

Dalgarno A and Kingston A E 1960 Proc. R. Soc. A 259 424-9

DePrima C R and Penner S S 1955 J.Chem. Phys. 23 757-8

Dalgarno A and Kingston A E 1960 Proc. R. Soc. A 259 424-9

DePrima C R and Penner S S 1955 J. Chem. Phys. 23 757-8

Driver R D and Snider J L 1976 Astrophys. J. 208 518-24

Düren R 1980 Adv. At. Mol. Phys. 17 55-100

Farr J M and Hindmarsh W R 1971 J. Phys. B: At. Mol. Phys. 4 568-73

Fermi E 1934 Nuovo Cim. 11 157-66

Foley H M 1946 Phys. Rev. 69 616-28

Giles R G and Lewis E L 1981 Spectral line Shape (Berlin: Walter de Gruyter)

Giusti-Suzor A and Roueff E 1975 J. Phys. B: At. Mol. Phys. 8 2708-17

Gombás P 1967 Pseudopotentiale (New York: Springer)

Griem H 1964 Plasma Spectroscopy (New York: McGraw-Hill)

— 1974 Spectral Line Broadening by Plasmas (New York: Academic Press)

Hammond G 1975 Ap. J. 196 291-305

Harima H, Tachibana K and Urano Y 1980 Ôyô Butsuri 49 124-8
(in Japanese)

Herzberg G 1950 Molecular Spectra and Molecular Structure I. Diatomic Molecules (New York: Van Nostrand Regional Offices)

Hindmarsh W R and Farr J M 1972 Collision Broadening of Spectral Lines by Neutral Atoms (Oxford: Pergamon)

Hindmarsh W R, Du Plessis A N and Farr J M 1970 J. Phys. B: At. Mol. Phys. 3 L5-8

Hindmarsh W R, Petford A D and Smith G 1967 Proc. R. Soc. A 297 296-304

Hindmarsh W R and Thomas K A 1961 Proc. Phys. Soc. 77 1193-6

Holmes Q A, Takeo M and Chen S Y 1969 J. Quant. Spectrosc. Radiat. Transfer 9 769-73

Holstein T 1950 Phys. Rev. 79 744

Honing R E and Kramer D A 1969 RCA Review 30 285-305

Jablonsky A 1945 Phys. Rev. 68 78-93

Julienne P 1981 private communication

— 1982 private communication

Kelley F M, Koh T K and Mathur M S 1974 Can. J. Phys. 52
795-802

Kielkopf J F 1978 J. Phys. B: At. Mol. Phys. 11 25-36

1981 Spectral Line Shapes (Berlin: Walter de
Gruyter)

Kirkwood J G 1932 Z. Physik 33 57-

Koide A 1976 J. Phys. B: At. Mol. Phys. 9 3173-83

Kosasa K, Maruyama Y and Urano Y 1976 Bunko Kenkyu 25 246-50
(in Japanese)

Kramer H L and Herschbach D R 1970 J. Chem. Phys. 53 2792-800

Ku R T, Verdeyen J T, Cherrington B E and Eden J G 1973 Phys.
Rev. A 8 3123-30

Kuratani K and Tsuchiya S 1968 Shock Wave in Chemistry and
Physics (in Japanese) (Tokyo: Shôkabô)

Lawrence G M 1968 Phys. Rev. 175 40-4

Lewis E L 1967 Proc. Phys. Soc. 92 817-25

1980 Phys. Rep. 58 1-71

Lindholm E 1945 Arkiv. Mat. Astr. Phys. 32 A, No.17

London F 1930 Z. Physik 63 245-79

Lorentz H A 1906 Proc. R. Acad. Sci. Amsterdam 8 591-

Mahan G D 1969 J. Chem. Phys. 50 2755-8

Malvern A R 1978 J. Phys. B: At. Mol. Phys. 11 831-45

Margenau H 1931 Phys. Rev. 38 747-56

Margenau H and Watson W W 1936 Rev. Mod. Phys. 8 22-53

Marlow W C 1967 Appl. Opt. 6 1715-24

McCartan D G and Farr J M 1976 J. Phys. B: At. Mol. Phys.
9 985-94

Michelson A A 1895 Astrophys. J. 2 251-63

Miles B M and Wiese W L 1969 At. Data 1 1-17

Mitchell A C G and Zemansky M W 1971 Resonance Radiation and
Excited Atoms (London: Cambridge University Press)

Moore C E 1971 Atomic Energy Levels, NBS Circular No 467,
vols 1,2,3. (Washington DC: US Govt Printing Office)

Müller A 1936 Proc. R. Soc. A 154 624-39

O'Malley T, Spruch L and Rosenberg L 1961 J. Math. 2 491-8

Omont A 1966 C. R. Acad. Soc. Paris 262 B 190-3

O'Neill and Smith G 1980 *Astron. Astrophys.* 81 100-107
Pascale J and Vandeplanque J 1974 *J. Chem. Phys.* 60 2278-89
Peach G 1980 *Adv. Phys.* 30 367-474
Penkin N P and Shabanova L N 1968 *Opt. Spectrosc.* 25 446-7
Phelps A V 1972 JILA Report No 110, University of Colorado,
Boulder, Colorado
Pollock D H and Jensen A O 1965 *J. Appl. Phys.* 36 3184-92
Roueff E 1970 *Astron. Astrophys.* 7 4-9
Slater J C and Kirkwood J G 1931 *Phys. Rev.* 37 682-97
Smith G 1972 *J. Phys. B: At. Mol. Phys.* 5 2310-9
Smirnov B M 1967 *Sov. Phys.-JETP* 24 314-9
Sobelman I I 1972 Introduction to the Theory of Atomic Spectra
(Oxford: Pergamon)
Sobelman I I, Vainstein L A and Yukov E A 1981 Excitation of Atoms
and Broadening of Spectral Lines (Berlin: Springer)
Sugino T, Shimizu H, Wada M and Itoh K 1979 *IEEE J. Quant. Electr.*
15 714-8
Szudy J and Baylis W E 1975 *J. Quant. Spectrosc. Radiat. Transfer*
15 641-68
Tachibana K, Harima H and Urano Y 1982 *J. Phys. B: At. Mol. Phys.*
15 (in press)
Takakura T, Iga K and Tako T 1980 *Japan. J. Appl. Phys.* L725-7
Thomann P, Burnett K and Cooper J 1980 *Phys. Rev. Lett.* 45 1325-8
Traving G 1960 Über die Theorie der Druckverbreiterung von
Spektrallinien (Karlsruhe: Braun)
Unsöld A 1955 Physik der Sternatmosphären (Berlin: Springer)
Urano Y, Kosasa K and Maruyama Y 1971 *Japan. J. Appl. Phys.* 10
1592-6
Vallee O, Ranson P and Chapelle J 1977 *IEEE J. Quant. Spectrosc.*
Radiat. Transfer 18 327-36
Varghese P L and Hanson R K 1981 *J. Quant. Spectrosc. Radiat.*
Transfer 26 339-47
Vaughan J M 1966 *Proc. R. Soc. A* 295 164-81
Vidal C R and Cooper J 1969 *J. Appl. Phys.* 40 3370-4
Wang S Y and Chen S Y 1979 *J. Quant. Spectrosc. Radiat. Transfer*
22 87-91

Weisskopf V 1933 Phys. Z. 34 1-24

Westerveld W B, Mulder Th F A and van Eck J 1979 J. Quant. Spectrosc. Radiat. Transfer 21 533-46

Whiting E E 1968 J. Quant. Spectrosc. Radiat. Transfer 21 533-46

York G and Gallagher A 1974 JILA Report No 114, University of Colorado, Boulder, Colorado

Zhuvikin G V, Penkin N P and Shabanova L N 1979 Opt. Spectrosc.

46 642-4

List of publications

1. "Empirical interatomic potentials for Ba-rare-gas systems deduced from an absorption measurement"
Harima H, Tachibana K and Urano Y 1982 J. Phys. B: At. Mol. Phys. 15 3679-93.
2. "Absorption coefficients for the wing of the Sr resonance line at 4607 Å broadened by Ar and Xe"
Harima H, Fukuzo Y, Tachibana K and Urano Y 1981 J. Phys. B: At. Mol. Phys. 14 3069-77.
3. "Measurement of broadening of absorption lines by image sensor"
Harima H, Tachibana K and Urano Y 1980 $\hat{O}y\hat{O}$ Butsuri 49 124-8.
4. "Measurement of oscillator strength of several lines of Ba I"
Harima H, Tachibana K and Urano Y 1978 J. Phys. Soc. Japan 45 357-8.
5. "Empirical interaction potentials between Sr and rare-gas atoms"
Harima H, Fukuzo Y, Tachibana K and Urano Y 1981 Abstracts of contributed papers, 12th International Conference on Physics of Electronic and Atomic Collisions, Gatlinburg, Tennessee, 503-4.
6. "Measurement of collisional broadening and shift of argon spectral lines using a tunable diode laser"
Tachibana K, Harima H and Urano Y 1982 J. Phys. B: At. Mol. Phys. 15 3169-78.
7. "Measurement of collision broadening of resonance lines of calcium ion by a low-resolution spectrometer"
Urano Y, Monju M, Harima H and Tachibana K 1981 Japan. J. Appl. Phys. 20 1021-5.

正誤表

$p(\text{行})$ $l(\text{行})$	誤	正
$p(2)l28$	upto	up to
$p12 l9, p22 l1, p27 l7, p29 l4,$ $p30 l17, p38 l12, p40 l4, p54 l19$ $p47 l2$	Eq.	Equation
$p53 l2, p56 l3, p57 l2, p58 l9,$ $p67 l12, p67 l27, p70 l8, p71 l22,$ $p73 l24, p80 l2, p83 l4, p83 l14,$ $p91 l7, p94 l3, p98 l22, p101 l2,$ $p110 l13, p113 l17, p116 l2, p119 l4$	Fig.	Figure
$p14 l10$	culculate	calculate
$p66 l7$	recieved	received
$p68 l1$	meaning	measuring
$p70 l8$	satisfying	satisfy
$p76 l11$	recentry	recently
$p76 l12$	attntion	attention
$p76 l18$	have	has
$p90 l19$	ergcm^{-6}	ergcm^6
$p91 l10$	a	an
$p99 l2$	reserved	reversed
$p101 l9$	serious	serious
$p101 l22$	monotonically	monotonously
$p104 l23$	to	with
$p106 l15$	crossing	crossings
$p106 l24$	occur	occurs
$p109 l2$	and	and yield
$p109 l10, p123 l18$	emmission	emission
$p110 l7$	kripton	krypton
$p113 l12$	compensated	compensated
$p113 l16, p121 l11$	were	was
$p115 l10$	Voight	Voigt
$p116 l7$	Lorenzian	Lorentzian
$p120 l10$	and	and we
$p120 l23$	assume	assume that
$p120 l21, p121 l2$	indicates	indicates that
$p128 l9$	line	Line
$p128 l24$	Nuetral	Neutral
$p129 l6$	Z. Physik 33 57-	Phys. Z 33 57-60
$p130 l14$	Sbelman	Sobelman
$p132 l13$	Tachibana K	Yoshida T